UCONN
LIBRARY

University of Connecticut
OpenCommons@UConn

Doctoral Dissertations

University of Connecticut Graduate School

5-23-2017

Adiabatic Expansion in Quantum Field Theory and Quantum Non-equilibrium Dynamics

Robert Dabrowski
University of Connecticut - Storrs, robdabrowski@gmail.com

Follow this and additional works at: https://opencommons.uconn.edu/dissertations

Recommended Citation
Dabrowski, Robert, "Adiabatic Expansion in Quantum Field Theory and Quantum Non-equilibrium Dynamics" (2017). *Doctoral Dissertations*. 1513.
https://opencommons.uconn.edu/dissertations/1513

Adiabatic Expansion in Quantum Field Theory and Quantum Non-equilibrium Dynamics

Robert Dabrowski, Ph.D.
University of Connecticut, 2017

In this dissertation we study semi-classical effects in Quantum Field Theory (QFT) and made use of the universal behavior of the asymptotic expansions to study of quantum non-equilibrium dynamics. We consider the evolution of quantum field theoretical systems subject to a time-dependent perturbation and demonstrate a universal form to the adiabatic particle number, corresponding to optimal truncation of the (divergent and asymptotic) adiabatic expansion. In this optimal basis, the particle number number evolves smoothly in time according to the universal smoothing of adiabatic evolution in the Stokes Phenomenon, thus providing a well-defined notion for evolution through a non-equilibrium process. The optimal basis also clearly illustrates interference effects associated with particle production for sequences of pulses in Schwinger and de Sitter particle production. We also demonstrate the basis dependence of the adiabatic particle number across several equivalent approaches, which revealed that particle production is a measure of small deviations between the exact and adiabatic solutions of the Ermakov-Milne equation for the associated time-dependent oscillators. Given a consistent formulation of the optimal time-dependent particle number, led us to explore the consequences for the back-reaction mechanism in particle production and provide a modification of Jarzynski's non-equilibrium work theorem to study non-equilibrium physics under adiabatic evolution. Lastly, we classify semiclassical saddle point (non-instanton) solutions in the asymptotically free $\mathbb{CP}^{N-1}$ model in QFT.

Adiabatic Expansion in Quantum Field Theory and Quantum Non-equilibrium Dynamics

Robert Dabrowski

B.S., Macaulay Honors College at The City College of New York, 2009

A Dissertation

Submitted in Partial Fulfillment of the

Requirements for the Degree of

Doctor of Philosophy

at the

University of Connecticut

2017

Copyright by

Robert Dabrowski

2017

APPROVAL PAGE

Doctor of Philosophy Dissertation

Adiabatic Expansion in Quantum Field Theory and Quantum Non-equilibrium Dynamics

Presented by

Robert Dabrowski, B.S.

Major Advisor

Gerald V. Dunne

Associate Advisor

Alex Kovner

Associate Advisor

Tom Blum

University of Connecticut

2017

For Nuha,

my wife and best friend

ACKNOWLEDGEMENTS

It has been an incredible journey to complete a Ph.D. and I am deeply appreciative of all those people who have supported me throughout the process. I would like to thank my advisor Dr. Gerald V. Dunne for his guidance across the years. Gerald has proven to be a great teacher and mentor, and I am grateful to have had the opportunity to work with him. I also thank my associate advisors Dr. Alex Kovner and Dr. Thomas Blum for all their help and efforts. Additionally, I would also like to thank my parents for their love, support, and encouragement to pursue science. They both passed away before they could see this moment, and I wish they were here with me today. I am also thankful for the support of my brother Artur, and my wife's family, especially for treating me as one of their own. Most of all, I thank my wife Nuha for her constant love, understanding, and encouragement all these years. This accomplishment is as much hers as it is mine and I could not have made it here without her.

TABLE OF CONTENTS

1. Introduction 1

2. Schwinger Particle Pair Production 5

2.1 Overview 5

2.2 Formalism 8

2.2.1 Scalar Quantum Electrodynamics 8

2.2.2 Mode Decomposition in a time-dependent External Classical Electric Field 9

2.2.3 Equivalent Representations of the Klein-Gordon Equation 11

2.2.4 Particle Production as a Scattering Problem 12

2.3 Bogoliubov Approach to Adiabatic Particle Number 14

2.4 Reflection Amplitude Approach to Adiabatic Particle Number 20

2.5 Wigner Approach to Adiabatic Particle Number 21

2.6 Schrödinger Picture Approach to Adiabatic Particle Number 27

2.7 Basis Ambiguity Problem of the Adiabatic Particle Number 33

2.8 Adiabatic Expansion & Bases: Going Beyond Leading Order WKB . 37

2.9 Adiabatic Particle Number Truncated at j-th Order 40

2.10 Universal Form to the Evolution of the Adiabatic Particle Number . 43

2.11 Illustrations of the Optimal Adiabatic Particle Number for various External Electric Fields 49

2.11.1 Illustrations of Simple External Electric Fields 49

2.11.2 Illustrations of Multi-pulse External Electric Fields 55

2.12 Approximate Universal Evolution for Multi-pulse External Fields . . 62

2.13 Particle Production as the Measure of Small Deviations 69

2.13.1 Optimal Adiabatic Approximation of the Ermakov-Milne Equation 71

2.13.2 Adiabatic Particle Number as a Measure of Small Deviations 79

2.14 Extroduction 83

3. Cosmological Particle Production 86

3.1 Overview 86

3.2 Scalar Fields conformally coupled to a de Sitter Spacetime 87

3.3 Spacetime Implications for Cosmological Particle Production 90

3.3.1 Optimal Adiabatic Particle Number in 4d de Sitter space: Coherent Constructive Interference 90

3.3.2 Optimal Adiabatic Particle Number in 3d de Sitter space: Coherent Destructive Interference 92

3.4 Extroduction 94

4. The Back-reaction Problem 96

4.1 Overview 96

4.2 Formalism 98

4.2.1 Induced Local Current 98

4.2.2 Mode Decomposition Conserved Current 99

4.3 Back-reaction Mechanism 100

4.4 Energy Conservation 101

4.4.1 Energy of the Produced Scalar Field and Electromagnetic Field . . 101

4.4.2 Implications of Energy Conservation 103

4.5 Components of the Current 105

4.6 Extroduction 110

5. Time-dependent Quantum Excitations and the Non-equilibrium Work Theorem 112

5.1 Introduction 112

5.2 Formalism 115

5.2.1 Quantum Harmonic Oscillator Dynamics and Adiabatic Evolution . 115

5.2.2 On the Time-dependence of the Adiabaticity Parameter 119

5.2.3 Adiabatic Approximation of the Energy 122

5.3 Work Characteristic Function 126

5.4 Recovering Jarzynski's Equality 129

5.5 Time-Dependent Work Probability Distribution 131

5.5.1 Work Probability Distribution for $\tilde{Q}^{(j)}(t) \approx 1$ 132

5.5.2 Work Probability Distribution for $\tilde{Q}^{(j)}(t) > 1$ 133

5.6 Statistical Properties of the System: Mean Work Probability and Dissipated Work 134

5.7 Extroduction 134

6. Fractionalized Non-self-dual Solutions in the $\mathbb{CP}^{N-1}$ Model . . 136

6.1 Introduction 136

6.2 Formalism: Classical solutions of $\mathbb{CP}^{N-1}$ 140

6.2.1 Action and Topological Charge 140

6.2.2 Self-dual (instanton) solutions 142

6.2.3 Non-self-dual solutions 142

6.2.4 Action and Topological Charge of Non-Self-Dual Classical Solutions 144

6.2.5 Fluctuation Modes 145

6.3 Explicit Examples on $\mathbb{R}^2$ and $\mathbb{S}^2$ 148

6.4 Explicit Examples on $\mathbb{S}^1_L \times \mathbb{R}^1$ 149

6.5 Conclusion 155

7. Conclusion 157

Appendices 158

A Schwinger Effect for Spinor QED 158

B Single-pulse Analytical Example 160

C Transition Amplitude Evaluation: Double Hermite Integral Solution . 161

D Hermite Bilinear Forms 162

E A Useful Integral 162

F $\mathbb{CP}^{N-1}$ Projector Identities 163

Bibliography 165

LIST OF FIGURES

2.1 Plots of $\xi_k(t)$ (left), and the real (blue-solid line) and imaginary (red-dashed line) parts of f_k (right), abiding the scattering conditions (2.24), for a single-pulse E-field: $E(t) = E_0\text{sech}^2(at)$, with $E_0 = 0.25$, $a = 0.1$, $k_\parallel = 0$, and $k_\perp = 0$, all in units with $m = 1$. For this case, both f_k and ξ_k can be obtained analytically (Appendix B), and ξ_k is plotted as a solid-red line in each subplot for comparison. 14

2.2 Density plots of $\mathcal{W}_k(t, k_0)$ with respect to t, and k_0, for a single-pulse E-field given by $E(t) = E_0\text{sech}^2(at)$, obtained by numerically evaluating equation (2.64) over $T \in (-T_0, +T_0)$, utilizing the exact solution $\xi_k(t)$ (see Appendix B). The upper left, upper right and lower left subplots are plotted with $E_0 = 0.25, a = 0.1$, $k_\parallel = 0.25$, and $k_\perp = 0$, in units with $m = 1$, with the upper left plot integrated with $T_0 = 20$, the upper right plot integrated with $T_0 = 40$, and the lower left subplot integrated with $T_0 = 60$. The lower right subplot is plotted for the physically unrealistic case with $m = 0, E_0 = 0.5, k_\parallel = 0.25, k_\perp = 0$, and integrated with $T_0 = 40$. In each subplot, $\mathcal{W}_k(t, k_0)$ is well matched by $-\omega_k(t)$ (2.17) (blue-dashed line), artificially plotted over each density subplot. 25

2.3 $\tilde{\mathcal{N}}_k(t)$, evaluated with respect to two different adiabatic bases, for the Schwinger effect in an E-field: $E(t) = E_0 \operatorname{sech}^2(at)$, with $E_0 = 0.25, a = 0.1, k_\perp = 0, k_\parallel = 0$, all in units with $m = 1$. The blue curves corresponds to the basis $W_k(t) = \omega_k(t)$ and $V_k(t) = 0$, while the red curves correspond to the basis $W_k(t) = \omega_k(t)$ and $V_k(t) = -\frac{\dot{\omega}_k(t)}{2\omega_k(t)}$, both determined by evaluating their respective evolution equations (2.89) and (2.91). The right-hand figure shows their late-time evolution. $\tilde{\mathcal{N}}_k(t)$ at intermediate times exhibits large differences in both scale and form of the oscillations, while the asymptotic value of the particle number is the same for both bases. 35

2.4 $\tilde{\mathcal{N}}_k(t)$, evaluated with respect to two different adiabatic bases, for particle creation in 4-dimensional de Sitter space with conformal coupling (see Chapter 3), with the physical de Sitter space parameters: $H = 0.5, k = 25$, in units with mass scale $m = 1$. The blue curves corresponds to the basis $W_k(t)=\omega_k(t)$ and $V_k(t)=0$, while the red curves correspond to the basis $W_k(t) = \omega_k(t)$ and $V_k(t) = -\frac{\dot{\omega}_k(t)}{2\omega_k(t)}$, both determined by evaluating their respective evolution equations (2.89) and (2.89). The right-hand figure shows their late-time evolution. Like Figure 2.3, the evolution of $\tilde{\mathcal{N}}_k(t)$ at intermediate times exhibits large differences in both scale and form of the oscillations, while the asymptotic value of the particle number is the same for both bases. 36

2.5 An order-by-order comparison of the truncation of the adiabatic expansion (solid-blue line) expressed in the phase integral form (2.108) with Dingle's universal large-order behavior of the expansion (2.109) (red-dashed line) for adiabatic orders $j = 1$ to $j = 8$, considering sQED Schwinger Effect in a single-pulse E-field. Dingle's universal form accurately captures the large-order behavior of the expansion and becomes valid even at relatively low orders. See text for additional details. 46

2.6 For a single complex conjugate pair of turning points, (t_c, t_c^*) joined by a Stokes line [dashed blue line], we define s_c as the time at which the Stokes line crosses the real axis axis. Particle production associated with this pair (t_c, t_c^*) corresponds to crossing the Stokes line at s_c. 47

2.7 $\tilde{\mathcal{N}}_k^{(j)}(t)$, here, obtained by numerically evaluating (2.100), for the first 6 orders of the adiabatic expansion, for Schwinger particle production in a constant E-field with $E = 0.25$, $k_\perp = 0$, $k_\parallel = 0$, in units with $m = 1$. $\tilde{\mathcal{N}}_k^{(j)}$ is plotted with solid-blue lines, and Berry's universal form (2.113) is plotted with red-dashed lines. The final value of the particle number is the same for all orders of truncation, but the oscillations in the particle number at intermediate times differ significantly. Note the smoothest evolution occurs at the optimal order, here, $j_{\rm opt} = 3$. 52

2.8 $\tilde{\mathcal{N}}_k^{(j)}(t)$, here, obtained by numerically evaluating (2.100), for the first 6 orders of the adiabatic expansion, for Schwinger particle production in a single-pulse E-field (2.119) with $E_0 = 0.25$, $a = 0.1$, $k_\perp = 0$, $k_\parallel = 0$, with units in $m = 1$. $\tilde{\mathcal{N}}_k^{(j)}$ and Berry's universal form (2.113) are plotted in the same style as for Figure 2.7. Again, the final value of the particle number is the same for all orders of truncation, but the oscillations in the particle number at intermediate times differ significantly. Here, $j_{\rm opt} = 3$. 54

2.9 A survey of illustrations that compares $\tilde{\mathcal{N}}_k^{(j_{\rm opt})}$ (solid-blue line), evaluated using (2.100) at the optimal order $j_{\rm opt}$, against its approximation by the universal form (2.113) (red-dashed line), for Schwinger particle production in a single-pulse E-field (2.119), across different field parameters E_0 and a, and different momenta $k_\parallel$ and $k_\perp$, in units with $m = 1$. In each example, $\tilde{\mathcal{N}}_k^{(j_{\rm opt})}$ (solid-blue line) is normalized by its final particle number to present each subplot on the same scale. The approximate universal form with (2.115) is plotted as a green-dashed curve. 56

2.10 $\tilde{\mathcal{N}}_k^{(j)}(t)(t)$ for the first 6 orders of the adiabatic expansion, for Schwinger particle production in alternating-sign double-pulse E-field (2.122), with $E_0 = 0.25$, $a = 0.1$, $b = 50$, $k_\perp = 0$, and $k_\parallel = 2.51555$, in units with $m = 1$. $k_\parallel$ is selected to show maximum constructive interference. The final particle number at future infinity is the same for all j, and is 4 times that of the intermediate plateau, consistent with coherent n^2-enhancement for constructive interference. Note the smoothening at the optimal order ($j_{\rm opt} = 3$) and the large oscillations that appear before and after. 57

2.11 As in Figure 2.10, but with $E_0 = 0.25$, $a = 0.1$, $b = 50$, $k_\perp = 0$, and $k_\parallel = 2.49887$, in units with $m = 1$. $k_\parallel$ is selected to show maximum destructive interference. The final asymptotic value of the particle number, at future infinity, vanishes for each order of truncation, consistent with coherent destructive quantum interference. Note the smoothening at the optimal order ($j_{\text{opt}} = 3$) and the large oscillations that appear before and after. 58

2.12 $\tilde{\mathcal{N}}_k^{(j)}(t)$ for an alternating-sign double pulse E-field (2.122) with $E_0 = 0.5$, $a = 0.2$, $b = 2.5$, $k_\perp = 0$, and $k_\parallel = 1.85$, in units with $m = 1$. Here, the pulses are closer together than in Figure 2.10 where the optimal order ($j_{\text{opt}} = 2$) provides a clear resolution of coherent destructive interference. 61

2.13 As in Figure 2.12, but with $k_\parallel = 1.22175$. Again, the pulses are closer together than in Figure 2.11 where the optimal order ($j_{\text{opt}} = 2$) provides a clear resolution of coherent destructive interference. . . 62

2.14 $\tilde{\mathcal{N}}_k^{(j)}(t)$, for the first 3 orders of the adiabatic expansion, considering an alternating-sign triple-pulse E-field (2.124) with $E_0 = 0.25$, $a = 0.1$, $b = 50$, $p_\perp = 0$, and $k_\parallel = 0.08336$, in units with $m = 1$. $k_\parallel$ is selected for maximum constructive interference. See Figure 2.15 for the next three orders. 63

2.15 As in Figure 2.14, but for the first 3 orders of the adiabatic expansion, $j = 3, 4, 5$. Here, $j_{\text{opt}} = 3$ and the ratios of the plateaux are $1 : 3.99 : 8.9$, very close to the expected $1 : 4 : 9$ for coherent constructive interference of three pulses. 64

2.16 Time evolution of $\tilde{\mathcal{N}}_k^{(j_{\text{opt}})}(t)$, normalized by its final particle number at future infinity, for two examples of coherent constructive interference: a double-pulse E-field (2.122) (left) as in Figure 2.10, and a triple-pulse E-field (2.124) (right) as in Figure 2.11. Here, $j_{\text{opt}} = 3$ for both, and the ratio of their plateaux follow $1 : 4$ and $1 : 4 : 9$, respectively. 65

2.17 The longitudinal momentum spectrum N_k as a function of the produced particle's longitudinal momentum for the single-, double-, and triple-pulse E-fields, (2.119), (2.122), and (2.124), respectively. The distribution, with constructive and destructive enhancement for certain modes, is of the n-slit interference form with the envelop being n^2 times the envelope for the single-pulse. 65

2.18 As in Figure 2.19, but plotted over specific time ranges, ending with cross sections at $t = \mp 7.5, +30$, to illustrate the time evolution of $k_{\parallel}$-momentum spectrum (red-filled) for different periods of particle creation due to pulse events at $t = 0, \pm 15$. The highlighted longitudinal momentum spectrum of each subplot follows the n-slit interference pattern (2.129), which can be compared to the asymptotic momentum spectra shown in Figure 2.17. Additional details found in text. 67

2.19 The approximate optimal adiabatic particle number (2.130) as a function of t and $k_{\parallel}$, for Schwinger pair production for alternating-sign triple-pulse (2.124) with $E_0 = 0.5$, $a = 0.25$, $b = 7.5$, and $k_{\perp} = 0$, in units with $m = 1$. A full time range realization of the cross-sections calculated in Figure (2.17) with particle creation events located at $t = 0, \pm 15$. Notice that $\tilde{\mathcal{N}}_k^{(j)}$ is critically dependent on the longitudinal momentum, indicating whether enhancement or cancellation occurs for produced particles with momentum $k_{\parallel}$. 68

2.20 The adiabatic approximation (2.131) of $1/(2\xi_k^2)$ (blue-solid line) compared to the adiabatic function $W_k^{(j)}$ (red-dashed line), for the first 3 orders of the adiabatic expansion, considering the single-pulse E-field (2.119) with $E_0 = 0.25$, $a = 0.1$, $k_\parallel = 0$, and $k_\perp = 0$, in units with $m = 1$. The central panels zoom in on time-scales near the pulse, while the right-hand panels zoom in on the late-time behavior. The deviations of the approximation from the exact form are typically very small, capturing well the averaged time dependence except near the the peak of the pulse, and except for tiny oscillations about the average value at late times. 70

2.21 As in Figure 2.20 but with plots of the next three adiabatic orders, $j = 3, 4, 5$ for the adiabatic approximation (2.131) of $1/(2\xi_k^2)$ (blue-solid line) compared to the adiabatic function $W_k^{(j)}$ (red-dashed line), considering the single-pulse E-field (2.119) with $E_0 = 0.25$, $a = 0.1$, $k_\parallel = k_\perp = 0$, in units with $m = 1$. The central panels zoom in on time-scales near the pulse, while the right-hand panels zoom in on the late-time behavior. The deviations of the approximation from the exact form are typically very small, capturing well the averaged time dependence except near the the peak of the pulse, and except for tiny oscillations about the average value at late times. The optimal order is reached at $j = 3$, after which the deviations begin to grow again. 71

2.22 Plots of approximation (2.132), the time derivative form of (2.131) as a ratio, by comparing $\dot{\xi}_k/\xi_k$ (blue-solid line) with the adiabatic function $V_k^{(j)} = -\dot{W}_k^{(j)}/(2W_k^{(j)})$ (red-dashed line), for the first three orders of the adiabatic expansion, considering the single-pulse E-field (2.119) with the same parameters as for Figure 2.20. The left-hand panels show the time-evolution over a wide time range, and the right-hand panels zoom in on the vicinity of the pulse. The approximate (red-dashed) curves accurately describe the averaged time evolution, but miss the late-time oscillations, which are more pronounced than those in Figures 2.20 and 2.21 because they are effectively the derivatives of those small oscillations. 73

2.23 As in Figure 2.22, but with plots of the next three adiabatic orders, $j = 3, 4, 5$, showing the approximation (2.132), the time derivative form of (2.131) as a ratio, by comparing $\dot{\xi}_k/\xi_k$ (blue-solid line) with the adiabatic function $V_k^{(j)} = -\dot{W}_k^{(j)}/(2W_k^{(j)})$ (red-dashed line), considering the single-pulse E-field (2.119) with the same parameters as for Figure 2.20. The left-hand panels show the time-evolution over a wide time range, and the right-hand panels zoom in on the vicinity of the pulse. The approximate (red-dashed) curves accurately describe the averaged time evolution, but miss the late-time oscillations, which are more pronounced than those in Figures 2.20 and 2.21 because they are effectively the derivatives of those small oscillations. 74

2.24 Plots of the approximation (2.132) at the optimal truncation order ($j = 3$), for the time derivative form of (2.131) as a ratio, by comparing $\dot{\xi}_k/\xi_k$ (blue-solid line) and $V_k^{(j)} = -\dot{W}_k^{(j)}/2W_k^{(j)}$ (red-dashed line), for the double-pulse E-field (2.122) with $E_0 = 0.25$, $a = 0.1$, $b = 50$, and $k_\perp = 0$, in units with $m = 1$. $k_\parallel$ was selected to correspond to maximum constructive ($k_\parallel = 2.51555$, left subplot), and maximum destructive interference ($k_\parallel = 2.49887$, right subplot) in the particle number at future infinity. In the maximum constructive case, the oscillations introduced after each pulse interfere to double in magnitude. In the maximum destructive case, the oscillations introduced by the first and second pulse interfere to completely cancel. 76

2.25 Zoomed-in view of the left subplot of Figure 2.24, plotted for a closer examination of the approximation (2.132) in the vicinity of the pulse centers ($t = \pm 50$), for the case of maximum constructive interference. 78

2.26 Zoomed-in view of the right subplot of Figure 2.24, plotted for a closer examination of the approximation (2.132) in the vicinity of the pulse centers ($t = \pm 50$), for the case of maximum destructive interference. 79

2.27 $\tilde{\mathcal{N}}_k^{(j)}(t)$ (2.133) (black-solid line), and its components, the first (blue-solid line) and second (red-solid line) terms on the right-hand-side of (2.133), for the first 6 orders of the adiabatic expansion, considering a single-pulse E-field (2.119) with $E_0 = 0.25, a = 0.1$, $k_{\|} = 0$, and $k_{\perp} = 0$, in units with $m = 1$. Notice that each of the components (blue and red curves) is highly oscillatory, and out of phase, but the sum is smooth except in the vicinity of the pulse. Also note the difference in scales in the various sub-plots. The deviations decrease dramatically as the optimal order ($j_{\text{opt}} = 3$) is approached, and then grow again after this order. See text for additional details. 80

2.28 $\tilde{\mathcal{N}}_k^{(j_{\text{opt}})}(t)$ (2.133) (black-solid line), and its components, the first (blue-solid line) and second (red-solid line) terms on the right-hand-side of (2.133), for the double-pulse E-field (2.122) with $E_0 = 0.25, a = 0.1, b = 50$, $k_{\|} = 2.51555$, and $k_{\perp} = 0$, in units with $m = 1$. $k_{\|}$ was selected for maximum constructive interference, with the final value being 4 times the intermediate plateau value between the two pulses. At intermediate times, notice the phase difference of the oscillatory components of (2.133), which remarkably sum to a smooth evolution of $\tilde{\mathcal{N}}_k^{(j_{\text{opt}})}$. 82

2.29 $\tilde{\mathcal{N}}_k^{(j_{\rm opt})}(t)$ (2.133) (black-solid line), and its components, the first (blue-solid line) and second (red-solid line) terms on the right-hand-side of (2.133), for the double-pulse E-field (2.122) with $E_0 = 0.25, a = 0.1, b = 50$, $k_\parallel = 2.49887$, and $k_\perp = 0$, in units with $m = 1$. $k_\parallel$ was selected for maximum destructive interference, with vanishing final particle number at future infinity. At intermediate times, notice the phase difference of the oscillatory components of (2.133), which remarkably sum to a smooth evolution of $\tilde{\mathcal{N}}_k^{(j_{\rm opt})}(t)$. 82

3.1 $\tilde{\mathcal{N}}_k^{(j)}(t)$ for the first 6 orders of the adiabatic expansion, for particle production in four-dimensional de Sitter space (3.12, 3.14), with $k = 25$ and $H = 0.5$, in units with $m = 1$. Here, $\eta_4 = \frac{1}{6}$ in $d = 4$. Note the similarity with Figure 2.10, the coherent constructive interference case for a double-pulse E-field, in terms of the 4 fold enhancement of the final particle number and the smoothing of the particle number with optimal truncation of the adiabatic expansion. 92

3.2 $\tilde{\mathcal{N}}_k^{(j)}(t)$ for the first 6 orders of the adiabatic expansion, for particle production in four-dimensional de Sitter space (3.12, 3.14), with $k = 25$ and $H = 0.5$, in units with $m = 1$. Here, $\eta_3 = \frac{1}{8}$ in $d = 3$. Note the similarity with Figure 2.11, the coherent destructive interference case for a double-pulse E-field, in terms of a vanishing final particle number and the smoothing of the particle number with optimal truncation of the adiabatic expansion. 93

4.1 The conduction current plotted for the first 6 orders of the adiabatic expansion, for Schwinger pair production in a single-pulse E-field (2.119, given by (2.120), with $E_0 = 0.25, a = 0.1, k_\perp = k_\parallel = 0$, in units of $m = 1$. As like Figure 2.8, the final value of the conduction current is same for all orders of truncation, but the oscillations differ significantly with the smoothest evolution occurring at the optimal order, here, $j_{\text{opt}} = 3$. 105

4.2 The conduction current plotted for the first six orders of the adiabatic expansion, for Schwinger pair production in a triple-pulse E-field (2.124), given by (2.125), with $E_0 = 0.25, a = 0.1, b = 50, k_\perp = k_\parallel = 0$, in units of $m = 1$. As like the particle number in Figure 2.8, the final value of the conduction current is same for all orders of truncation, but the oscillations differ significantly. The smoothest evolution of the conduction current occurs at the optimal order, here, $j_{\text{opt}} = 3$. 109

5.1 Time evolution of $\tilde{Q}^{(j)}(t)$ (5.14) for the first six orders of the adiabatic expansion, considering an Schwinger particle production effective frequency (2.17), with parameters as in Figure 2.8. Note that $\tilde{Q}^{(j)}(t)$ has the same intermediate time behavior as the adiabatic particle number $\tilde{\mathcal{N}}^{(j)}(t)$ except shifted and twice the magnitude, as related by (5.15). 120

5.2 The residual of $h(t)$ (5.18) and its approximation by (5.21) for the first six orders of the adiabatic expansion, considering the sQED particle production effective frequency (2.17) with the same pulse parameters as used in Figure 2.8. Here, $j_{\text{opt}} = 3$, which is consistent with Figure 2.8. The adiabatic order-by-order residual of both quantities show minor differences at intermediate times but agreement at asymptotically late times. 123

6.1 The change (6.18) in the action under the fluctuation (6.17), for the $Q = 0$ non-self-dual configuration plotted in the second row of Figure 6.2. The horizontal axis denotes the (symmetric) distance of each object from the center. At large separation this fluctuation is a zero mode, while at finite separation it becomes a negative mode. 145

6.2 The Action and Charge Density configurations due to successive mappings from the ansatz solution (6.19) in $\mathbb{CP}^2$ on $\mathbb{R}^2$, where $a = a_1 + i\, a_2$ and $b = b_1 + i\, b_2$, with $\lambda, \mu = 2$, $a_1, a_2 = 0$, $b_1, b_2 = 4$, $\forall\ \theta_1, \theta_2 \in [0, 2\pi)$. $\omega_{(0)}$ corresponds to two instantons, while $\omega_{(1)}$ corresponds to two instantons and two anti-instantons, and $\omega_{(2)}$ corresponds to two anti-instantons. All are exact solutions to (6.7) but $\omega_{(1)}$ is non-self-dual. 147

6.3 The Action and Charge Density configurations due to successive mappings from the ansatz solution (6.22) in $\mathbb{CP}^2$ on $\mathbb{S}^1_L \times \mathbb{R}^1$, with $\lambda = 4000, \mu = 1, \forall\, \theta_1, \theta_2 \in [0, 2\pi)$. $\omega_{(0)}$ corresponds to two fractionalized instantons, while $\omega_{(1)}$ corresponds to a single fractionalized instanton and two anti-instantons, and $\omega_{(2)}$ corresponds to a single fractionalized anti-instanton. All are exact solutions to (6.7) but $\omega_{(1)}$ is non-self-dual. 150

6.4 The Action and Charge Density configurations due to successive mapping from an ansatz solution with more structure (6.24) in $\mathbb{CP}^2$ on $\mathbb{S}^1_L \times \mathbb{R}^1$, with $\lambda = 10^4, \mu = 10^{-2}, \nu = 10^4,\ \theta_1 = \pi, \theta_2 = 0,\ \forall$ $\theta_3 \in [0, 2\pi)$. See text for quantitative details on the mapping. $\omega_{(0)}$, $\omega_{(1)}$ and $\omega_{(2)}$ are all exact solutions to (6.7), but $\omega_{(1)}$ is non-self-dual. 151

6.5 A magnified cross section of the charge density of the highly localized charge-1 instanton and anti-instanton that appear in the fourth and sixth plots in Figure 6.4. Both are plotted with the same parameters used in Figure 6.4. 152

Chapter 1

Introduction

A question yet to be fully addressed in Quantum Field Theory (QFT) is what happens during time-dependent far-from-equilibrium evolution of a quantum system. Often, one speaks of quasi-particles since the concept of a particle is ambiguous at intermediate times: one is trying to ascribe energy states to identify particles and anti-particles with respect to a vacuum influenced by an interaction. For this reason, discussions are restricted to considering equilibrium states of the system and making use of perturbative methods close to equilibrium. In this dissertation, we explore semi-classical effects in QFT, and apply the universal behavior of asymptotic expansions to address far-from-equilibrium effects undergoing time-dependent driving. This work is motivated by questions of whether particle production can be seen in real-time, on how to address the non-equilibrium effect of back-reaction in particle production mechanisms, and motivated by remarkable formulations such as Jarzynski's non-equilibrium work theorem in which the study of the equilibrium configurations of a dynamical system yields information regarding the non-equilibrium evolution of the system. With respect to Schwinger particle production, a real-time formulation of the particle number has the potential to provide additional insights into the design of laser pulses to reduce the critical electric field threshold necessary to observe the effect and exert quantum control. It could also yield a means to study the time-dependent process of pair recombination, the back-reaction of pairs that reduce the particle production, potentially providing insights to experimental realizations of the Schwinger Effect, and other particle production mechanisms, with direct implications for cosmology. In addition, a time-dependent formulation of Jarzynski's work theorem could yield additional insights into particle production, and other dynamical quantum systems.

A key new contribution made in this dissertation is the use of the universal results of Dingle's work on asymptotic expansions and Berry's application of Dingle's work to characterize the adiabatic evolution of dynamical quantum mechanical systems. Berry's work demonstrated the adiabatic approximation of the evolution of the system can be characterized by the (divergent and asymptotic) adiabatic expansion, in which the study beyond the leading order of the expansion, corresponding to a Wentzel-Kramers-Brillouin (WKB)-type approximation, leads to changes in the effective approximation of the adiabatic evolution of the system. The truncation of this adiabatic expansion has a well-defined large-order behavior and exhibits an optimal order corresponding to a minimum error approximation, implying an optimal adiabatic approximation. In the context of QFT, it provides a means to optimally approximate the positive and negative energy states of a dynamical system necessary for particle and anti-particle identification at intermediate times. The work of Berry also identifies an approximate universal form for the time evolution of the system corresponding to truncation at the optimal order of the adiabatic expansion. The work presented in this dissertation is the first application of these mathematical adiabatic expansion results to the physical context of QFT.

The dissertation is structured as follows. In Chapter 2 we characterize the adiabatic expansion, we derive a time-dependent particle number using a variety of equivalent yet different approaches in sQED Schwinger particle production, and show that particle production is the manifestation of the Stokes Phenomenon. Illustrations of the universal behavior of the optimally truncated time-dependent particle number are demonstrated for a variety of applied external electric fields, which clearly demonstrates the effect of quantum interference. In Chapter 3, we apply the universal results of the adiabatic expansion to de Sitter particle production, and demonstrated that the difference between a vanishing particle number in odd dimensional de Sitter space and non-vanishing particle production in even de Sitter space is due to quantum interference. In Chapter 4, we address and outline the technical difficulties of incorporating the back-reaction mechanism in sQED Schwinger particle production. In Chapter 5 we construct a *time-dependent* formulation of Jarzynski's non-equilibrium work theorem using the universal results from optimally truncating the adiabatic expansion. Chapter 7 is devoted to concluding remarks, and some supporting calculations and identities are presented in the Appendices.

Chapter 2

Schwinger Particle Pair Production

2.1 Overview

The stimulated production of particles from the vacuum is a remarkable feature of quantum field theory that manifests when the vacuum is subjected to an external perturbation, such as gauge or gravitational curvature. Notable examples include the Schwinger effect from applying an external electric field to the electrodynamical (QED) vacuum [1–5], expanding cosmologies [6–9] and de Sitter space times [10–19], Hawking Radiation due to blackholes and gravitational horizon effects [20–25], and Unruh Radiation seen by an accelerating observer [26,27]. These types of particle production have an important role in the physics of non-equilibrium processes in heavy-ion collisions [28–32], astrophysical phenomena [33], and the search for nonlinear and non-perturbative effects in ultra-intense laser systems [34–37]. There are also close technical analogues with driven two-level systems, relevant for atomic and condensed matter processes [38,39], such as Landau-Zener-Stückelberg transitions [40], the dynamical Casimir effect and its analogues [41,42], Ramsey processes and tunnel junctions [43,44]. Of particular relevance to this dissertation chapter is the development of sophisticated ultra-intense laser systems, such as Extreme Light Infrastructure (ELI) and European XFEL, which will soon become operational to probe this ultra-relativistic regime with a field strength close to the necessary threshold set by the Schwinger Limit [3,36].

Particle production involves evolution of a quantum system from an initial (free) equilibrium configuration to a new final (free) equilibrium configuration through an intervening non-equilibrium evolution set by the background. Quantifying a final particle number then involves relating the final equilibrium configuration to the initial one, a comparison of well-defined asymptotic vacua where the identification of positive (particles) and negative (anti-particles) energy states is unambiguous and exact. A quantitative description of particle production at all times, not just at asymptotically early and late times, requires a well-defined notion of time-dependent particle number also at *intermediate times*. This is a challenging conceptual and computational problem, especially if one wants to include also back-reaction effects and the full non-equilibrium dynamics.

At intermediate times, when the system is out equilibrium, the exact distinction of energy states is unclear and a standard approach is by *adiabatic approximation* [6–8,45–62]: specifying a reference basis set of approximate states under the assumption of a slowly varying dynamical background. In this way, a time-dependent particle number can be defined by the projection of the system evolution onto these approximate states. With this procedure, the final particle number at asymptotically late times is independent of the basis choice. However, the particle number at intermediate times differ significantly for different basis choices, which raises questions about whether any physically meaningful interpretation can be made for the particle number at intermediate times. However, a remarkable mathematical universality of adiabatic expansions was discovered by Berry and Dingle. Dingle [63] identified a simple large-order universal behavior to the (divergent and asymptotic) adiabatic expansion, which provided a universal form for truncation of the adiabatic expansion at the optimal order. Berry [64–66] then applied a Borel summation using the Dingle large-order form to determine that the smoothest evolution across a Stokes Line, in the context of the Stokes Phenomenon, corresponds to optimal truncation of the expansion and identified a universal form for the evolution.

The universality of truncating the adiabatic expansion at the optimal order makes for a well-defined notion for the adiabatic particle number at intermediate times and corresponds to an *optimal adiabatic approximation* of the evolution. At the optimal order, the adiabatic particle number also evolves the smoothest in time as compared to any order with a given approximate universal form. To test the optimal order, we examine the truncation of the adiabatic expansion using several common (and equivalent) formulations of particle production: the Bogoliubov [13,14,47–49,53], Riccati [67,68], Spectral Function [69,70] and Schrödinger [20–23] approaches. The analysis presented can also be used in other formalisms such as quantum kinetic approach [53,54,71–75], and the Dirac-Heisenberg-Wigner approach with time-dependent background fields [76,77].

2.2 Formalism

2.2.1 Scalar Quantum Electrodynamics

We consider scalar QED for simplicity[1]. The action of a charged massive scalar field is given by a Klein-Gordon Lagrangian

$$S = \int d^4x \left[|D_\mu \Phi|^2 - m^2 |\Phi|^2 - \frac{1}{4} F_{\mu\nu} F^{\mu\nu} \right] \tag{2.1}$$

where extremizing the action with the respect to $\Phi^*(\mathbf{x}, t)$ yields the *Klein-Gordon Equation* for the field $\Phi(\mathbf{x}, t)$:

$$\left(D_\mu D^\mu + m^2 \right) \Phi(\mathbf{x}, t) = 0 \tag{2.2}$$

while extremizing the action with respect to the gauge field A^ν yields

$$\partial_\mu F^{\mu\nu} = j^\nu \tag{2.3}$$

with the conserved local current

$$j^\nu = i \left[(D^\nu \Phi) \Phi^* - \Phi (D^\nu \Phi)^* \right] \tag{2.4}$$

---

[1] Apart from opposite phase of interference effects, the physics is very similar to that of spinor QED but notationally simpler.

The proceeding sections of this chapter consider only the Klein-Gordon equation and neglect any back-reaction mechanism. This mechanism is discussed later in Chapter 4.

2.2.2 Mode Decomposition in a time-dependent External Classical Electric Field

For a charged scalar field $\Phi(\mathbf{x}, t)$ in a time-dependent and spatially homogeneous classical electric field, the scalar field can be decomposed into spatial Fourier modes. The decomposition is characterized by

$$\Phi(\mathbf{x}, t) = \int \frac{d^3k}{(2\pi)^3} \phi_{\mathbf{k}}(t) e^{i\mathbf{k}\cdot\mathbf{x}} \qquad \Phi^*(\mathbf{x}, t) = \int \frac{d^3k}{(2\pi)^3} \phi^*_{\mathbf{k}}(t) e^{-i\mathbf{k}\cdot\mathbf{x}} \tag{2.5}$$

with the conjugate momentum of the fields $\Phi(\mathbf{x}, t)$ and $\Phi^*(\mathbf{x}, t)$ decomposed as

$$\Pi(\mathbf{x}, t) = \dot{\Phi}^*(\mathbf{x}, t) = \int \frac{d^3k}{(2\pi)^3} \dot{\phi}^*_{\mathbf{k}}(t) e^{-i\mathbf{k}\cdot\mathbf{x}} = \int \frac{d^3k}{(2\pi)^3} \pi_{\mathbf{k}}(t) e^{-i\mathbf{k}\cdot\mathbf{x}} \tag{2.6}$$

$$\Pi^*(\mathbf{x}, t) = \dot{\Phi}(\mathbf{x}, t) = \int \frac{d^3k}{(2\pi)^3} \dot{\phi}_{\mathbf{k}}(t) e^{i\mathbf{k}\cdot\mathbf{x}} = \int \frac{d^3k}{(2\pi)^3} \pi^*_{\mathbf{k}}(t) e^{i\mathbf{k}\cdot\mathbf{x}} \tag{2.7}$$

The fields satisfy the equal-time commutation relations

$$[\Phi(\mathbf{x}, t)\, ,\, \Pi(\mathbf{y}, t)] = i\delta^{(3)}(\mathbf{x} - \mathbf{y}) \tag{2.8}$$

$$[\Phi^*(\mathbf{x}, t)\, ,\, \Pi^*(\mathbf{y}, t)] = i\delta^{(3)}(\mathbf{x} - \mathbf{y}) \tag{2.9}$$

with the mode decomposed fields satisfying

$$[\phi_{\mathbf{k}}(\mathbf{x}, t)\, ,\, \pi_{\mathbf{k}}(\mathbf{y}, t)] = i(2\pi)^3\delta^{(3)}(\mathbf{x} - \mathbf{y}) \tag{2.10}$$

$$[\phi^*_{\mathbf{k}}(\mathbf{x}, t)\, ,\, \pi^*_{\mathbf{k}}(\mathbf{y}, t)] = i(2\pi)^3\delta^{(3)}(\mathbf{x} - \mathbf{y}) \tag{2.11}$$

The spatial mode decomposition is made complete by introducing time-independent creation/annihilation operators $a_{\mathbf{k}}, b_{-\mathbf{k}}$ and the time-dependent, spatially homogenous, complex mode function $f_{\mathbf{k}}(t)$ as

$$\begin{aligned}\phi_{\mathbf{k}}(t) &= f_{\mathbf{k}}(t)a_{\mathbf{k}} + f^*_{\mathbf{k}}(t)b^\dagger_{-\mathbf{k}} \\ \pi_{\mathbf{k}}(t) &= \dot{f}^*_{\mathbf{k}}(t)a^\dagger_{\mathbf{k}} + \dot{f}_{\mathbf{k}}(t)b_{-\mathbf{k}}\end{aligned} \tag{2.12}$$

where Bosonic commutation relations,

$$\left[a_{\mathbf{k}}\, ,\, a^\dagger_{\mathbf{k}'}\right] = (2\pi)^3\delta^{(3)}(\mathbf{k}-\mathbf{k}') \tag{2.13}$$

$$\left[b_{-\mathbf{k}}\, ,\, b^\dagger_{-\mathbf{k}'}\right] = (2\pi)^3\delta^{(3)}(\mathbf{k}-\mathbf{k}') \quad , \tag{2.14}$$

impose the Wronskian condition on the mode functions $f_k(t)$ as

$$\mathrm{Wr}[f_k(t), f^*_k(t)] \equiv f_k(t)\dot{f}^*_k(t) - \dot{f}_k(t)f^*_k(t) = i \tag{2.15}$$

The mode decomposition of the Klein-Gordon Equation (2.1) using (2.5) then reduces to a set of decoupled linear time-dependent oscillator equations spanned by the momenta k:

$$\ddot{f}_k(t) + \omega_k^2(t)f_k(t) = 0 \tag{2.16}$$

Here, the effective time-dependent frequency $\omega_k(t)$ is [47–49,53]

$$\omega_k(t) = \sqrt{m^2 + p_\perp^2 + (k_\parallel - A_\parallel(t))^2} \tag{2.17}$$

where $k_\perp$ and $k_\parallel$, respectively, denotes the momenta of the produced particles transverse and longitudinal to the direction of the electric field. The magnitude of the electric field varies with time as $E_{\parallel}(t) = -\dot{A}_{\parallel}(t)$. As shown in Chapter 3, an analogous mode decomposition exists for particle production in spinor QED (see Appendix A) and cosmological de Sitter gravitational backgrounds [6–8,12–14,20,21].

2.2.3 Equivalent Representations of the Klein-Gordon Equation

Writing the complex mode function $f_k(t)$ in terms of its real amplitude $\xi_k(t)$ and phase $\lambda_k(t)$,

$$f_k(t) = \xi_k(t) e^{-i\lambda_k(t)} \quad , \tag{2.18}$$

the Klein-Gordon equation (2.16) reduces to the Ermakov-Milne [78–82] equation for the amplitude function $\xi_k(t)$:

$$\ddot{\xi}_k(t) + \omega_k^2(t)\xi_k(t) - \frac{1}{4\xi^3(t)} = 0 \tag{2.19}$$

Unitarity determines the time-dependent phase $\lambda_k(t)$ in terms of $\xi_k(t)$ as

$$\lambda_k(t) = \int^t \frac{dt}{2\xi_k^2(t)} \tag{2.20}$$

Note that with the definition (2.18), the Ermakov-Milne equations (2.19,2.20) are completely equivalent to the original Klein-Gordon equation (2.16).

Another equivalent way to express the time-evolution is achieved by defining the square of the amplitude function, $G_k(t) = \xi_k^2(t)$, which satisfies a nonlinear second-order equation, and its corresponding linear third-order equation:

$$2G_k\ddot{G}_k - \dot{G}_k^2 + 4\omega_k^2(t)G_k^2 = 1 \tag{2.21}$$

$$\dddot{G}_k + 4\omega_k^2(t)\dot{G}_k + 4\omega_k(t)\dot{\omega}_k(t)G_k = 0 \tag{2.22}$$

This is known as the Gel‘fand-Dikii equation [83,84], arising in the analysis of the resolvent Green function for Schrödinger operators, which can be written in terms of products of solutions to the Klein-Gordon equation (2.16). The resolvent approach has been used in the analysis of Schwinger effect [85,86].

2.2.4 Particle Production as a Scattering Problem

The particle production problem consists of the following physical situation: at initial time the vacuum is defined with respect to the (time-independent) creation and annihilation operators in (2.12). Then as time evolves the vacuum is subjected to a time-dependent electric field, which turns off again as $t \to +\infty$. At $t = +\infty$, after the electric field has been turned off, the production of particles from vacuum can be inferred from the fraction of negative frequency modes in the evolved mode functions. As is well known [47–49,67,68], this can be expressed as an "over-the-barrier" quantum mechanical scattering problem, in the time domain, by interpreting the Klein-Gordon equation (2.16) as a Schrödinger-like equation

$$-\ddot{f}_k(t) - \left(k_\parallel - A_\parallel(t)\right)^2 f_k(t) = \left(m^2 + k_\perp^2\right) f_k(t) \tag{2.23}$$

with physical “scattering” boundary conditions [47–52]:

$$f_k(t) \sim \begin{cases} \frac{1}{\sqrt{2\omega_k(-\infty)}} e^{-i\omega_k(-\infty)t} & , \quad t \to -\infty \\ \frac{1}{\sqrt{2\omega_k(+\infty)}} \left(A_k e^{-i\omega_k(+\infty)t} + B_k e^{i\omega_k(+\infty)t} \right) & , \quad t \to +\infty \end{cases} \tag{2.24}$$

The scattering coefficients A_k and B_k defined asymptotically at $t = +\infty$ satisfy $|A_k|^2 - |B_k|^2 = 1$. Thus, we can evolve the mode oscillator equation (2.16) with the initial boundary conditions

$$\begin{aligned} f_k(t \to -\infty) &\sim \frac{1}{\sqrt{2\omega_k(-\infty)}} e^{-i\omega_k(-\infty)t} \\ \dot{f}_k(t \to -\infty) &\sim -i\sqrt{\frac{\omega_k(-\infty)}{2}} e^{-i\omega_k(-\infty)t} \end{aligned} \tag{2.25}$$

or, equivalently the Ermakov-Milne equation (2.19) with initial conditions

$$\begin{aligned} \xi_k(t \to -\infty) &= \frac{1}{\sqrt{2\omega_k(-\infty)}} \\ \dot{\xi}_k(t \to -\infty) &= 0 \end{aligned} \tag{2.26}$$

A numerical advantage of the Ermakov-Milne equation is that the amplitude function $\xi_k(t)$ typically varies more smoothly than the mode function $f_k(t)$ [and recall from (2.20) that the phase $\lambda_k(t)$ is determined by $\xi_k(t)$]. This is illustrated in Figure 2.1, for an explicit example of a single-pulse electric field, for which a well-known analytic exact solution is possible, as reviewed in Appendix B. Note the smoothness of $\xi_k(t)$, with small oscillations about the final asymptotic value $1/\sqrt{2\omega_k(+\infty)}$ shown in the left inset figure. As shown in Section 2.13, these small oscillations encode the particle production phenomenon.

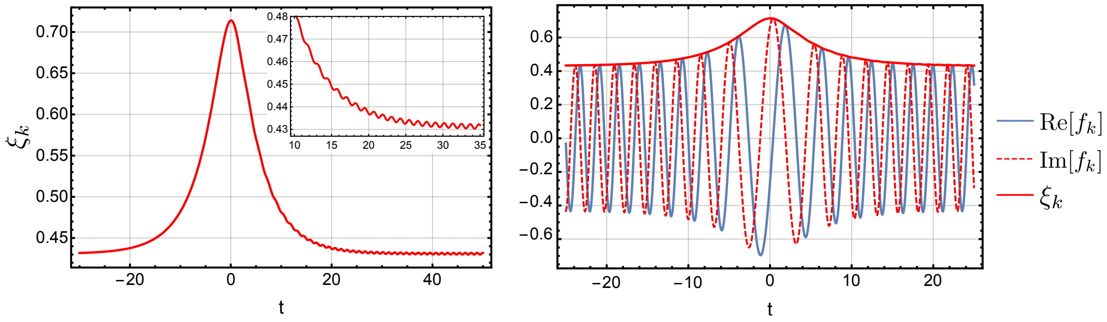

Fig. 2.1: Plots of $\xi_k(t)$ (left), and the real (blue-solid line) and imaginary (red-dashed line) parts of f_k (right), abiding the scattering conditions (2.24), for a single-pulse E-field: $E(t) = E_0 \text{sech}^2(at)$, with $E_0 = 0.25$, $a = 0.1$, $k_\parallel = 0$, and $k_\perp = 0$, all in units with $m = 1$. For this case, both f_k and ξ_k can be obtained analytically (Appendix B), and ξ_k is plotted as a solid-red line in each subplot for comparison.

2.3 Bogoliubov Approach to Adiabatic Particle Number

In processes that involve a time-dependent background field, a unique separation into positive and negative energy states with which to identify particles and antiparticles is only possible at asymptotic times [47–49], when the electric field is turned off. This is the same as the non-uniqueness of defining left- and right-moving modes inside an inhomogeneous dielectric medium [87,88].

To proceed, we define a time-dependent adiabatic particle number in the presence of a slowly varying time-dependent background, with respect to a particular set of reference mode functions $\tilde{f}_k(t)$ defined as

$$\tilde{f}_k(t) \equiv \frac{1}{\sqrt{2W_k}} e^{-i\int^t W_k(t)} \xrightarrow{t\to-\infty} \frac{1}{\sqrt{2\omega_k(-\infty)}} e^{-i\omega_k(-\infty)t} \tag{2.27}$$

Clearly there is an infinite number of such reference mode functions, all having the same initial asymptotic behavior. This is related to needing to specify also the initial time derivative [see also Eq. (2.33) below]. The problem is to define a physically suitable set of mode functions for use at intermediate times.

Insisting that $\tilde{f}_k(t)$, as defined in (2.27), be a solution to the Klein-Gordon equation (2.16), the function $W_k(t)$ is related to the effective frequency $\omega_k(t)$ by the well-known Schwarzian derivative form:

$$W_k^2(t) = \omega_k^2(t) - \left[\frac{\ddot{W}_k}{2W_k(t)} - \frac{3}{4}\left(\frac{\dot{W}_k}{W_k}\right)^2\right] \tag{2.28}$$

This can be solved by a systematic adiabatic expansion in which the leading order is the standard leading WKB solution to the mode oscillator equation (2.16) of the form $W_k^{(0)}(t) = \omega_k(t)$ [64–66]. Higher order terms are analyzed in detail in Section 2.8.

The Bogoliubov Transformation is a linear canonical transformation that defines a set of time-dependent creation and annihilation operators, $\tilde{a}_k(t)$ and $\tilde{b}_k^\dagger(t)$, from the original time-independent operators, a_k and $b_k^\dagger$, defined at the initial time in (2.12) [48,49]. They are related by

$$\begin{pmatrix} \tilde{a}_k(t) \\ \tilde{b}^\dagger_{-k}(t) \end{pmatrix} = \begin{pmatrix} \alpha_k(t) & \beta_k^*(t) \\ \beta_k(t) & \alpha_k^*(t) \end{pmatrix} \begin{pmatrix} a_k \\ b^\dagger_{-k} \end{pmatrix} \tag{2.29}$$

where unitarity requires $|\alpha_k(t)|^2 - |\beta_k|^2 = 1$ for scalar fields, for all t. As a result of the Bogoliubov transformation, the equivalent decomposition of the scalar field operator in terms of these reference mode functions is

$$\phi_k(t) = \tilde{f}_k(t)\tilde{a}_k(t) + \tilde{f}_k^*(t)\tilde{b}^\dagger_{-k}(t) \tag{2.30}$$

This can also be interpreted as a linear transformation between the exact mode functions $f_k(t)$ and the reference adiabatic mode functions $\tilde{f}_k(t)$, as

$$f_k(t) = \alpha_k(t)\tilde{f}_k(t) + \beta_k(t)\tilde{f}_k^*(t) \tag{2.31}$$

The transformation of the scalar field momentum operator $\pi_k^\dagger = \dot{\phi}(t)$:

$$\pi_k^\dagger(t) = Q_k(t)\tilde{f}_k(t)\tilde{a}_k(t) + Q_k^*(t)\tilde{f}_k^*(t)\tilde{b}_{-k}^\dagger(t) \tag{2.32}$$

with a corresponding decomposition of the first derivative

$$\dot{f}_k(t) = Q_k(t)\alpha_k(t)\tilde{f}_k(t) + Q_k^*(t)\beta_k(t)\tilde{f}_k^*(t) \tag{2.33}$$

Here $Q_k(t)$ is defined as

$$Q_k(t) \equiv -iW_k(t) + V_k(t) \tag{2.34}$$

The inclusion of the real time-dependent function $V_k(t)$, specified later, in the decompositions (2.31) and (2.33) represents the most general decomposition of the exact solution $f_k(t)$ that is consistent with unitarity (the preservation of the bosonic commutation relations, or equivalently the Wronskian condition (2.15)). This can also be understood technically by the fact that in (2.31) we trade one complex function $f_k(t)$ for two complex coefficient functions: $\alpha_k(t)$ and $\beta_k(t)$. Physically, the freedom in the choice of $W_k(t)$ and $V_k(t)$ encodes the arbitrariness of specifying positive and negative energy states at intermediate times. We will see later that a 'natural' choice is $V_k(t) = -\dot{W}_k/(2W_k)$, coming from the derivative of the $1/\sqrt{2W_k(t)}$ factor in the definition of the reference mode functions (2.27).

The scattering coefficients in (2.24) are realized as the Bogoliubov coefficients evaluated at asymptotically late time, after the perturbation has turned off: $A_k = \alpha_k(+\infty)$ and $B_k = \beta_k(+\infty)$. The time-dependent adiabatic particle number, for each mode k, is defined as the expectation value of the time-dependent number operator $\tilde{a}_k^\dagger(t)\tilde{a}_k(t)$ with respect to the asymptotic vacuum state. Assuming no particles are initially present, the time-dependent adiabatic particle number is

$$\tilde{\mathcal{N}}_k(t) \equiv \left\langle \tilde{a}_k^\dagger(t)\tilde{a}_k(t) \right\rangle = |\beta_k(t)|^2 \tag{2.35}$$

This reduces the problem to the direct evaluation of the time evolution of the Bogoliubov transformation parameters $\alpha_k(t)$ and $\beta_k(t)$. The decompositions (2.31) and (2.33) are exact provided they satisfy the mode oscillator equation (2.16), which implies the following evolution equations for the Bogoliubov transformation parameters $\alpha_k(t)$ and $\beta_k(t)$:

$$\begin{pmatrix} \dot{\alpha}_k(t) \\ \dot{\beta}_k(t) \end{pmatrix} = \begin{pmatrix} \delta_k(t) & [\delta_k(t) + \Delta_k(t)]\, e^{2i\int^t W_k} \\ [\delta_k^*(t) + \Delta_k(t)]\, e^{-2i\int^t W_k} & \delta_k^*(t) \end{pmatrix} \begin{pmatrix} \alpha_k(t) \\ \beta_k(t) \end{pmatrix} \tag{2.36}$$

where

$$\delta_k(t) = \frac{1}{2iW_k}\left(\omega_k^2(t) - W_k^2(t) + \left(\dot{V}_k(t) + V_k^2(t)\right)\right) \tag{2.37}$$

$$\Delta_k(t) = \frac{\dot{W}_k(t)}{2W_k(t)} + V_k(t) \tag{2.38}$$

Note that $\delta_k(t)$ vanishes with the choice $V_k(t) = -\dot{W}_k/(2W_k)$. The numerical evaluation of this coupled differential equation completely determines the time evolution of $\alpha_k(t)$ and $\beta_k(t)$ with respect to the basis (W_k, V_k). The time evolution of the adiabatic particle number $\tilde{\mathcal{N}}_k(t)$ is obtained by the modulus squared of the time evolution of the Bogoliubov coefficient following (2.36), solved using the initial conditions $\alpha_k(-\infty) = 1$ and $\beta_k(-\infty) = 0$, consistent with the scattering scenario in (2.24) and the assumption of no particles being initially present. The evolution equations (2.36) are dependent on the choice made for the basis functions $W_k(t)$ and $V_k(t)$, which influences the time evolution of the adiabatic particle number at intermediate times but does not affect its final asymptotic value at future infinity, $|B_k|^2$ [54]. This is because the final value is determined by the global information of the Stokes phenomenon [67,68].

The time evolution of the coefficients $\alpha_k(t)$ and $\beta_k(t)$ can also be expressed directly through the time evolution of the amplitude $\xi_k(t)$ via the Wronskian of the exact (2.18) and reference mode function (2.27). Solving the linear equations (2.31) and (2.33) we find

$$\alpha_k(t) = -i\mathrm{Wr}\Big[f_k(t), \tilde{f}_k^*(t)\Big] = i\tilde{f}_k^*(t)\left(\dot{f}_k(t) - Q_k^*(t)f_k(t)\right) \tag{2.39}$$

$$\beta_k(t) = i\mathrm{Wr}\Big[f_k(t), \tilde{f}_k(t)\Big] = -i\tilde{f}_k(t)\left(\dot{f}_k(t) - Q_k(t)f_k(t)\right) \tag{2.40}$$

Furthermore, from (2.18) and its time-dependent phase (2.20). we find the identity

$$\frac{\dot{f}_k(t)}{f_k(t)} = \frac{\dot{\xi}_k(t)}{\xi_k(t)} - \frac{i}{2\xi_k^2(t)} \quad , \tag{2.41}$$

Thus, the Bogoliubov coefficients may be rewritten in the uncoupled form as

$$\alpha_k(t) = \frac{\xi_k}{\sqrt{2W_k}} \left[\left(\frac{1}{2\xi_k^2} + W_k \right) + i \left(\frac{\dot{\xi}_k}{\xi_k} - V_k \right) \right] e^{-i \int^t \left(\frac{1}{2\xi_k^2} - W_k \right)} \tag{2.42}$$

$$\beta_k(t) = -\frac{\xi_k}{\sqrt{2W_k}} \left[\left(\frac{1}{2\xi_k^2} - W_k \right) + i \left(\frac{\dot{\xi}_k}{\xi_k} - V_k \right) \right] e^{-i \int^t \left(\frac{1}{2\xi_k^2} + W_k \right)} \tag{2.43}$$

This expresses the time evolution of the Bogoliubov coefficients as a comparison between the time evolution of the amplitude function, $\xi_k(t)$, obtained by solving the Ermakov-Milne equation (2.19), and the reference mode basis (W_k, V_k). The Adiabatic Particle Number then follows as

$$|\alpha_k(t)|^2 = \frac{\xi_k^2}{2W_k} \left[\left(\frac{1}{2\xi_k^2} + W_k \right)^2 + \left(\frac{\dot{\xi}_k}{\xi_k} - V_k \right)^2 \right] \tag{2.44}$$

$$\tilde{\mathcal{N}}_k(t) \equiv |\beta_k(t)|^2 = \frac{\xi_k^2}{2W_k} \left[\left(\frac{1}{2\xi_k^2} - W_k \right)^2 + \left(\frac{\dot{\xi}_k}{\xi_k} - V_k \right)^2 \right] \tag{2.45}$$

It is straightforward to confirm that unitarity is preserved: $|\alpha_k(t)|^2 - |\beta_k(t)|^2 = 1$.

The form of (2.45) emphasizes clearly the dependence of the adiabatic particle number on the basis choice of reference mode functions (W_k, V_k). It is not enough to know the time evolution of $\xi_k(t)$: one must also compare it to the reference functions. With the choice $V_k = -\dot{W}_k/(2W_k)$, the expression for the adiabatic particle number simplifies further to a direct comparison between $\xi_k(t)$ and $W_k(t)$:

$$\tilde{\mathcal{N}}_k(t) = \frac{\xi_k^2}{2W_k} \left[\left(\frac{1}{2\xi_k^2} - W_k \right)^2 + \left(\frac{\dot{\xi}_k}{\xi_k} + \frac{\dot{W}_k}{2W_k} \right)^2 \right] \tag{2.46}$$

In subsequent sub-sections we show how exactly the same expression arises in other different but equivalent, methods for defining and computing the adiabatic particle number. In later sections we illustrate the adiabatic particle number with different electric field configurations, and then in Section 2.13 we show how in the adiabatic expansion in the expression (2.46) can be viewed as a measure of the tiny deviations between the exact solution $\xi_k(t)$ of the Ermakov-Milne equation and various orders of the adiabatic approximation for $W_k(t)$.

2.4 Reflection Amplitude Approach to Adiabatic Particle Number

The time evolution of the Bogoliubov coefficients can be re-expressed in Riccati form by defining the ratio [48,49,67,68]

$$R_k(t) \equiv \frac{\beta_k(t)}{\alpha_k(t)} \tag{2.47}$$

which can be viewed as a local (in time) reflection amplitude for this Schrödinger-like equation (2.23) [48,49,47]. Using the unitarity condition, $|\alpha_k(t)|^2 - |\beta_k(t)|^2 = 1$, the time-dependent adiabatic particle can be rewritten as

$$\tilde{\mathcal{N}}_k(t) = \frac{|R_k(t)|^2}{1 - |R_k(t)|^2} \tag{2.48}$$

In the semi-classical limit in which m is the dominant scale (as is relevant in QED), this over-the-barrier scattering problem has an exponentially small reflection probability, which implies that the adiabatic particle number is well approximated by $\tilde{\mathcal{N}}_k(t) \simeq |R_k(t)|^2$.

Using (2.47), the Bogoliubov coefficient evolution equations (2.36), with the basis (W_k, V_k), become a Riccati equation:

$$\dot{R}_k = (\Delta_k - \delta_k)\, e^{-2i\int^t W_k} - 2\delta_k R_k - (\Delta_k + \delta_k)\, e^{2i\int^t W_k} R_k^2 \tag{2.49}$$

with $\delta_k(t)$ and $\Delta_k(t)$ defined by equations (2.37, 2.38). This is straightforward to evaluate numerically with the initial conditions $R_k(-\infty) = 0$, and an initial phase of zero. It can also be solved semi-classically for $R_k(+\infty)$, thereby yielding the final particle number $\tilde{\mathcal{N}}_k(+\infty)$, using complex turning points and the Stokes phenomenon [67,68].

Alternatively, using the forms calculated previously for $\alpha_k(t)$ and $\beta_k(t)$, equations (2.42,2.43), we obtain an analytic representation of the reflection probability as

$$|R_k(t)|^2 = \frac{\left(\frac{1}{2\xi_k^2} - W_k\right)^2 + \left(\frac{\dot{\xi}_k}{\xi_k} - V_k\right)^2}{\left(\frac{1}{2\xi_k^2} + W_k\right)^2 + \left(\frac{\dot{\xi}_k}{\xi_k} - V_k\right)^2} \tag{2.50}$$

Expression (2.48) for the adiabatic particle number then yields

$$\tilde{\mathcal{N}}_k(t) = \frac{\xi_k^2}{2W_k}\left[\left(\frac{1}{2\xi_k^2} - W_k\right)^2 + \left(\frac{\dot{\xi}_k}{\xi_k} - V_k\right)^2\right] \tag{2.51}$$

confirming the consistency with the Bogoliubov transformation expression (2.45).

2.5 Wigner Approach to Adiabatic Particle Number

Another physically interesting formalism to describe particle production at intermediate times is to define the time-dependent adiabatic particle number through the use of Spectral Functions [70,69], which are constructed in terms of correlation functions of the time-dependent creation and annihilation operators (2.12) used in (2.46). In this Section we show how the basis dependence arises in this formalism.

The Spectral Approach defines the adiabatic particle number through unequal time correlators of time-dependent creation and annihilation operators, in a limit that recovers the equal-time adiabatic particle number:

$$\tilde{\mathcal{N}}_k(t) = \lim_{t_1,t_2\to t} \left\langle \tilde{a}_k^\dagger(t_1)\tilde{a}_k(t_2)\right\rangle \tag{2.52}$$

Using (2.12), the time-dependent creation and annihilation operators can be written in terms of the decomposed field operators as

$$\tilde{a}_k(t) = i\tilde{f}_k^*(t)\left[\partial_0 - Q_k^*(t)\right]\phi_k(t) \tag{2.53}$$

$$\tilde{b}_{-k}^\dagger(t) = -i\tilde{f}_k(t)\left[\partial_0 - Q_k(t)\right]\phi_k(t) \tag{2.54}$$

which match smoothly to the initial creation and annihilation operators. Note the dependence on the choice of basis $(W_k(t), V_k(t))$, through the function $Q_k(t) \equiv -iW_k(t) + V_k(t)$, defined in (2.34). We thus obtain

$$\tilde{\mathcal{N}}_k(t) = \frac{1}{2W_k(t)} \lim_{t_1,t_2\to t}\left(\left[\partial_1 - Q_k(t_1)\right]\left[\partial_2 - Q_k^*(t_2)\right]\right)\left\langle \phi_k^\dagger(t_1)\phi_k(t_2)\right\rangle \quad , \tag{2.55}$$

where ∂_j denotes a derivative with respect to time t_j. This expression shows a clear separation between the computation of the correlation function $\left\langle \phi_k^\dagger(t_1)\phi_k(t_2)\right\rangle$, and the projection onto a set of reference modes, characterized by $Q_k(t)$ in (2.34). In [70,69] a particular basis choice was made, $W_k = \omega_k$ and $V_k = 0$, corresponding to a leading-order adiabatic expansion and a particular phase choice via V_k. (2.55) makes it clear that this is just one of an infinite set of possible choices, for which the final particle number at late asymptotic time is always the same, but for which the particle number at intermediate times can be very different.

Spatially homogeneous time-dependent external electric fields decouple the modes k allowing the spectral functions, the Wigner transformed Pauli-Jordan function $\mathcal{A}_k(t,k_0)$ and Hadamard function $\mathcal{D}_k(t,k_0)$, to be expressed as [70,69]

$$\mathcal{A}_k(t,k_0) = \frac{1}{\mathcal{V}}\int dT\, e^{ik_0T}\left\langle\left[\phi_k\left(t+\tfrac{T}{2}\right),\phi_k^\dagger\left(t-\tfrac{T}{2}\right)\right]\right\rangle \tag{2.56}$$

$$\mathcal{D}_k(t,k_0) = \frac{1}{\mathcal{V}}\int dT\, e^{ik_0T}\left\langle\left\{\phi_k\left(t+\tfrac{T}{2}\right),\phi_k^\dagger\left(t-\tfrac{T}{2}\right)\right\}\right\rangle \tag{2.57}$$

with the conjugate variable pair being the energy k_0 and the time separation T. The spatial volume is denoted by $\mathcal{V}$.

The correlation function in (2.55) can be expressed through a linear combination of the inverse Wigner transformed functions (2.56, 2.57) as

$$\begin{aligned}\left\langle\phi_k^\dagger\left(t-\tfrac{T}{2}\right)\phi_k\left(t+\tfrac{T}{2}\right)\right\rangle &= \frac{\mathcal{V}}{2}\int\frac{dk_0}{2\pi}e^{-ik_0T}\mathcal{W}_k(t,k_0) & (2.58)\\ &= \frac{\mathcal{V}}{2}\int\frac{dk_0}{2\pi}e^{-ik_0T}\left(\mathcal{D}_k(t,k_0)-\mathcal{A}_k(t,k_0)\right) & (2.59)\end{aligned}$$

where the total spectral function is defined as $\mathcal{W}_k(t,k_0)\equiv\mathcal{D}_k(t,k_0)-\mathcal{A}_k(t,k_0)$. Inserting this expression into (2.55), and taking the limit, yields an expression for the time-dependent adiabatic particle number in terms of the transformed correlation function as

$$\tilde{\mathcal{N}}_k(t) = \frac{\mathcal{V}}{4W_k}\int\frac{dk_0}{2\pi}\left[\frac{1}{4}\partial_t^2 - V_k\partial_t + (W_k+k_0)^2 + V_k^2\right]\mathcal{W}_k(t,k_0) \tag{2.60}$$

This expression (2.60) is the natural extension of Fukushima's result [70,69], which employed the leading adiabatic approximation choice of basis functions as $W_k(t) = \omega_k(t)$ and $V_k(t) = 0$, to a general basis specified by $W_k(t)$ and $V_k(t)$.

It is important to appreciate that the spectral function $\mathcal{W}_k(t, k_0)$ in (2.60) can be expressed directly in terms of the solutions to the Klein-Gordon equation or the Ermakov-Milne equation, without reference to the reference mode basis functions. Assuming no particles are initially present in the vacuum, the expectation value of the field operator commutator and anti-commutator are

$$\left\langle\left[\phi_k\left(t+\tfrac{T}{2}\right), \phi_k^\dagger\left(t-\tfrac{T}{2}\right)\right]\right\rangle = f_k\left(t+\tfrac{T}{2}\right) f_k^*\left(t-\tfrac{T}{2}\right) - f_k^*\left(t+\tfrac{T}{2}\right) f_k\left(t-\tfrac{T}{2}\right) \tag{2.61}$$

$$\left\langle\left\{\phi_k\left(t+\tfrac{T}{2}\right), \phi_k^\dagger\left(t-\tfrac{T}{2}\right)\right\}\right\rangle = f_k\left(t+\tfrac{T}{2}\right) f_k^*\left(t-\tfrac{T}{2}\right) + f_k^*\left(t+\tfrac{T}{2}\right) f_k\left(t-\tfrac{T}{2}\right) \tag{2.62}$$

Therefore, the spectral function $\mathcal{W}_k(t, k_0)$ assumes the form

$$\mathcal{W}_k(t, k_0) = \frac{2}{\mathcal{V}} \int dT\, e^{ik_0 T} f_k\left(t-\tfrac{T}{2}\right) f_k^*\left(t+\tfrac{T}{2}\right) \tag{2.63}$$

Alternatively, this can be rewritten in terms of the amplitude function $\xi_k(t)$:

$$\mathcal{W}_k(t, k_0) = \frac{2}{\mathcal{V}} \int dT\, e^{ik_0 T} \xi_k\left(t-\tfrac{T}{2}\right) \xi_k\left(t+\tfrac{T}{2}\right) \exp\left[i \int_{t-T/2}^{t+T/2} \frac{dt'}{2\xi_k^2(t')}\right] \tag{2.64}$$

Thus, the spectral function $\mathcal{W}_k(t, k_0)$ is determined without any knowledge of the basis functions $(W_k(t), V_k(t))$ and is exact provided that integration is performed over all possible values of the separation T. The behavior of the spectral function (2.64) is shown in Figure 2.2 for the soluble case of a single-pulse electric field (see Appendix B), integrated over a finite range $T = -T_0$ to $T = +T_0$, for

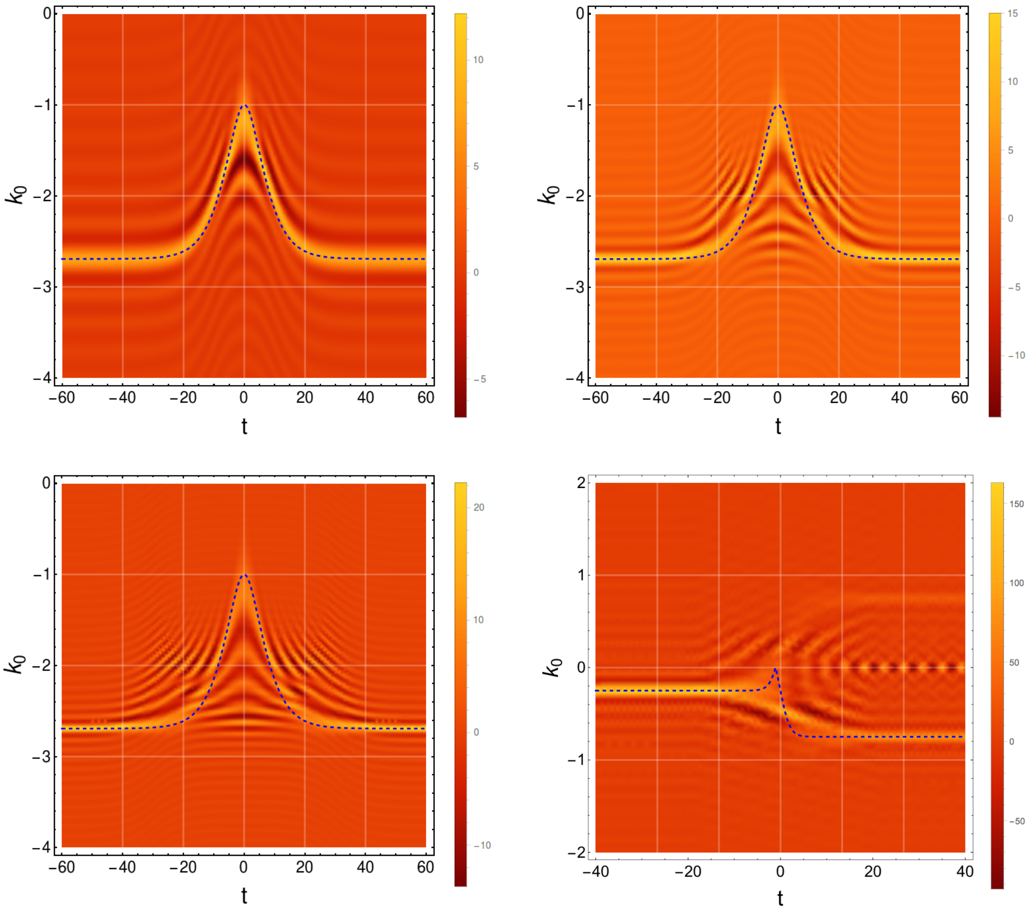

Fig. 2.2: Density plots of $\mathcal{W}_k(t, k_0)$ with respect to t, and k_0, for a single-pulse E-field given by $E(t) = E_0 \text{sech}^2(at)$, obtained by numerically evaluating equation (2.64) over $T \in (-T_0, +T_0)$, utilizing the exact solution $\xi_k(t)$ (see Appendix B). The upper left, upper right and lower left subplots are plotted with $E_0 = 0.25, a = 0.1$, $k_\parallel = 0.25$, and $k_\perp = 0$, in units with $m = 1$, with the upper left plot integrated with $T_0 = 20$, the upper right plot integrated with $T_0 = 40$, and the lower left subplot integrated with $T_0 = 60$. The lower right subplot is plotted for the physically unrealistic case with $m = 0, E_0 = 0.5, k_\parallel = 0.25, k_\perp = 0$, and integrated with $T_0 = 40$. In each subplot, $\mathcal{W}_k(t, k_0)$ is well matched by $-\omega_k(t)$ (2.17) (blue-dashed line), artificially plotted over each density subplot.

various values of the cutoff T_0. The two upper subplots and the lower left subplots in Figure 2.2 are plotted for the case when $E_0 = 0.25, a = 0.1, k_\perp = k_\parallel = 0$, in units with $m = 1$, with the upper left plot integrated with $T_0 = 20$, the upper right plot integrated with $T_0 = 40$, and the lower left plot integrated with $T_0 = 60$. The lower right plot was plotted with the parameters used in [70], with $m = 0, E_0 = 0.5, k_\parallel = 0.25, k_\perp = 0$ and integration with $T_0 = 40$. In each subplot of Figure 2.2, the dominant features of $\mathcal{W}_k(t, k_0)$ (2.64) are well approximated by the negative effective frequency $-\omega_k(t)$, plotted with a blue-dashed line, which demonstrates that the spectral function $\mathcal{W}_k(t, k_0)$ represents the projection of the fundamental frequency on a plane spanned by time and the conjugate energy variable k_0. Furthermore, we see that the oscillating features of the spectral function decrease as $T_0 \to \infty$. Lastly, we compared the results obtained in [70], calculated by numerically evaluating the mode function $f_k(t)$ and the subsequent integral in (2.64), with the exact solution to the mode-oscillator equation (see Appendix B), which indicates that the numerical approach suffers from sensitive numerical instabilities in the evaluation of (2.64) and the mode function $f_k(t)$.

We next show how the expression for the time-dependent adiabatic particle number that was previously derived in the Bogoliubov (2.45) and Riccati formalisms (2.51) is obtained in the Spectral Representation formalism. From equation (2.60), and using the spectral function (2.63), the expression is recovered by first re-writing the derivatives in terms of t, and reorganizing the resulting terms via integration by parts to eliminate, apart from the exponential term $e^{ik_0 T}$, the k_0 dependence in the integrand. The k_0 integration produces a Dirac Delta function which, when integrated over T, eliminates all integrations. Two terms appear: one corresponding directly to the adiabatic particle number, and the other to a surface boundary term. Recast in terms of ξ_k using the identity (2.41), this lengthy but straightforward calculation leads to an expression for the time-dependent adiabatic particle number (2.60) as

$$\tilde{\mathcal{N}_k}(t) = \frac{\xi_k^2}{2W_k}\left[\left(\frac{1}{2\xi_k^2} - W_k\right)^2 + \left(\frac{\dot{\xi}_k}{\xi_k} - V_k\right)^2\right] \tag{2.65}$$

noting that the total surface boundary term vanishes when $T_0 \to \infty$. This agrees precisely with the Bogoliubov and Riccati expressions in (2.45). We see again that the adiabatic particle number is basis dependent at intermediate times, through the choice of the W_k and V_k functions. As before, ξ_k is solved exactly without any knowledge of the basis functions, and the selected basis functions are inserted into the expression (2.55) to determine the adiabatic particle number with respect to that basis. In the spectral function approach this follows because the spectral function (2.64) is determined once and for all by the solution $\xi_k(t)$, and then the basis-dependent particle number is obtained by the transform in (2.60).

2.6 Schrödinger Picture Approach to Adiabatic Particle Number

Another common way to define adiabatic particle number is through the solution to the time-dependent oscillator problem, for each momentum mode k

[20–23,48,49,89]. We consider Schwinger vacuum pair production via the Schrödinger Picture time evolution of an infinite collection of time-dependent quantum harmonic oscillators, in the presence of a time-dependent background. The sQED hamiltonian becomes

$$\hat{H}(t) = \sum_k \left(\frac{1}{2} p_k^2 + \frac{1}{2} \omega_k^2(t) q_k^2 \right) \tag{2.66}$$

where k labels each independent spatial momentum mode, and the field operators map to their quantum mechanical counterparts as $\phi_k \to q_k$ and $\pi_k \to p_k$. The exact solution of the corresponding time-dependent Schrödinger equation can be written as [89–94]

$$\psi(q_k, t) = \sum_n c_{n,k} \, \psi_n(q_k, t) \tag{2.67}$$

where

$$\psi_n(q_k, t) = \frac{1}{\sqrt{2^n n!}} \left(\frac{1}{2\pi \xi_k^2(t)} \right)^{1/4} e^{-\frac{1}{2}\Omega_k(t) q_k^2} H_n\left(\frac{q_k}{\sqrt{2}\xi_k(t)} \right) e^{-i(n+\frac{1}{2})\lambda_k(t)} \tag{2.68}$$

Here $\xi_k(t)$ is the solution to the Ermakov-Milne equation (2.19), $\lambda_k(t)$ is defined by (2.20), and the time-dependent function $\Omega_k(t)$ in the Gaussian factor is defined as

$$\Omega_k(t) = -i \frac{\dot{\xi}_k}{\xi_k} + \frac{1}{2\xi_k^2} \quad . \tag{2.69}$$

These $\psi_n(q_k, t)$ are normalized eigenfunctions of the exact invariant operator

$$\hat{I}_k(t) = q_k^2 \left(\dot{\xi}_k^2 + \frac{1}{4\xi_k^2} \right) + \xi_k^2 p_k^2 - \xi_k \, \dot{\xi}_k \left(p_k q_k + q_k p_k \right) \tag{2.70}$$

satisfying

$$\frac{\partial \hat{I}_k}{\partial t} + i\,[\hat{H}, \hat{I}_k] = 0 \tag{2.71}$$

and

$$\hat{I}_k(t)\,\psi_n(q_k, t) = \left(n + \frac{1}{2}\right)\,\psi_n(q_k, t) \tag{2.72}$$

The function $\Omega_k(t)$ in (2.69) is directly related to the Riccati formalism of Section 2.4, and the mode decomposition of the operator q_k, the analog of the field (2.12), in the Heisenberg picture:

$$i\Omega_k(t) = \frac{\dot{\xi}_k}{\xi_k} + \frac{i}{2\xi_k^2} = \frac{\dot{f}_k^*}{f_k^*} = iW_k\left(\frac{1 - r_k^*}{1 + r_k^*}\right) + V_k \tag{2.73}$$

Here, $\xi_k(t)$ is again the solution to the Ermakov-Milne equation (2.19), $f_k(t)$ is the solution to the Klein-Gordon equation (2.16), and the function $r_k(t)$ is related to the reflection amplitude (2.47) by an extra phase:

$$r_k(t) = R_k(t)e^{2i\int^t W_k(t)} \tag{2.74}$$

Note that solving for $r_k^*(t)$ in (2.73) in terms of $\xi_k(t)$ leads directly to the analytical form (2.50) of the Riccati reflection probability.

We now define the adiabatic particle number by projecting these states onto a basis set of adiabatically evolving eigenstates of the time-dependent Hamiltonian. The most general expression for the adiabatically evolving eigenfunction $\zeta_n(q_k, t)$, motivated by the assumption of a slowly varying potential given by

$\omega_k(t)$, takes the form

$$\zeta_n(q_k,t) = \frac{1}{\sqrt{2^n n!}} \left(\frac{W_k(t)}{\pi}\right)^{1/4} e^{\frac{i}{2}Q_k^*(t)q_k^2} H_n\left(\sqrt{W_k(t)}q_k\right) e^{-i(n+\frac{1}{2})\int^t W_k(t)} \tag{2.75}$$

where $W_k(t)$ and $V_k(t)$ are basis functions, with the function $Q_k(t)$ defined as in (2.34).

At asymptotic early and late times, these adiabatic eigenfunctions reduce to well-defined stationary harmonic oscillator eigenfunctions

$$\begin{aligned} \zeta_n(q_k,t\to\pm\infty) \sim & \frac{1}{\sqrt{2^n n!}} \left(\frac{\omega_k(\pm\infty)}{\pi}\right)^{1/4} e^{-\frac{1}{2}\omega_k(\pm\infty)q_k^2} H_n\left(\sqrt{\omega_k(\pm\infty)}q_k\right) \\ & \times e^{-i(n+\frac{1}{2})\omega_k(\pm\infty)t} \end{aligned} \tag{2.76}$$

A state initially prepared at a particular time can evolve to become a superposition of a variety of states at a later time t. Assuming that the system is prepared in the m-th state at $t = -\infty$, the probability amplitude of making a transition to the n-th state is obtained by projecting the adiabatic eigenfunctions $\zeta_n(q_k,t)$ (2.76) onto the exact eigenfunction (2.68) for the m-th state $\psi_m(q_k,t)$, where $\psi_n(q_k,t) \sim \zeta_n(q_k,t)$. Using the integral solution in Appendix C, the amplitude for the transition then simplifies to

$$C_{nm,k}(t) = \int_{-\infty}^{+\infty} dq_k \, \zeta_n^*(q_k,t)\psi_m(q_k,t) \tag{2.77}$$

$$= \begin{cases} \dfrac{(-1)^{\frac{n}{2}}}{(\frac{n}{2})!(\frac{m}{2})!}\sqrt{\dfrac{n!m!}{2^{n+m}}}\left(\dfrac{2W_k}{\xi_k^2 J_{+,k}^2}\right)^{\frac{1}{4}}\left(\dfrac{J_{-,k}}{J_{+,k}}\right)^{\frac{n}{2}}\left(\dfrac{J_{-,k}^*}{J_{+,k}}\right)^{\frac{m}{2}} \cdot & \\ \qquad \cdot \, {}_2F_1\left[-\dfrac{m}{2}, -\dfrac{n}{2}, \dfrac{1}{2}, \dfrac{-2W_k}{\xi_k^2|J_{-,k}|^2}\right] e^{i(n+\frac{1}{2})\int^t W_k - i(m+\frac{1}{2})\lambda_k}, & \text{for} \quad m,n = \text{even} \\ \dfrac{(-1)^{\frac{n-1}{2}}}{(\frac{m-1}{2})!(\frac{n-1}{2})!}\sqrt{\dfrac{n!m!}{2^{n+m}}}\left(\dfrac{2W_k}{\xi_k^2 J_{+,k}^2}\right)^{\frac{3}{4}}\left(\dfrac{J_{-,k}}{J_{+,k}}\right)^{\frac{n-1}{2}}\left(\dfrac{J_{-,k}^*}{J_{+,k}}\right)^{\frac{m-1}{2}} \cdot & \\ \qquad \cdot \, {}_2F_1\left[\dfrac{1-m}{2}, \dfrac{1-n}{2}, \dfrac{3}{2}, \dfrac{-2W_k}{\xi_k^2|J_{-,k}|^2}\right] e^{i(n+\frac{1}{2})\int^t W_k - i(m+\frac{1}{2})\lambda_k}, & \text{for} \quad m,n = \text{odd} \\ 0\,, & \text{for} \quad m+n = \text{odd} \end{cases} \tag{2.78}$$

where the functions $J_{\pm,k}(t)$ are defined as

$$J_{\pm,k}(t) \equiv \left(\frac{1}{2\xi_k^2} \pm W_k\right) - i\left(\frac{\dot{\xi}_k}{\xi_k} - V_k\right) \tag{2.79}$$

and the following simplifications were used:

$$\frac{2W_k}{J_{+,k}} - 1 = -\frac{J_{-,k}}{J_{+,k}} \qquad\qquad \frac{1}{J_{+,k}\xi_k^2} - 1 = \frac{J_{-,k}^*}{J_{+,k}} \tag{2.80}$$

Across the different formalisms, its modulus squared is related to the Bogoliubov coefficients $\alpha_k(t)$ and $\beta_k(t)$, the Riccati reflection probability (2.50) and the adiabatic particle number (2.46) as

$$\frac{\xi_k^2}{2W_k}\,|J_{+,k}(t)|^2 = |\alpha_k(t)|^2 = \frac{1}{1-|R_k(t)|^2} = 1 + \tilde{\mathcal{N}}_k(t) \tag{2.81}$$

$$\frac{\xi_k^2}{2W_k}\,|J_{-,k}(t)|^2 = |\beta_k(t)|^2 = \frac{|R_k(t)|^2}{1-|R_k(t)|^2} = \tilde{\mathcal{N}}_k(t) \tag{2.82}$$

Thus the final form for the time-dependent transition probability from the m-th state to the n-th state can be expressed in terms of the adiabatic particle number $\tilde{\mathcal{N}}_k(t)$ (2.46), for instance, as

$$P_{nm,k}(t) = \left|C_{nm,k}(t)\right|^2 \tag{2.83}$$

$$= \begin{cases} \dfrac{n!m!}{2^{n+m}\left[(\frac{n}{2})!(\frac{m}{2})!\right]^2} \dfrac{1}{\sqrt{1+\tilde{\mathcal{N}}_k}} \left(\dfrac{\tilde{\mathcal{N}}_k}{1+\tilde{\mathcal{N}}_k}\right)^{\frac{n+m}{2}} {}_2F_1\left[-\dfrac{m}{2}, -\dfrac{n}{2}, \dfrac{1}{2}, -\dfrac{1}{\tilde{\mathcal{N}}_k}\right]^2, \\ \qquad\qquad\qquad\qquad\qquad\qquad\qquad\qquad \text{for} \quad m, n = \text{even} \\ \dfrac{n!m!}{2^{n+m}\left[(\frac{n-1}{2})!(\frac{m-1}{2})!\right]^2} \left(\dfrac{1}{1+\tilde{\mathcal{N}}_k}\right)^{\frac{3}{2}} \left(\dfrac{\tilde{\mathcal{N}}_k}{1+\tilde{\mathcal{N}}_k}\right)^{\frac{n+m-2}{2}} {}_2F_1\left[\dfrac{1-m}{2}, \dfrac{1-n}{2}, \dfrac{3}{2}, -\dfrac{1}{\tilde{\mathcal{N}}_k}\right]^2, \\ \qquad\qquad\qquad\qquad\qquad\qquad\qquad\qquad \text{for} \quad m, n = \text{odd} \\ 0\,, \qquad\qquad\qquad\qquad\qquad\qquad\qquad\qquad \text{for} \quad m+n = \text{odd} \end{cases} \tag{2.84}$$

For example, the time-dependent vacuum persistence probability, the probability of the system occupying the ground state at time t, is

$$P_{00,k}(t) = \sqrt{1-|R_k(t)|^2} = |\alpha_k(t)|^{-1} = \frac{1}{\sqrt{1+\tilde{\mathcal{N}}_k(t)}} \quad , \tag{2.85}$$

as expected.

The vacuum expectation value of the state occupation number for a system that adiabatically evolves from being initially prepared in the ground state at $t = -\infty$ is the weighted sum of the transition probabilities (2.84). Utilizing the

$\tilde{\mathcal{N}}_k$-representation for convenience, the sum simplifies to

$$\sum_{n=0,2,4,\ldots}^{\infty} n\,|C_{n0,k}(t)|^2 = \frac{1}{\sqrt{1+\tilde{\mathcal{N}}_k(t)}} \sum_{n=0,2,4,\ldots}^{\infty} \frac{n!}{2^n\left[(\frac{n}{2})!\right]^2}\left(\frac{\tilde{\mathcal{N}}_k(t)}{1+\tilde{\mathcal{N}}_k(t)}\right)^{\frac{n}{2}} \tag{2.86}$$

$$= \tilde{\mathcal{N}}_k(t) = \frac{\xi_k^2}{2W_k}\left[\left(\frac{1}{2\xi_k^2} - W_k\right)^2 + \left(\frac{\dot{\xi}_k}{\xi_k} - V_k\right)^2\right] \tag{2.87}$$

Thus, we find exactly the same expression as before, in the Bogoliubov, Riccati and Spectral Function approaches to adiabatic particle number. In the Schrödinger picture approach the basis dependence enters through the arbitrariness in (2.75) of specifying the adiabatic eigenstates $\zeta_n(q_k, t)$ of the time-dependent Hamiltonian.

2.7 Basis Ambiguity Problem of the Adiabatic Particle Number

In the preceding sections the expression (2.45) for the time evolution of the adiabatic particle number was equivalently derived through the Bogoliubov, Riccati, Spectral Function and Schrödinger approaches. However, the adiabatic reference mode functions (W_k, V_k) were left unspecified, and the arbitrariness of defining positive and negative energy states implies that an infinite number of consistent choices could be made.

Conventional choices for $W_k(t)$ and $V_k(t)$ are based on a WKB approximation, taking $W_k(t) = \omega_k(t)$, following the argument that the next-to-leading order term, and thus subsequent orders, is negligibly small in comparison to $\omega_k(t)$, for parameters of the effective frequency where $\omega_k(t)$ varies slowly in time:

$$W_k(t) \simeq \omega_k(t) \gg \frac{1}{4}\left(\frac{\ddot{\omega}_k}{\omega_k} - \frac{3}{2}\frac{\dot{\omega}_k^2}{\omega_k^3}\right) \tag{2.88}$$

For example, adiabaticity in the effective frequency for Schwinger particle production (2.17) is ensured by the dominant m scale: $m \gg E_0$ and $m \gg a$.

Two common choices are:

1. $W_k(t) = \omega_k(t)$ and $V_k(t) = 0$. This choice is made for example in [20,21,47–49,67–70]. Inserting this choice into the couple evolution equations (2.36) we obtain the time evolution of the Bogoliubov coefficients $\alpha_k(t)$ and $\beta_k(t)$ as

$$\begin{pmatrix} \dot{\alpha}_k(t) \\ \dot{\beta}_k(t) \end{pmatrix} = \frac{\dot{\omega}_k(t)}{2\omega_k(t)} \begin{pmatrix} 0 & e^{2i\int^t \omega_k} \\ e^{-2i\int^t \omega_k} & 0 \end{pmatrix} \begin{pmatrix} \alpha_k(t) \\ \beta_k(t) \end{pmatrix} \tag{2.89}$$

   or, using the direct form of the adiabatic particle number (2.45) as

$$\tilde{\mathcal{N}}_k(t) = \frac{\xi_k^2}{2\omega_k}\left[\left(\frac{1}{2\xi_k^2} - \omega_k\right)^2 + \frac{\dot{\xi}_k^2}{\xi_k^2}\right] , \tag{2.90}$$

   with the evolution of $\xi_k(t)$ determined by (2.19).

2. $W_k(t) = \omega_k(t)$ and $V_k(t) = -\frac{\dot{W}_k(t)}{2W_k(t)} = -\frac{\dot{\omega}_k(t)}{2\omega_k(t)}$. This choice is made for example in [53,64,65]. Inserting this choice into the couple evolution equations (2.36) we obtain the time evolution of the Bogoliubov coefficients $\alpha_k(t)$ and

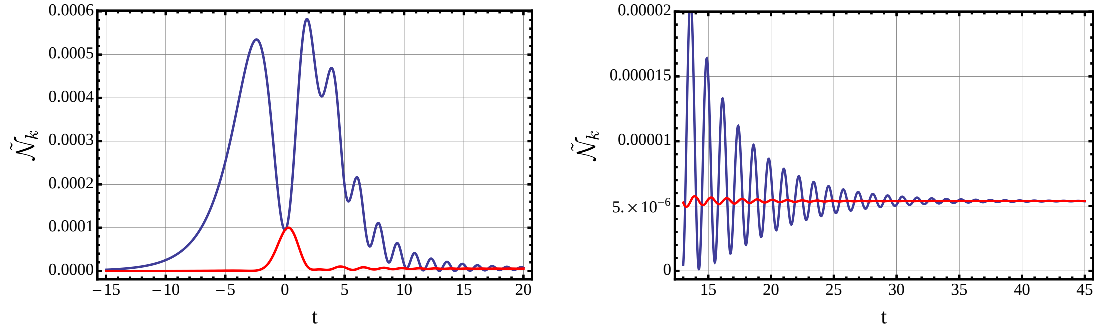

Fig. 2.3: $\tilde{\mathcal{N}}_k(t)$, evaluated with respect to two different adiabatic bases, for the Schwinger effect in an E-field: $E(t) = E_0\,\mathrm{sech}^2(at)$, with $E_0 = 0.25, a = 0.1, k_\perp = 0, k_\parallel = 0$, all in units with $m = 1$. The blue curves corresponds to the basis $W_k(t) = \omega_k(t)$ and $V_k(t) = 0$, while the red curves correspond to the basis $W_k(t) = \omega_k(t)$ and $V_k(t) = -\frac{\dot{\omega}_k(t)}{2\omega_k(t)}$, both determined by evaluating their respective evolution equations (2.89) and (2.91). The right-hand figure shows their late-time evolution. $\tilde{\mathcal{N}}_k(t)$ at intermediate times exhibits large differences in both scale and form of the oscillations, while the asymptotic value of the particle number is the same for both bases.

$\beta_k(t)$ as

$$\begin{pmatrix} \dot{\alpha}_k(t) \\ \\ \dot{\beta}_k(t) \end{pmatrix} = \frac{1}{4i}\left(\frac{3}{2}\frac{\dot{\omega}_k^2(t)}{\omega_k^3(t)} - \frac{\ddot{\omega}_k(t)}{\omega_k^2(t)}\right)\begin{pmatrix} 1 & e^{2i\int^t \omega_k} \\ \\ -e^{-2i\int^t \omega_k} & -1 \end{pmatrix}\begin{pmatrix} \alpha_k(t) \\ \\ \beta_k(t) \end{pmatrix} \tag{2.91}$$

or, using the alternate definition of the adiabatic particle number (2.45), as

$$\tilde{\mathcal{N}}_k(t) = \frac{\xi_k^2}{2\omega_k}\left[\left(\frac{1}{2\xi_k^2} - \omega_k\right)^2 + \left(\frac{\dot{\xi}_k}{\xi_k} + \frac{\dot{\omega}_k}{2\omega_k}\right)^2\right] \tag{2.92}$$

Note the first basis choice, $W_k(t) = \omega_k(t)$ and $V_k(t) = 0$, implies that $\delta_k(t) = 0$ and $\Delta_k(t) = \frac{\dot{\omega}_k(t)}{2\omega_k(t)}$, while the second choice, $W_k(t) = \omega_k(t)$ and $V_k(t) = -\frac{\dot{W}_k(t)}{2W_k(t)} = -\frac{\dot{\omega}_k(t)}{2\omega_k(t)}$, implies that $\Delta_k(t) = 0$ and $\delta_k(t) = \frac{1}{4i}\left(\frac{3}{2}\frac{\dot{\omega}_k^2(t)}{\omega_k^3(t)} - \frac{\ddot{\omega}_k(t)}{\omega_k^2(t)}\right)$.

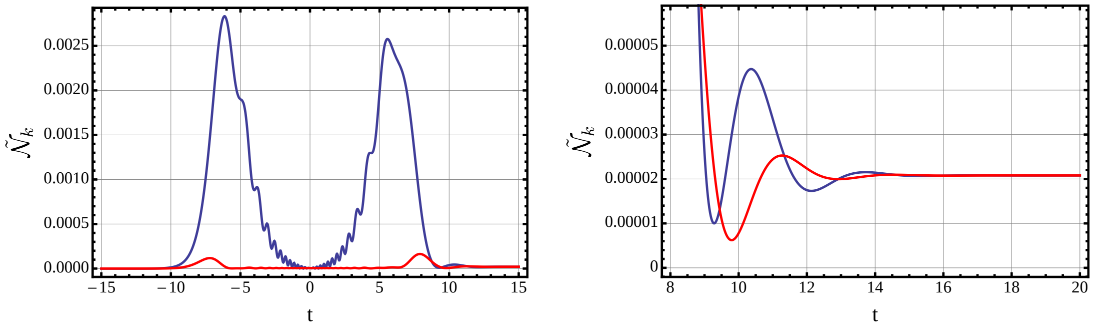

Fig. 2.4: $\tilde{\mathcal{N}}_k(t)$, evaluated with respect to two different adiabatic bases, for particle creation in 4-dimensional de Sitter space with conformal coupling (see Chapter 3), with the physical de Sitter space parameters: $H = 0.5, k = 25$, in units with mass scale $m = 1$. The blue curves corresponds to the basis $W_k(t) = \omega_k(t)$ and $V_k(t) = 0$, while the red curves correspond to the basis $W_k(t) = \omega_k(t)$ and $V_k(t) = -\frac{\dot{\omega}_k(t)}{2\omega_k(t)}$, both determined by evaluating their respective evolution equations (2.89) and (2.89). The right-hand figure shows their late-time evolution. Like Figure 2.3, the evolution of $\tilde{\mathcal{N}}_k(t)$ at intermediate times exhibits large differences in both scale and form of the oscillations, while the asymptotic value of the particle number is the same for both bases.

Since the evolution of the adiabatic particle number $\tilde{\mathcal{N}}_k(t)$ depends on the choice made for the mode functions $W_k(t)$ and $V_k(t)$, the time evolution of $\alpha_k(t)$ and $\beta_k(t)$, and hence of the adiabatic particle number $\tilde{\mathcal{N}}_k(t)$, will depend on the basis choice. A crucial observation is that the final asymptotic value, the total particle number $N_k = \tilde{\mathcal{N}}_k(t = +\infty)$ is independent of the choice of basis. This is illustrated in Figure 2.3 for the case of Schwinger particle production in a single-pulse electric field, and in Figure 2.4 for particle production in dS_4 (see Chapter 3), using the two different choices of mode functions listed above in (2.89) and (2.91). The final particle number is the same for the two bases, but the adiabatic particle number $\tilde{\mathcal{N}}_k(t)$ is different at intermediate times. These differences include both differences in the scale, and in the actual form of the oscillatory behavior at intermediate times.

Despite the next-to-leading order behavior (2.88), which also holds for subsequent orders of the expansion, we show in later sections that going beyond leading order WKB produces tangible effects in the evolution of the adiabatic particle number. The next section characterizes the possible choices for $W_k(t)$ and, subsequently, $V_k(t)$.

2.8 Adiabatic Expansion & Bases: Going Beyond Leading Order WKB

In Section 2.3 we introduced adiabaticity and specified approximate reference mode functions (2.27), which led to a definition of the time-dependent adiabatic particle number that is dependent on the choice of basis (2.45). We now study and characterize the basis choices.

Insisting that the reference mode functions (2.27) be a solution to the Klein-Gordon equation (2.16) requires that the function $W_k(t)$ satisfy equation (2.28). This equation can be solved by an adiabatic expansion [64–66], in which the leading order is the standard leading WKB solution to (2.28). This adiabatic expansion is divergent and asymptotic. Successive orders of the adiabatic expansion of $W_k(t)$ are obtained by expanding (2.28) in time-derivatives and truncating the expansion at a certain order of derivatives of the fundamental frequency $\omega_k(t)$

(2.17). The up-to-$(j+1)$th order expansion of $W_k(t)$, with the superscript (j) denoting the order of the adiabatic expansion, is then generated by the iterative expansion of

$$W_k^{(j+1)}(t) = \sqrt{\omega_k^2(t) - \left[\frac{\ddot{W}_k^{(j)}(t)}{2W_k^{(j)}(t)} - \frac{3}{4}\left(\frac{\dot{W}_k^{(j)}(t)}{W_k^{(j)}(t)}\right)^2\right]} \tag{2.93}$$

truncated at terms involving at most $2(j+1)$ derivatives with respect to t. The first three orders are:

1. Leading Order:

$$W_k^{(0)}(t) = \omega_k(t) \tag{2.94}$$

2. Next-to-leading order:

$$W_k^{(1)}(t) = W_k^{(0)}(t) - \frac{1}{4}\left(\frac{\ddot{\omega}_k}{\omega_k^2} - \frac{3}{2}\frac{\dot{\omega}_k^2}{\omega_k^3}\right) \tag{2.95}$$

3. Next-to-next-to-leading order:

$$\begin{aligned} W_k^{(2)}(t) = W_k^{(1)}(t) - \frac{1}{8}\Bigg(&\frac{13}{4}\frac{\ddot{\omega}_k^2(t)}{\omega_k^5(t)} - \frac{99}{4}\frac{\dot{\omega}_k^2(t)\ddot{\omega}_k(t)}{\omega_k^6(t)} + 5\frac{\dot{\omega}_k(t)\dddot{\omega}_k(t)}{\omega_k^5(t)} + \\ &- \frac{1}{2}\frac{\overset{(4)}{\omega}_k(t)}{\omega_k^4(t)} + \frac{297}{16}\frac{\dot{\omega}_k^4(t)}{\omega_k^7(t)}\Bigg) \end{aligned} \tag{2.96}$$

For backgrounds that become constant at asymptotic times it follows that $W_k^{(j)}(\pm\infty) = \omega_k(\pm\infty)$, and $\dot{W}_k^{(j)}(\pm\infty) = 0$ for all j.

Despite ambiguity in its explicit form at intermediate times, a critical feature of the real time-dependent function $V_k(t)$ is the necessary requirement that it vanish at asymptotic times

$$V_k(\pm\infty) = 0 \ . \tag{2.97}$$

At asymptotically late time, the function V_k is no longer ambiguous since the background becomes constant and the identification of particles and anti-particles becomes exact. In terms of the time-dependent adiabatic particle number (2.45), this implies that the particle number at future infinity is independent of the choice of V_k (as well as W_k). At intermediate times, however, the choice critically influences the time evolution of the adiabatic particle number. In the Schrödinger approach the basis function V_k is identified from (2.75) as an unphysical time-dependent phase. This is equivalently observed in the Bogoliubov, Riccati, and Spectral Function formalisms through the Wronskian condition (2.15) where the normalization of the mode function is unaffected by the inclusion of the function V_k in the mode decompositions (2.31,2.33), and thus admits the same interpretation as purely a time-dependent phase.

We argue that the choice

$$V_k(t) \equiv -\frac{\dot{W}_k(t)}{2W_k(t)} \tag{2.98}$$

is the most suitable and 'natural' form. In the Bogoliubov, Riccati, and Spectral Function approaches the choice (2.98) arises in the specified mode function decomposition (2.33) by retaining the contribution from the time-derivative of the $1/\sqrt{2W_k}$ factor in the definition of the reference mode function (2.27). In the Schrödinger approach, the choice (2.98) appears from insisting that the general form of the adiabatically evolving eigenfunction (2.75) be a solution to the time-dependent Schrödinger equation. It is a solution provided that the basis function $V_k(t)$ has the form (2.98), and yields the same condition on the function W_k as (2.28), consistent with the Bogoliubov, Riccati, and Spectral Function approaches. We adopt this 'natural' choice (2.98) and in later Sections we explore the dependence on the choice of $W_k(t)$.

2.9 Adiabatic Particle Number Truncated at j-th Order

Now we consider the specification of the function $W_k(t)$, via various orders of expansion of the adiabatic expansion (2.93). The time evolution of the adiabatic particle number at j-th adiabatic order is obtained by utilizing the preferred basis (2.98) and setting $W_k(t) = W_k^{(j)}(t)$ throughout the expressions used in its evaluation. This section also serves to summarize and contrast the forms developed across different, but equivalent, approaches to the adiabatic particle number.

At j-th order (recall that k labels the longitudinal momentum, while the superscript (j) labels the order of the adiabatic expansion), they read:

1. Evolution equation (2.45), the Adiabatic Particle Number obtained from the projection of the exact solution to the oscillator equation (2.16) onto a basis

of adiabatic evolving reference functions,

$$\tilde{\mathcal{N}}_k^{(j)}(t) = \frac{\xi_k^2(t)}{2W_k^{(j)}(t)}\left[\left(\frac{1}{2\xi_k^2(t)} - W_k^{(j)}(t)\right)^2 + \left(\frac{\dot{\xi}_k(t)}{\xi_k(t)} + \frac{\dot{W}_k^{(j)}(t)}{2W_k^{(j)}(t)}\right)^2\right] \tag{2.99}$$

This expression is completely characterized by the amplitude function $\xi_k(t)$ and the basis function $W_k^{(j)}$, where the general procedure to evaluate (2.99) is the following: solve the Klein-Gordon equation (2.16), or equivalently the Ermakov-Milne equation (2.19), to obtain $\xi_k(t)$, and compute $W_k^{(j)}(t)$ from the truncation of the adiabatic expansion at the desired adiabatic order.

2. Bogoliubov evolution equations (2.36):

$$\begin{pmatrix} \dot{\alpha}_k^{(j)}(t) \\ \dot{\beta}_k^{(j)}(t) \end{pmatrix} = \Lambda_k^{(j)}(t) \begin{pmatrix} 1 & e^{2i\int^t W_k^{(j)}} \\ -e^{-2i\int^t W_k^{(j)}} & -1 \end{pmatrix} \begin{pmatrix} \alpha_k^{(j)}(t) \\ \beta_k^{(j)}(t) \end{pmatrix} \tag{2.100}$$

where

$$\Lambda_k^{(j)}(t) = \frac{1}{2iW_k^{(j)}}\left[\omega_k^2 - \left(W_k^{(j)}\right)^2 + \left(\frac{3}{4}\left(\frac{\dot{W}_k^{(j)}}{W_k^{(j)}}\right)^2 - \frac{\ddot{W}_k^{(j)}}{2W_k^{(j)}}\right)\right] , \tag{2.101}$$

and their decoupled form, expressed in terms of the amplitude function $\xi_k(t)$:

$$\begin{aligned} \alpha_k^{(j)}(t) &= \frac{\xi_k}{\sqrt{2W_k^{(j)}}}\left[\left(\frac{1}{2\xi_k^2} + W_k^{(j)}\right) + i\left(\frac{\dot{\xi}_k}{\xi_k} + \frac{\dot{W}_k^{(j)}}{W_k^{(j)}}\right)\right] e^{-i\int^t\left(\frac{1}{2\xi_k^2} - W_k^{(j)}\right)} \\ \beta_k^{(j)}(t) &= -\frac{\xi_k}{\sqrt{2W_k^{(j)}}}\left[\left(\frac{1}{2\xi_k^2} - W_k^{(j)}\right) + i\left(\frac{\dot{\xi}_k}{\xi_k} + \frac{\dot{W}_k^{(j)}}{W_k^{(j)}}\right)\right] e^{-i\int^t\left(\frac{1}{2\xi_k^2} + W_k^{(j)}\right)} \end{aligned} \tag{2.102}$$

The evolution of the Bogoliubov coefficients in (2.100) are determined solely by the adiabatic function $W_k^{(j)}(t)$, truncated at the desired order, while its equivalent decoupled form (2.102) are additionally dependent on the amplitude function $\xi_k(t)$.

3. Riccati evolution equation (2.49):

$$\dot{R}_k^{(j)}(t) = -\Lambda_k^{(j)}(t)\left[e^{-2i\int^t W_k^{(j)}} + 2R_k^{(j)}(t) + e^{2i\int^t W_k^{(j)}}\left(R_k^{(j)}(t)\right)^2\right] \tag{2.103}$$

where $\Lambda_k^{(j)}(t)$ is defined as in (2.101), and:

$$R_k^{(j)}(t) = -e^{-2i\int^t W_k^{(j)}}\left[\frac{\left(\frac{1}{2\xi_k^2} - W_k^{(j)}\right) + i\left(\frac{\dot{\xi}_k}{\xi_k} + \frac{\dot{W}_k^{(j)}}{2W_k^{(j)}}\right)}{\left(\frac{1}{2\xi_k^2} + W_k^{(j)}\right) + i\left(\frac{\dot{\xi}_k}{\xi_k} + \frac{\dot{W}_k^{(j)}}{2W_k^{(j)}}\right)}\right] \tag{2.104}$$

The Reflection amplitude in (2.103) is completely determined by the specification of the adiabatic function $W_k^{(j)}(t)$, truncated at order j, while its solution (2.104) is expressed in terms of the amplitude function $\xi_k(t)$ and $W_k^{(j)}(t)$.

4. Evolution equation (2.60), the adiabatic particle number in the Wigner formalism:

$$\tilde{\mathcal{N}}_k^{(j)}(t) = \frac{\mathcal{V}}{4W_k^{(j)}}\int\frac{dk_0}{2\pi}\left[\frac{1}{4}\partial_t^2 + \frac{\dot{W}_k^{(j)}}{2W_k^{(j)}}\partial_t + \left(W_k^{(j)} + k_0\right)^2 + \left(\frac{\dot{W}_k^{(j)}}{2W_k^{(j)}}\right)^2\right]\mathcal{W}_k(t, k_0) \tag{2.105}$$

with $W_k^{(j)}(t)$ truncated at the desired order and $\mathcal{W}_k(t, k_0)$, equation (2.63) or (2.64), determined by the exact solution to the oscillator equation (2.16).

5. and, lastly, the adiabatic evolving wave function (2.75), the approximation

of the exact solution (2.68) to the time-dependent Schrödinger equation:

$$\zeta_n^{(j)}(q_k,t)=\frac{1}{\sqrt{2^n n!}}\left(\frac{W_k^{(j)}}{\pi}\right)^{1/4} e^{-\frac{1}{2}\left(W_k^{(j)}+i\frac{\dot{W}_k^{(j)}}{2W_k^{(j)}}\right)q_k^2} H_n\left(\sqrt{W_k^{(j)}}q_k\right) e^{-i(n+\frac{1}{2})\int^t W_k^{(j)}} \tag{2.106}$$

where, again, the expression is completely characterized by the adiabatic function $W_k^{(j)}(t)$ truncated at the desired order.

These different, yet equivalent, approaches to the adiabatic particle number have a clear dependence of the adiabatic function $W_k^{(j)}(t)$, in which the order of truncation of the adiabatic expansion critically influences the evolution of the particle number but leaves the final particle number unaffected.

2.10 Universal Form to the Evolution of the Adiabatic Particle Number

The adiabatic expansion is a *divergent* asymptotic expansion, and at higher orders j the expressions for $W_k^{(j)}(t)$ in terms of the original frequency $\omega_k(t)$ rapidly increase in complexity: see equations (2.94)-(2.96). In fact, terms in the expansion grow approximately as 2^j. This would discourage their study but Dingle found a simple universal large-order behavior for the adiabatic expansion [63] that was then capitalized by Berry to provide a *universal* form to the evolution of the adiabatic particle number.

Define the *Singulant* variable

$$F_k(t) = 2i \int_{t_c}^{t} dt' \, \omega_k(t') \tag{2.107}$$

where t_c is a turning point, a solution of $\omega_k(t_c) = 0$ that is closest to the real axis and located in the upper half plane. Then if we characterize the higher-orders of the adiabatic expansion through the terms generated in the phase-integral approach to WKB [96],

$$W_k(t) = \omega_k(t) \sum_{j=0,2,4}^{\infty} \varphi_k^{(j)}(t) \tag{2.108}$$

then there is a simple and universal large-order behavior in terms of the singulant:

$$\varphi_k^{(j+1)} \sim -\frac{j!}{\pi \, F_k^{j+1}} \qquad , \quad j \gg 1 \tag{2.109}$$

In Figure 2.5 we plot a sequential order-by-order comparison of Dingle's universal form (2.109) against different truncations of the adiabatic expansion expressed in the phase integral form (2.108) for the sQED Schwinger Effect, considering a single-pulse electric field: $E_{\|}(t) = E_0 \text{sech}^2 \, [at]$ with $E_0 = 0.25$, $a = 0.1$, $k_{\perp} = 0$, $k_{\|} = 0$, with units in $m = 1$. From evaluating the singulant (2.107) with respect to the dominant turning point pair, Dingle's universal large-order behavior for the expansion are plotted in red-dashed lines, and the adiabatic expansion truncated at j-th order are plotted in solid-blue lines in each subplot. Note the vertical scale changes across plotted orders. The figure demonstrates that Dingle's universal form accurately captures the large-order behavior of the expansion and becomes valid even for relatively low orders of the expansion. In addition, Dingle's universal expression works for effective frequencies dominated by a pair of turning points, as realized in the single-pulse field configuration.

Berry used this large-order behavior to resum the adiabatic expansion, to give a universal time-dependent form of the transition across a turning point [64,65]. Each (complex) turning point can be identified with a particle creation event (equivalently, in the scattering language, the "birth of a reflection" [64,65]). Berry's result can be stated as follows. For real $\omega_k^2(t)$, the turning points occur in complex conjugate pairs. Consider the situation of a single dominant complex conjugate pair of turning points, as sketched in Figure 2.6. Then Berry found that when the adiabatic expansion is truncated at optimal order $j_{\rm opt}$, the Bogoliubov coefficient $\beta_k(t)$ evolves across the associated Stokes line according to the *universal* approximate expression

$$\beta_k^{(j_{\rm opt})}(t) \approx \frac{i}{2}\,\mathrm{Erfc}\left(-\sigma_k(t)\right)\, e^{-F_k^{(0)}} \quad , \tag{2.110}$$

where Erfc is the error function [95], and the natural time evolution parameter $\sigma_k(t)$ is expressed in terms of the real and imaginary parts of the singulant function:

$$\sigma_k(t) \equiv \frac{\mathrm{Im}\, F_k(t)}{\sqrt{2\,\mathrm{Re}\, F_k(t)}} \tag{2.111}$$

The amplitude $e^{-F_k^{(0)}}$ is determined by the singulant between the complex conju-

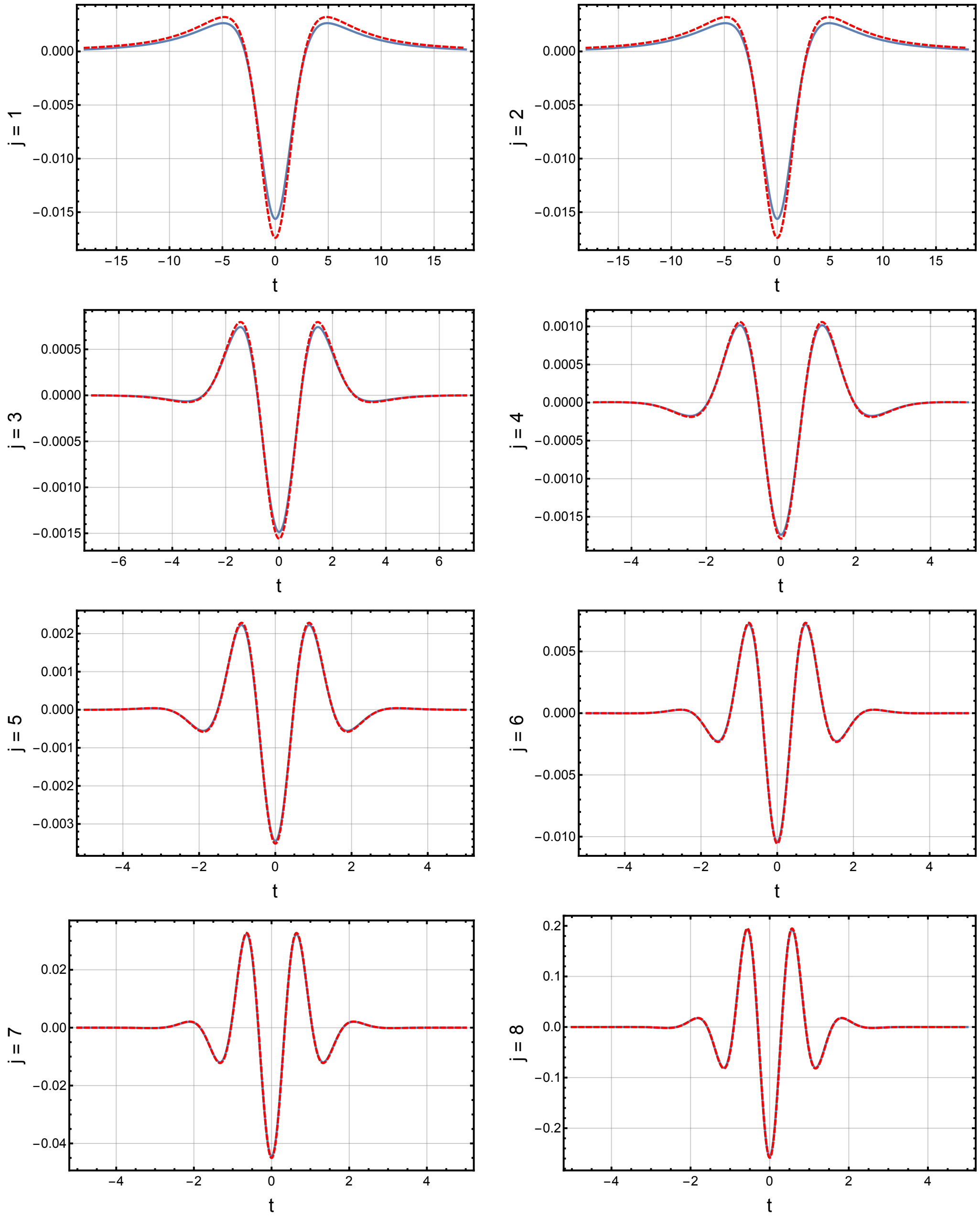

Fig. 2.5: An order-by-order comparison of the truncation of the adiabatic expansion (solid-blue line) expressed in the phase integral form (2.108) with Dingle's universal large-order behavior of the expansion (2.109) (red-dashed line) for adiabatic orders $j = 1$ to $j = 8$, considering sQED Schwinger Effect in a single-pulse E-field. Dingle's universal form accurately captures the large-order behavior of the expansion and becomes valid even at relatively low orders. See text for additional details.

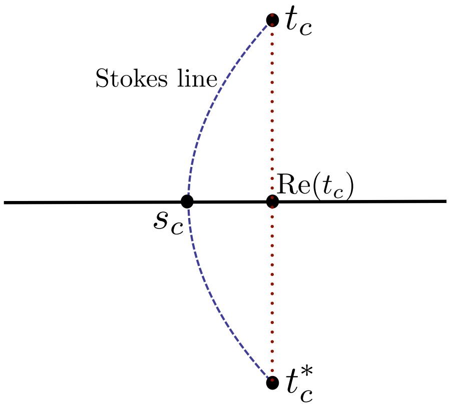

Fig. 2.6: For a single complex conjugate pair of turning points, (t_c, t_c^*) joined by a Stokes line [dashed blue line], we define s_c as the time at which the Stokes line crosses the real axis axis. Particle production associated with this pair (t_c, t_c^*) corresponds to crossing the Stokes line at s_c.

gate turning points:

$$F_k^{(0)} = i \int_{t_c}^{t_c^*} \omega_k(t)\, dt \quad , \tag{2.112}$$

where the integral is taken along the Stokes line joining the two turning points. In fact, the integral can be taken along the straight line connecting t_c and t_c^*, and with proper choices of branches the result is real and positive [64,65,96]. Thus, the Bogoliubov coefficient makes a smooth jump of universal shape when crossing a Stokes line, which suggests the interpretation of the "time of particle creation" as the time s_c at which the Stokes line connecting t_c and t_c^* crosses the real axis, as sketched in Figure 2.6; this is the time at which $\sigma_k(t)$ vanishes.

Recalling (2.35), we immediately deduce that in the context of particle production, the time evolution of the adiabatic particle number $\tilde{\mathcal{N}}_k(t)$ is given by the *universal* approximate expression

$$\tilde{\mathcal{N}}_k^{(j_{\rm opt})}(t) \approx \frac{1}{4} \left| \mathrm{Erfc}\left(-\sigma_k(t)\right) e^{-F_k^{(0)}} \right|^2 \tag{2.113}$$

Furthermore, in the vicinity of the real crossing point s_c of the Stokes line,

$$F_k(t) \approx F_k(s_c) + 2i\, \omega_k(s_c)(t - s_c) \tag{2.114}$$

which leads to the simplified approximation:

$$\sigma_k(t) \approx \frac{2\, \omega_k(s_c)\, (t - s_c)}{\sqrt{2\, F_k(s_c)}} \tag{2.115}$$

Finally, the order j at which the adiabatic approximation should be optimally truncated depends on the parameters associated with the turning points, and can be estimated in terms of $F_k^{(0)}$ defined in (2.112): the optimal order $j_{\rm opt}$ is the integer closest to

$$j_{\rm opt} \approx \mathrm{Int}\left[\frac{1}{2}\left(\left|F_k^{(0)}\right| - 1\right)\right] \tag{2.116}$$

In practice it is often a good approximation to estimate this optimal order by computing the absolute value of the singulant (2.107), evaluated at the real part of t_c.

The *universality* of these remarkable results makes the notion of an optimally truncated adiabatic particle number a useful and well-defined concept. As a result of this universality, it is not necessary to make an explicit large-order truncation of the adiabatic expansion, which grows in complexity for higher orders, and moreover would be truncated at different orders for different parameters. The results of Dingle and Berry imply that this is not needed: the universal form of the time-dependence in (2.113) applies in general with optimal truncation of the expansion.

2.11 Illustrations of the Optimal Adiabatic Particle Number for various External Electric Fields

We illustrate Berry's result for Schwinger particle production for various time-dependent electric fields in the context of the Stokes interpretation of particle production. The results are illustrated for simple fields involving a single pair of dominant complex-conjugate turning points, and later multi-pulse configurations involving multiple dominant turning point pairs, which give rise to distinct interference effects.

2.11.1 Illustrations of Simple External Electric Fields

We first consider simple electric field configurations that have just a single pair of dominant complex-conjugate turning points: the constant electric field and an example of a single-pulse electric field.

Constant Electric Field

We first consider the simplest case, that of a constant electric field: $E_\parallel(t) = E_0$. There is one pair of complex-conjugate turning points located at

$$t_c = \frac{i\,(m^2 + k_\perp^2) - k_\parallel}{E_0} \tag{2.117}$$

and its complex conjugate. A thorough discussion is provided, for example, in [13,14]. In Figure 2.8 we plot the time evolution of the adiabatic particle number $\tilde{\mathcal{N}}_k^{(j)}(t)$ for the first six orders of the adiabatic expansion, where the subscript j denotes the order of truncation. The numerical results, from integrating (2.100) with the basis (2.98) are plotted in solid-blue lines, and Berry's universal form (2.113) is plotted as a red-dashed curve in each plot. The final asymptotic value of the particle number, at future infinity, is the same for all orders of truncation j. Note the vertical scales changes across plotted orders. At zeroth order of the adiabatic expansion we see at intermediate times large oscillations in the particle number, roughly 30 times the scale of the final value. The magnitude of the oscillations decreases as we approach the optimal order, $j_{\text{opt}} = 3$, and then they rapidly grow again if we continue beyond the optimal order. Recall that such behavior is characteristic of asymptotic expansions, where the order of truncation depends crucially on the size of the expansion parameter, and going beyond this optimal order typically yields increasingly worse results. For the physical parameters used in Figure 2.7, we have $F_k^{(0)} = 2\pi \approx 6.283$, consistent with the estimate (2.116) for the optimal truncation order, and $\exp(-2\,F_k^{(0)}) \approx 3.49 \times 10^{-6}$, consistent with the universal formula (2.113) for final particle number at future infinity. Evaluating (2.112), the value of the final particle number for the constant electric field is

$$\tilde{\mathcal{N}}_k(+\infty) = e^{-2F_k^{(0)}} = \mathrm{Exp}\left[-\frac{\pi}{E_0}\left(m^2 + k_\parallel^2 + k_\perp^2\right)\right] \quad , \tag{2.118}$$

independent of the adiabatic basis.

Single-pulse Electric Field

A slightly more physical example is that of a single-pulse electric field,

$$E_\parallel(t) = E_0\,\mathrm{sech}^2(at) \quad , \tag{2.119}$$

for which we use the time-dependent vector potential:

$$A_\parallel(t) = -\frac{E}{a}\tanh(at) \tag{2.120}$$

A field configuration that initially begins turned off, becomes active, and then turns off once again, in contrast to the constant electric field example. This field configuration yields an infinite tower of pairs of complex-conjugate turning points is enumerated by the set:

$$t_c = \begin{cases} \dfrac{1}{a}\,\mathrm{artanh}\Big[\dfrac{a}{E}\left(iM - k_\parallel\right)\Big] + \dfrac{i\pi}{a}l \\ \dfrac{1}{a}\,\mathrm{artanh}\Big[\dfrac{a}{E}\left(-iM - k_\parallel\right)\Big] + \dfrac{i\pi}{a}(l+1) \end{cases} \tag{2.121}$$

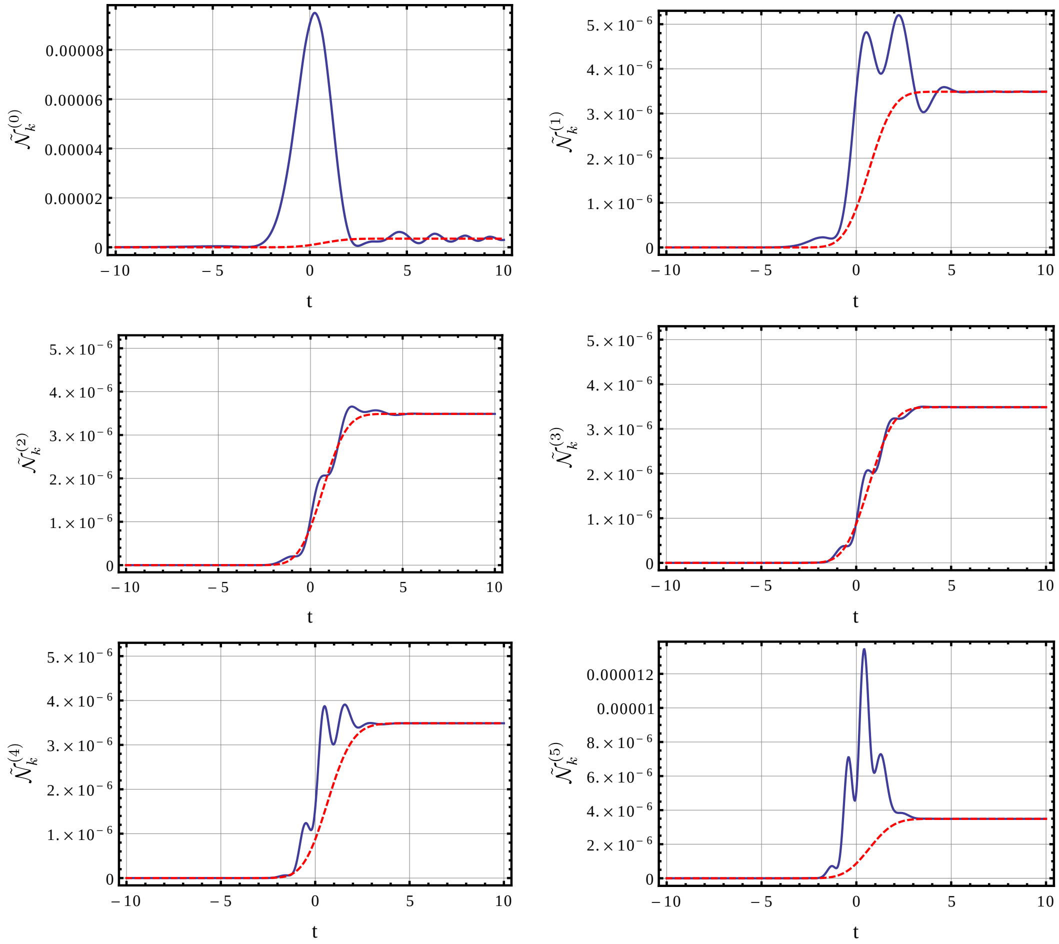

Fig. 2.7: $\tilde{\mathcal{N}}_k^{(j)}(t)$, here, obtained by numerically evaluating (2.100), for the first 6 orders of the adiabatic expansion, for Schwinger particle production in a constant E-field with $E = 0.25$, $k_\perp = 0$, $k_\parallel = 0$, in units with $m = 1$. $\tilde{\mathcal{N}}_k^{(j)}$ is plotted with solid-blue lines, and Berry's universal form (2.113) is plotted with red-dashed lines. The final value of the particle number is the same for all orders of truncation, but the oscillations in the particle number at intermediate times differ significantly. Note the smoothest evolution occurs at the optimal order, here, $j_{\text{opt}} = 3$.

for $l = 0, 1, 2, \ldots$, with $M^2 \equiv m^2 + k_\perp^2$. However, operating in the semiclassical regime, where $E \ll m^2$ and $a \ll m$, the effect is dominated by the pair closest to the real axis [67,68]. This manifests in behavior quite similar to that of the constant electric field configuration. The results are shown in Figure 2.8, and we observe the close similarity to the constant E-field results in Figure 2.7. Again there are large oscillations at intermediate times for low orders of the adiabatic expansion. These subside as the optimal order ($j_{\rm opt} = 3$) is reached, and then grow again as one goes to higher orders in the adiabatic expansion. The red-dashed curves show Berry's universal error-function form (2.113), with excellent agreement with the optimal order of truncation. For the physical parameters used in Figure 2.8, we have $F_k^{(0)} \approx 6.050$, consistent with the estimate (2.116) for the optimal truncation order, and $\exp(-2\,F_k^{(0)}) \approx 5.558 \times 10^{-6}$, consistent with the universal formula (2.113) for the particle number at future infinity.

In Figure 2.9 we illustrate the universal nature of the optimally truncated form (2.113), by comparing the optimally truncated order, for different field and momentum parameters, for Schwinger pair production in a single-pulse electric field. Recall that the parameters found in the effective frequency $\omega_k(t)$ (2.17) affects which order corresponds to the the optimal order of truncation. In order to show all plots on the same scale, we have normalized the adiabatic particle number by its final value $N_k \equiv \tilde{\mathcal{N}}_k(t = +\infty)$. In each plot the order j denotes the optimal order of truncation associated with the pulse and momenta parameters selected and is indicated by the subscript (j) in $\tilde{\mathcal{N}}_k^{(j)}(t)$. The red-dashed curves show the universal error function form in (2.113) with the local action (2.111), while the green-dot-dashed curves show the universal form with the approximate expression (2.115) for the local action $\sigma_k(t)$. For the parameter values used in

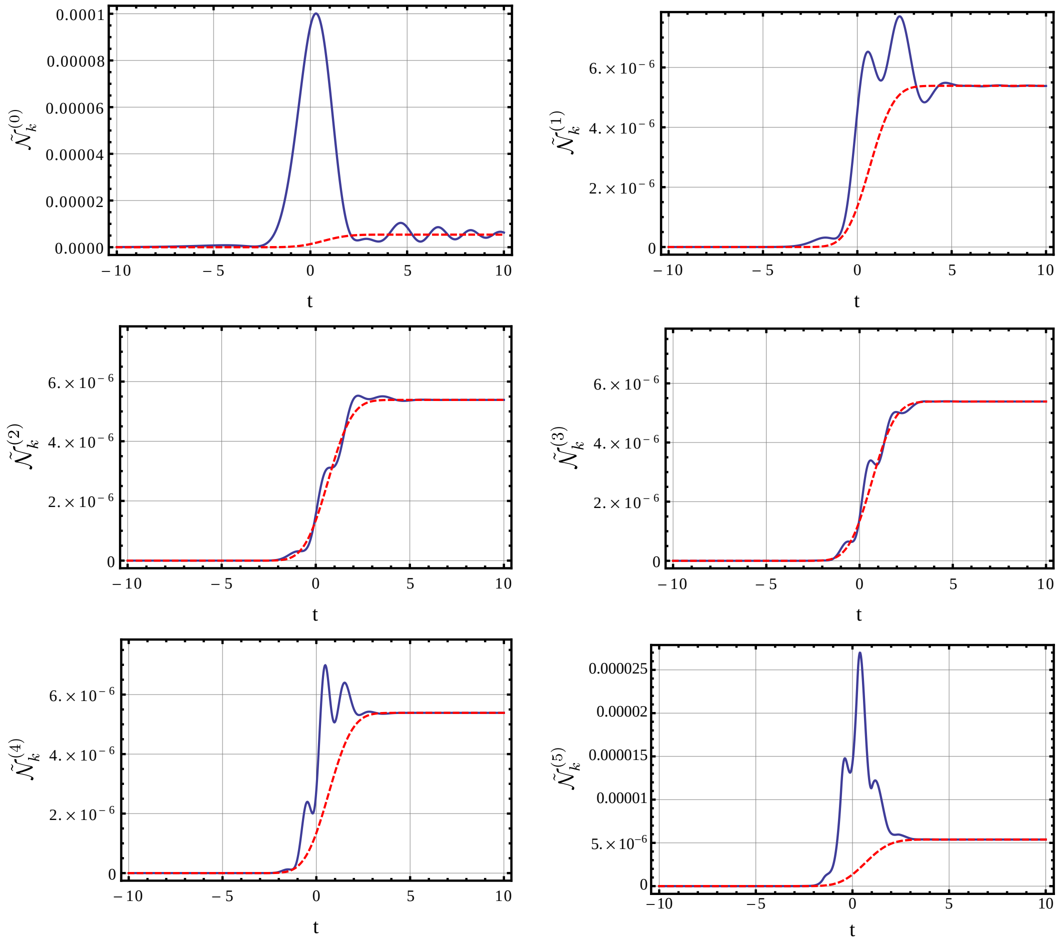

Fig. 2.8: $\tilde{\mathcal{N}}_k^{(j)}(t)$, here, obtained by numerically evaluating (2.100), for the first 6 orders of the adiabatic expansion, for Schwinger particle production in a single-pulse E-field (2.119) with $E_0 = 0.25$, $a = 0.1$, $k_\perp = 0$, $k_\parallel = 0$, with units in $m = 1$. $\tilde{\mathcal{N}}_k^{(j)}$ and Berry's universal form (2.113) are plotted in the same style as for Figure 2.7. Again, the final value of the particle number is the same for all orders of truncation, but the oscillations in the particle number at intermediate times differ significantly. Here, $j_{\text{opt}} = 3$.

these plots, $F_k^{(0)}$ takes values 7.416, 2.967, 6.050, and 6.956, respectively, consistent with the estimate (2.116) for the optimal truncation order. These results illustrate that across a wide range of different field parameters, the universal form of the adiabatic particle number (2.113) agrees well with the particle number at the optimal truncation of the adiabatic expansion. Furthermore, the approximation (2.115), valid in the vicinity of a simple dominant turning point pair, works very well. Finally, the optimal order gives a clear physical picture of the particle creation event as a single smoothed jump across the Stokes line, in contrast to the leading order of the adiabatic expansion which has large unphysical oscillations in this time region. This feature is even more pronounced for the fields studied in the subsequent sections, as particle production in these fields involves quantum interference between different creation events.

2.11.2 Illustrations of Multi-pulse External Electric Fields

In this Section we show how the adiabatic particle number with respect to the optimal adiabatic basis evolves in time for various classes of time-dependent electric fields having nontrivial temporal structure, to illustrate the time-dependence of the associated quantum interference effects. We concentrate on sequences of alternating-sign pulses, as these have been shown to permit maximal constructive interference, via an analogy with the Ramsey effect of atomic physics, leading to a coherent enhancement of the Schwinger effect [43]. For certain longitudinal momenta of the produced particles, the final particle number is enhanced, while for others it is reduced by destructive interference, producing a momentum spectrum that is a precise time-domain analogue of the interference pattern of the multiple slit interferometer [43]. We note that such interferometric effects have been ex-

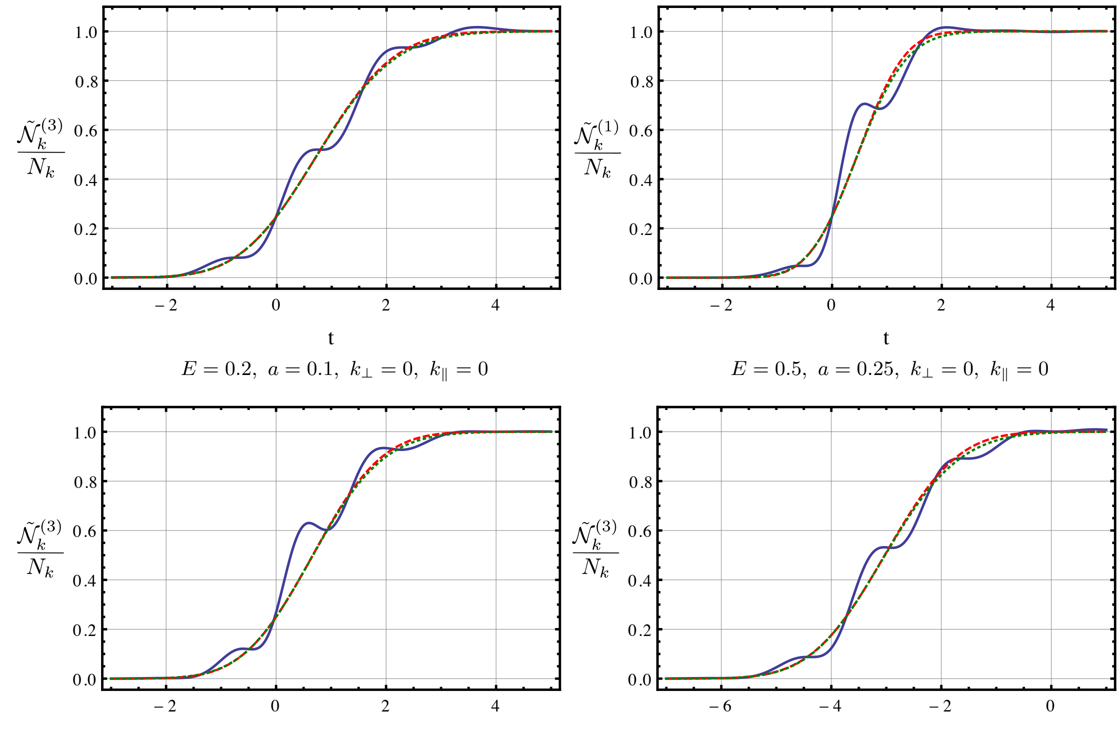

$E = 0.2,\ a = 0.1,\ k_\perp = 0,\ k_\parallel = 0$

$E = 0.5,\ a = 0.25,\ k_\perp = 0,\ k_\parallel = 0$

$E = 0.25,\ a = 0.1,\ k_\perp = 0,\ k_\parallel = 0$

$E = 0.25,\ a = 0.1,\ k_\perp = 0,\ k_\parallel = 1$

Fig. 2.9: A survey of illustrations that compares $\tilde{\mathcal{N}}_k^{(j_{\text{opt}})}$ (solid-blue line), evaluated using (2.100) at the optimal order j_{opt}, against its approximation by the universal form (2.113) (red-dashed line), for Schwinger particle production in a single-pulse E-field (2.119), across different field parameters E_0 and a, and different momenta $k_\parallel$ and $k_\perp$, in units with $m = 1$. In each example, $\tilde{\mathcal{N}}_k^{(j_{\text{opt}})}$ (solid-blue line) is normalized by its final particle number to present each subplot on the same scale. The approximate universal form with (2.115) is plotted as a green-dashed curve.

perimentally observed in analogue atomic ionization systems [97–101], and more recently in a polariton system with two-color fields [102].

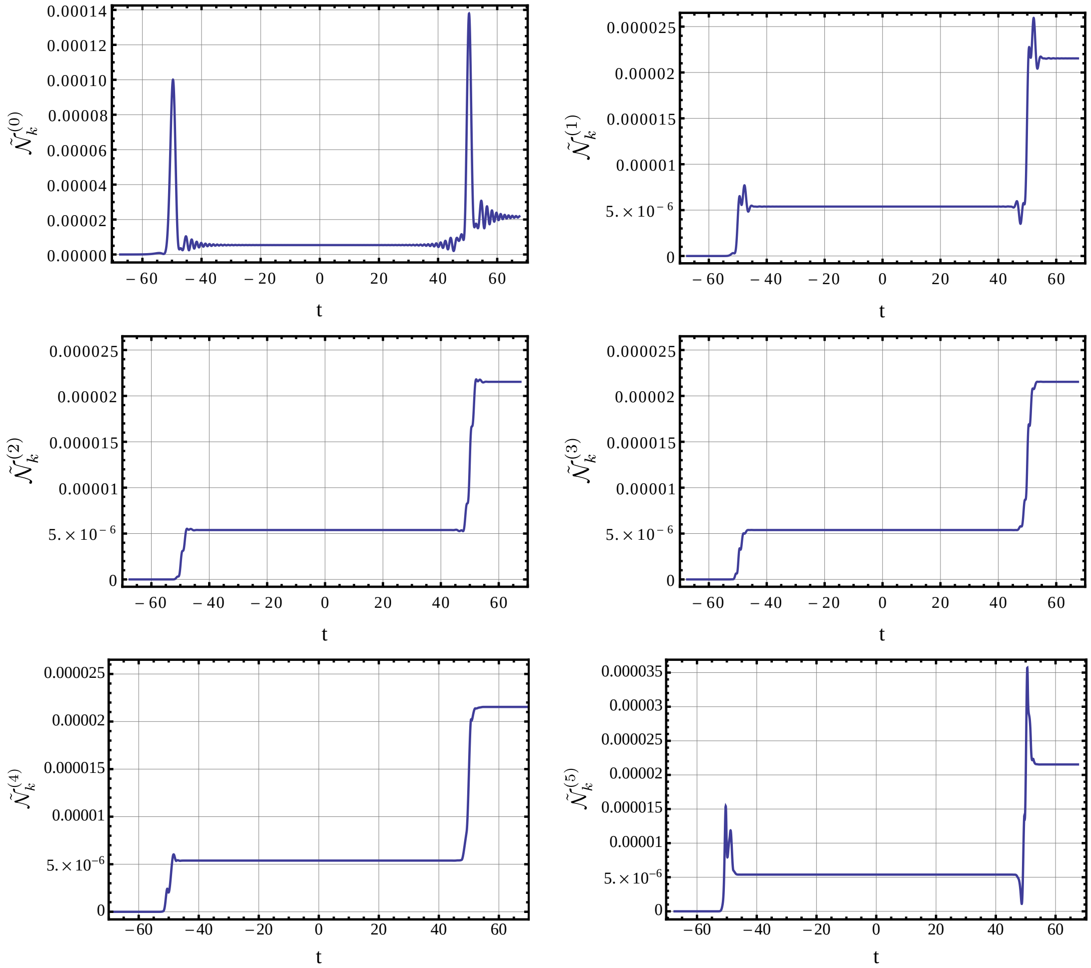

Fig. 2.10: $\tilde{\mathcal{N}}_k^{(j)}(t)(t)$ for the first 6 orders of the adiabatic expansion, for Schwinger particle production in alternating-sign double-pulse E-field (2.122), with $E_0 = 0.25$, $a = 0.1$, $b = 50$, $k_\perp = 0$, and $k_\parallel = 2.51555$, in units with $m = 1$. $k_\parallel$ is selected to show maximum constructive interference. The final particle number at future infinity is the same for all j, and is 4 times that of the intermediate plateau, consistent with coherent n^2-enhancement for constructive interference. Note the smoothening at the optimal order ($j_{\mathrm{opt}} = 3$) and the large oscillations that appear before and after.

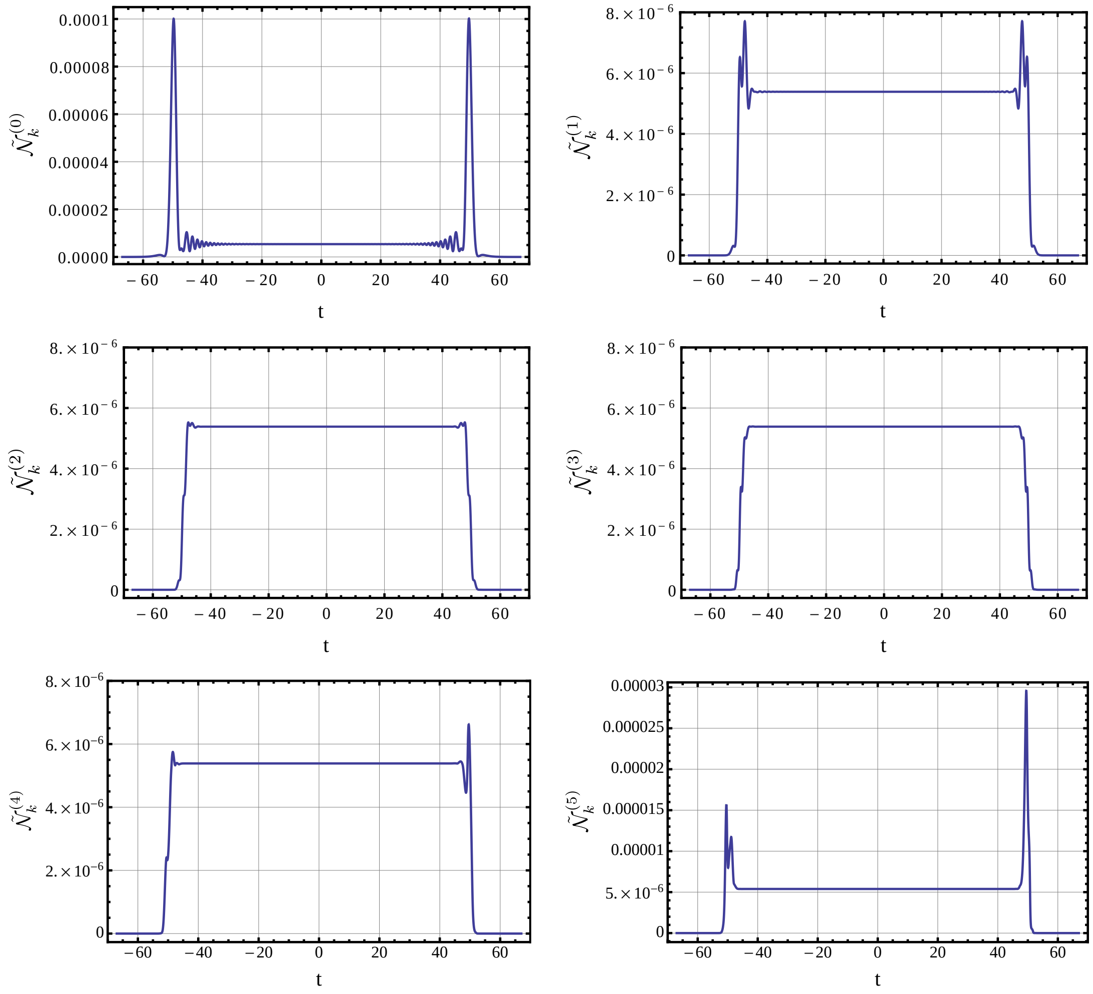

Fig. 2.11: As in Figure 2.10, but with $E_0 = 0.25$, $a = 0.1$, $b = 50$, $k_\perp = 0$, and $k_\parallel = 2.49887$, in units with $m = 1$. $k_\parallel$ is selected to show maximum destructive interference. The final asymptotic value of the particle number, at future infinity, vanishes for each order of truncation, consistent with coherent destructive quantum interference. Note the smoothening at the optimal order ($j_{\text{opt}} = 3$) and the large oscillations that appear before and after.

Two Alternating-sign Electric Field Pulses

We now consider an electric field consisting of the two successive pulses, of alternating sign:

$$E(t) = -E_0 \operatorname{sech}^2 [a(t+b)] + E_0 \operatorname{sech}^2 [a(t-b)] \tag{2.122}$$

for which we can choose a time-dependent vector potential:

$$A_{\parallel}(t) = -\frac{E}{a}\Big(- \tanh \big[a(t+b)\big] + \tanh \big[a(t-b)\big]\Big) \tag{2.123}$$

In addition to choosing the field parameters, we can choose to probe the momentum of the produced particles. Following [43,67,68], we consider the cases of maximal constructive interference and maximal destructive interference by choosing two different values of the particle momenta, associated with the central maximum and the first minimum of the momentum spectrum. The results are shown in Figures 2.10 and 2.11, respectively. In these plots the pulses occur at $t = \mp 50$. These plots show that in low orders of the adiabatic expansion there are large oscillations at non-asymptotic times in the vicinity of the pulses, but at the optimal order of truncation (here $j = 3$) the time evolution becomes smooth. Furthermore, we clearly see the coherent constructive interference in Figure 2.10, as the final plateau is four times the value of the plateau between the two pulses. On the other hand, Figure 2.11 shows destructive interference, as the optimal adiabatic particle number rises to a value corresponding to a single pulse, and then falls back to zero after the second pulse. In both Figure 2.10 and Figure 2.11, the physical parameters are such that $F_k^{(0)} \approx 6.050$, consistent with the estimate (2.116) for the optimal truncation order, and $\exp(-2F_k^{(0)}) \approx 5.56 \times 10^{-6}$, consistent with the intermediate plateau value of the particle number in both cases.

Examples with pulses closer together in time, are shown in Figures 2.12 and 2.13. Note that while in Figures 2.10 and 2.11 it is easy to resolve the adiabatic particle number into two separate events, even at the lowest order of the adiabatic expansion, it is more difficult to make such a distinction for the parameters of Figures 2.12 and 2.13. But at the optimal order (here $j \approx 1-2$) one can clearly resolve the situation of two separate creation events, with characteristic plateaux amplitudes in the ratio 1 : 4 in the case of constructive interference (Figure 2.12), and destructive interference (Figure 2.13). In Figure 2.12 and Figure 2.13, the physical parameters are such that $F_k^{(0)} \approx 4.303$ and 4.405, respectively, and $\exp(-2F_k^{(0)}) \approx 1.83 \times 10^{-4}$ and 1.49×10^{-4}, respectively, consistent with the estimates in (2.113) and (2.116).

Three Alternating-sign Electric Field Pulses

We now consider an electric field consisting of the three successive pulses, of alternating sign:

$$E(t) = E\,\mathrm{sech}^2\left[a(t+2b)\right] - E\,\mathrm{sech}^2\left[at\right] + E\,\mathrm{sech}^2\left[a(t-2b)\right] \tag{2.124}$$

for which we can choose a time-dependent vector potential:

$$A_{\parallel}(t) = -\frac{E}{a}\Big(\tanh[a(t+2b)] - \tanh(at) + \tanh[a(t-2b)]\Big) \tag{2.125}$$

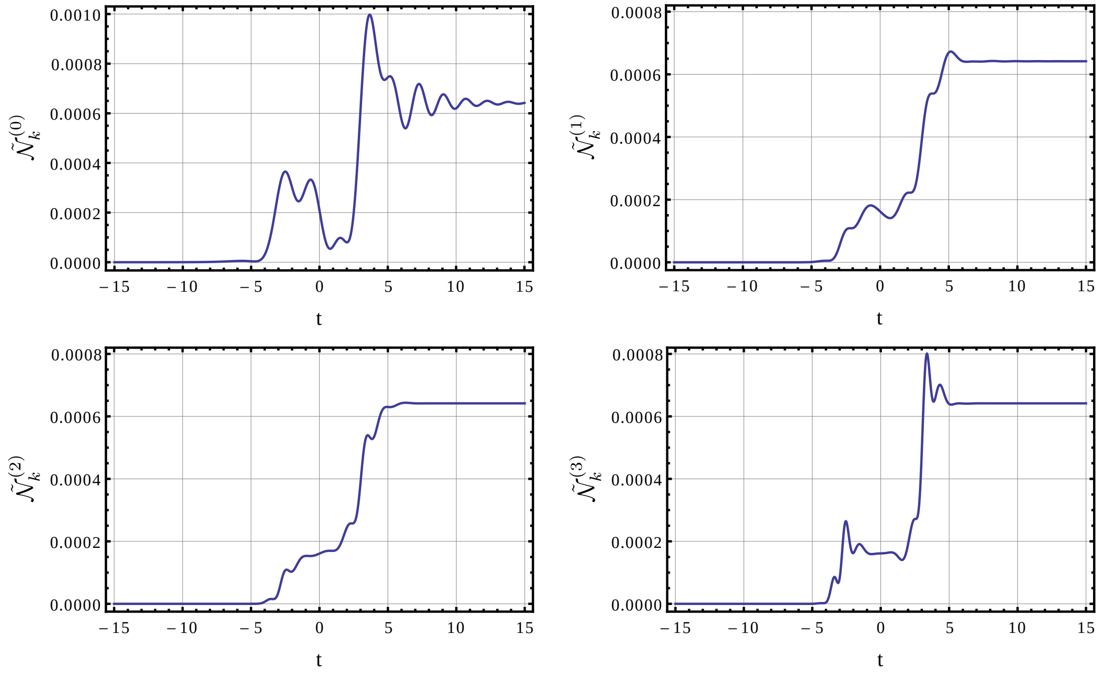

Fig. 2.12: $\tilde{\mathcal{N}}_k^{(j)}(t)$ for an alternating-sign double pulse E-field (2.122) with $E_0 = 0.5$, $a = 0.2$, $b = 2.5$, $k_\perp = 0$, and $k_\parallel = 1.85$, in units with $m = 1$. Here, the pulses are closer together than in Figure 2.10 where the optimal order ($j_{\text{opt}} = 2$) provides a clear resolution of coherent destructive interference.

The results are shown in Figures 2.14 and 2.15, with longitudinal momentum $k_\parallel$ associated with coherent constructive interference. Notice the large oscillations that shrink and smooth out as the optimal order of truncation ($j = 3$) is approached, and return after this order is passed. Also notice the coherence effect that the three plateaux are in the ratio 1 : 4 : 9.

Figure 2.16 emphasizes this coherence effect, as the successive plateaux occur in the ratio 1 : 4 for two pulses, and in the ratio 1 : 4 : 9 for three pulses, when the momentum of the produced particles corresponds to a maximum in the momentum spectrum [43,67,68].

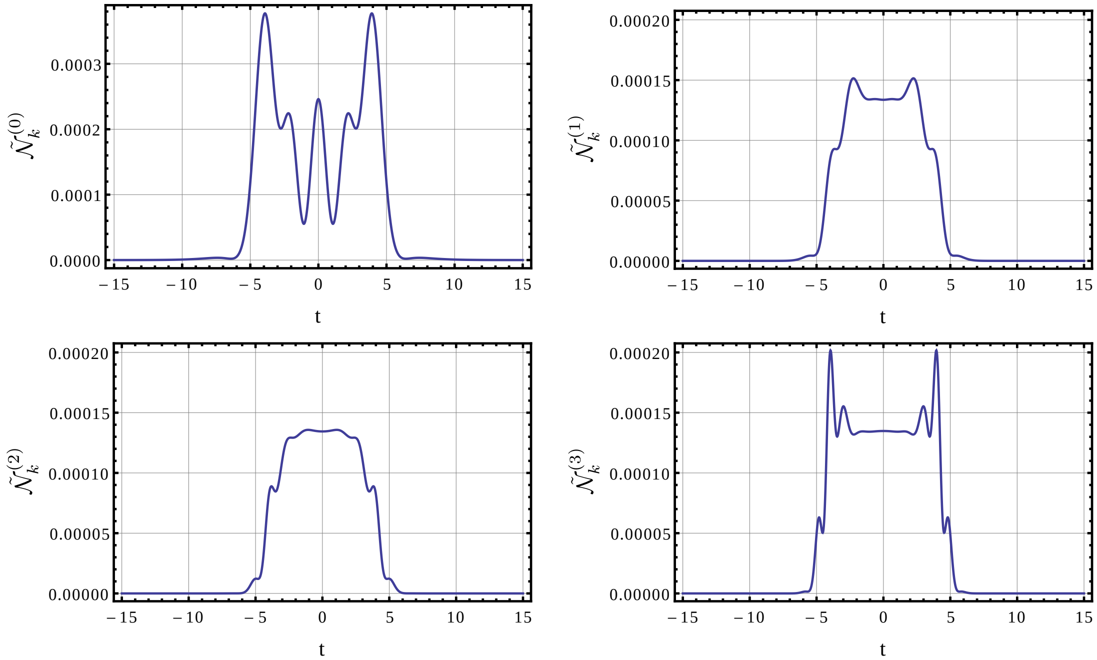

Fig. 2.13: As in Figure 2.12, but with $k_\parallel = 1.22175$. Again, the pulses are closer together than in Figure 2.11 where the optimal order ($j_{\text{opt}} = 2$) provides a clear resolution of coherent destructive interference.

2.12 Approximate Universal Evolution for Multi-pulse External Fields

These interference effects arise due to phase differences between different sets of complex-conjugate turning points, and have a significant effect on the final total particle number [43,67,68], providing a simple semiclassical interpretation of the numerical results in [103] which showed an intricate dependence of the momentum spectrum of the produced particles on the carrier phase of the sub-cycle structure of a time-dependent laser pulse. The results of [43,67,68] are that the final particle number can be expressed as a sum over contributions from each set of turning

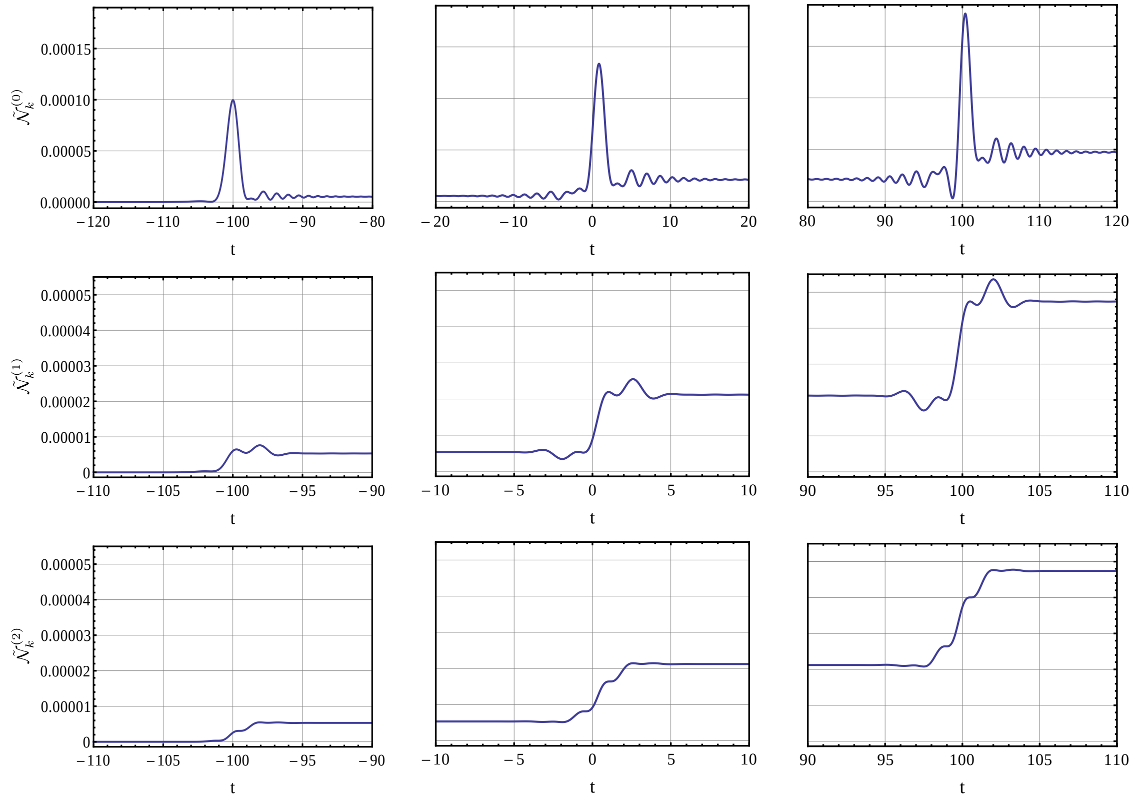

Fig. 2.14: $\tilde{\mathcal{N}}_k^{(j)}(t)$, for the first 3 orders of the adiabatic expansion, considering an alternating-sign triple-pulse E-field (2.124) with $E_0 = 0.25$, $a = 0.1$, $b = 50$, $p_\perp = 0$, and $k_\parallel = 0.08336$, in units with $m = 1$. $k_\parallel$ is selected for maximum constructive interference. See Figure 2.15 for the next three orders.

points. For scalar QED we have

$$N_k \equiv \tilde{\mathcal{N}}_k(t = +\infty) \approx \left| \sum_{t_p} \exp\left(2i\theta_k^{(p)}\right) \exp\left(-F_{k,t_p}^{(0)}\right) \right|^2 \qquad (2.126)$$

where the exponent of the magnitude of the contribution of the turning point t_p is

$$F_{k,t_p}^{(0)} \equiv i \int_{t_p}^{t_p^*} \omega_k(t)\, dt \qquad (2.127)$$

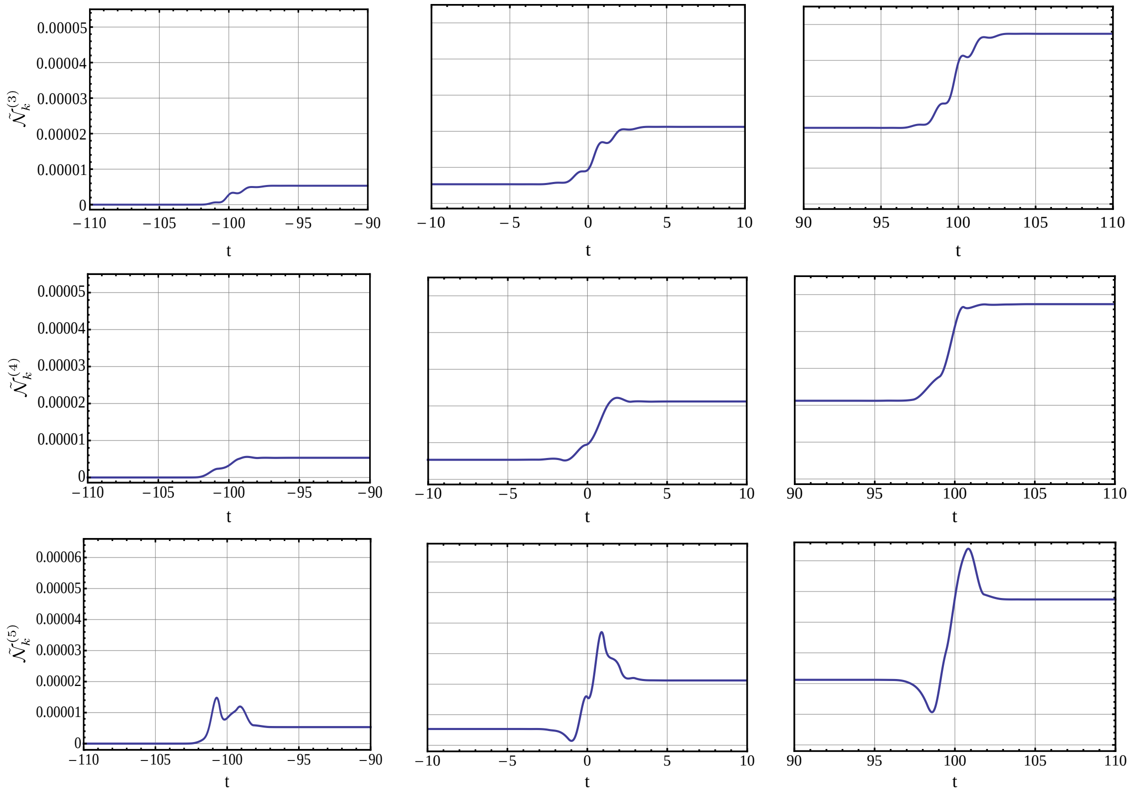

Fig. 2.15: As in Figure 2.14, but for the first 3 orders of the adiabatic expansion, $j = 3, 4, 5$. Here, $j_{\rm opt} = 3$ and the ratios of the plateaux are $1 : 3.99 : 8.9$, very close to the expected $1 : 4 : 9$ for coherent constructive interference of three pulses.

while the accumulated phase (measured relative to the first real Stokes point s_1, the point where the Stokes line connecting t_1 and t_1^* crosses the real axis) for turning point t_p is

$$\theta_k^{(p)} \equiv \int_{s_1}^{s_p} \omega_k(t)\, dt \approx \int_{\mathrm{Re}[t_1]}^{\mathrm{Re}[t_p]} \omega_k(t)\, dt \qquad (2.128)$$

If the pulse-sequence consists of alternating sign pulses of the same shape, then all the $\left| e^{-F_{k,t_p}^{(0)}} \right|^2$ factors are approximately equal, and we can have constructive or destructive interference depending on the relative phases. These phases

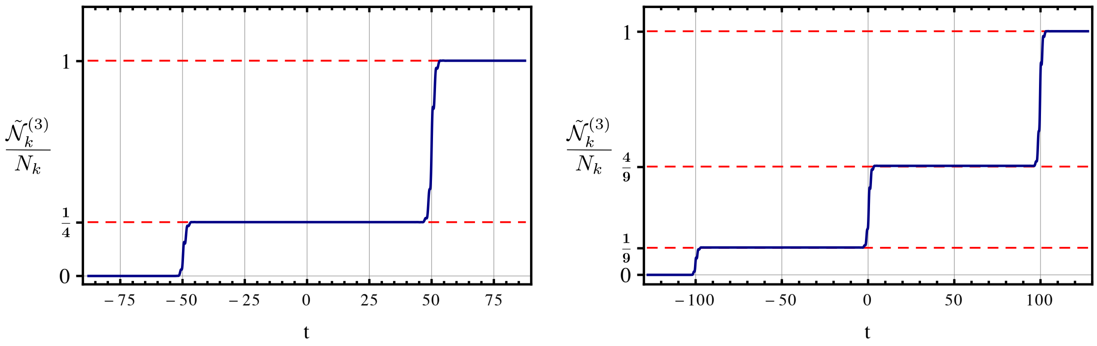

Fig. 2.16: Time evolution of $\tilde{\mathcal{N}}_k^{(j_{\mathrm{opt}})}(t)$, normalized by its final particle number at future infinity, for two examples of coherent constructive interference: a double-pulse E-field (2.122) (left) as in Figure 2.10, and a triple-pulse E-field (2.124) (right) as in Figure 2.11. Here, $j_{\mathrm{opt}} = 3$ for both, and the ratio of their plateaux follow 1 : 4 and 1 : 4 : 9, respectively.

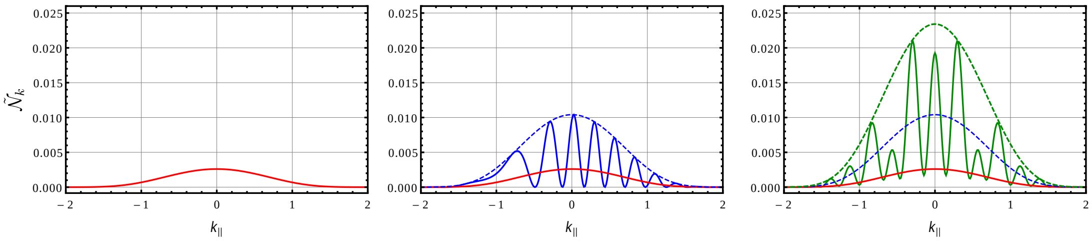

Fig. 2.17: The longitudinal momentum spectrum N_k as a function of the produced particle's longitudinal momentum for the single-, double-, and triple-pulse E-fields, (2.119), (2.122), and (2.124), respectively. The distribution, with constructive and destructive enhancement for certain modes, is of the n-slit interference form with the envelop being n^2 times the envelope for the single-pulse.

depend both on the pulse parameters and on the produced particle's longitudinal momentum $k_{\parallel}$. In particular, for equally-spaced alternating-sign pulses, we have approximately equal phase differences between successive turning point pairs, leading to coherent interference:

$$N_k^{\text{n-pulse}} \approx \begin{cases} N_k^{\text{1-pulse}} \sin^2\left[n\,\theta_k\right] / \cos^2\left[\theta_k\right] \quad , \quad n \text{ even} \\ \\ N_k^{\text{1-pulse}} \cos^2\left[n\,\theta_k\right] / \cos^2\left[\theta_k\right] \quad , \quad n \text{ odd} \end{cases} \tag{2.129}$$

Note that as a function of the longitudinal momentum k, these particle spectra represent the n-slit interference pattern, here probed in the time-domain from the quantum vacuum [43]. In Figure 2.17 we show these momentum spectra (for the final asymptotic particle number $N_k = \tilde{\mathcal{N}}_k(t = +\infty)$), for the cases of one, two and three pulses, of the forms (2.119), (2.122), and (2.124), respectively. There, we clearly see a distribution of the n-slit interference form with the envelope being n^2 times the envelope for one pulse. When integrated over k, the total particle number is just n times that for a single pulse, but the modes are redistributed into the n-slit form, with constructive enhancement in some modes, and destructive interference in other modes.

In this dissertation we consider not just these final values for the asymptotic particle number, but also the *time evolution* of the adiabatic particle number. Since Berry's universal time-evolution corresponds to the behavior in the vicinity of a single turning point pair, we need to generalize the result (2.113) to the case with several (complex conjugate pairs of) turning points, as occurs for electric fields with nontrivial temporal substructure [67,68]. Some steps in this direction were taken for non-relativistic two-level systems [104,105].

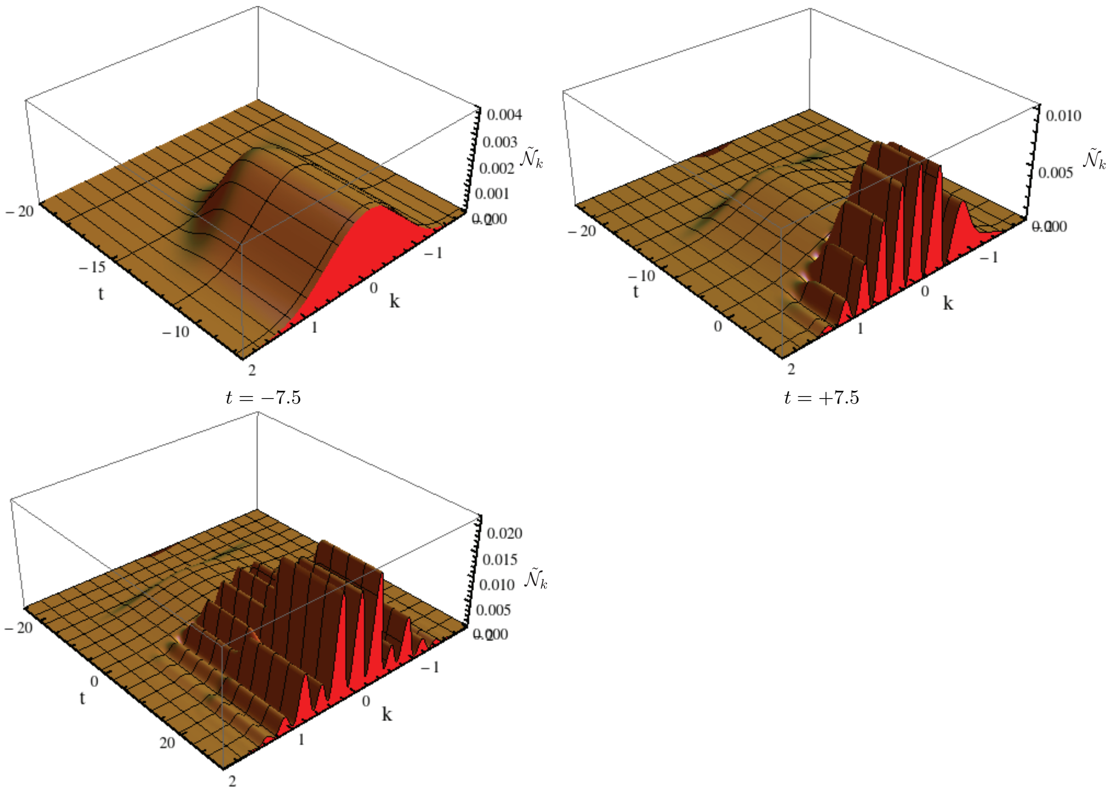

$t = -7.5$ $t = +7.5$

$t = +30$

Fig. 2.18: As in Figure 2.19, but plotted over specific time ranges, ending with cross sections at $t = \mp 7.5, +30$, to illustrate the time evolution of $k_\parallel$-momentum spectrum (red-filled) for different periods of particle creation due to pulse events at $t = 0, \pm 15$. The highlighted longitudinal momentum spectrum of each subplot follows the n-slit interference pattern (2.129), which can be compared to the asymptotic momentum spectra shown in Figure 2.17. Additional details found in text.

The natural generalization of (2.113) is the following:

$$\tilde{\mathcal{N}}_k(t) \approx \frac{1}{4}\left|\sum_{t_p}\exp\left(2i\theta_k^{(p)}\right)\exp\left(-F_{k,t_p}^{(0)}\right)\mathrm{Erfc}\left(-\sigma_k^{(p)}(t)\right)\right|^2 \tag{2.130}$$

We have verified numerically that this form fits well with the time evolution of the optimal adiabatic particle number for sequences of time-dependent pulses for different field parameters and different momenta. In Figures 2.19 and 2.18 we show plots of the approximation of the optimal adiabatic particle number (2.113)

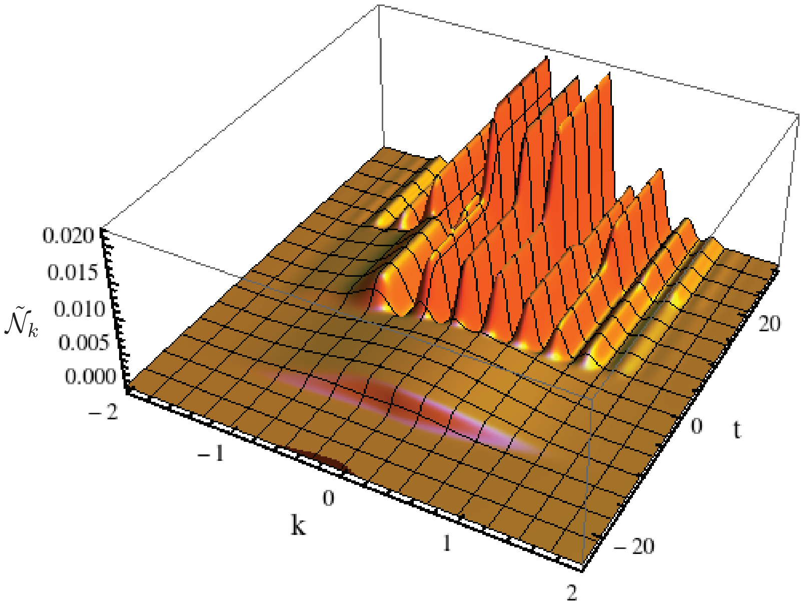

Fig. 2.19: The approximate optimal adiabatic particle number (2.130) as a function of t and $k_{\|}$, for Schwinger pair production for alternating-sign triple-pulse (2.124) with $E_0 = 0.5$, $a = 0.25$, $b = 7.5$, and $k_{\perp} = 0$, in units with $m = 1$. A full time range realization of the cross-sections calculated in Figure (2.17) with particle creation events located at $t = 0, \pm 15$. Notice that $\tilde{\mathcal{N}}_k^{(j)}$ is critically dependent on the longitudinal momentum, indicating whether enhancement or cancellation occurs for produced particles with momentum $k_{\|}$.

as a function of both time and the longitudinal momentum of the produced particles. These plots show the smooth evolution of the quantum interference effects due to three separate particle creation events and how they critically dependent on the value of the longitudinal momentum . After the first pulse, and before the second pulse, the momentum distribution has the form that would be obtained asymptotically at future infinity from just a single pulse. But after the second pulse, and before the third pulse, the momentum distribution has the form that would be obtained asymptotically at future infinity from a sequence of two alternating-sign pulses. Finally, after the third pulse, we observe a momentum distribution of the form that would be obtained asymptotically at future infinity from the full sequence of three alternating-sign pulses. In Figure 2.18 we emphasize the interference effects of the time dependent optimal adiabatic particle number with cross-sections of the momentum distributions at times in-between the pulses. These time-slices coincide with the final future infinity particle number momentum distributions shown in Figure 2.17 for one, two and three pulses, respectively.

2.13 Particle Production as the Measure of Small Deviations

We now study the fine details of the time dependence of the adiabatic particle number using the definition of the adiabatic particle number (2.45) first presented in Section 2.3 with the Bogoliubov formalism and equivalently shown through the Riccati (Section 2.4), Spectral Function (Section 2.5), and Schrödinger Picture (Section 2.6): a time-dependent adiabatic particle number determined by the minute differences between the adiabatic basis (W_k, V_k) and the exact solution to the Ermakov equation (2.19). Recall that truncating the adiabatic expansion at different orders typically has only a small effect on $W_k(t)$, compared to the leading order of the expansion $W_k = \omega_k(t)$, but nonetheless have a large and non-trivial effect on the time evolution of the adiabatic particle number. In this section we explore how these small deviations of the adiabatic approximation influence the evolution of the adiabatic particle number, and show how this manifests in the physical phenomenon of quantum interference.

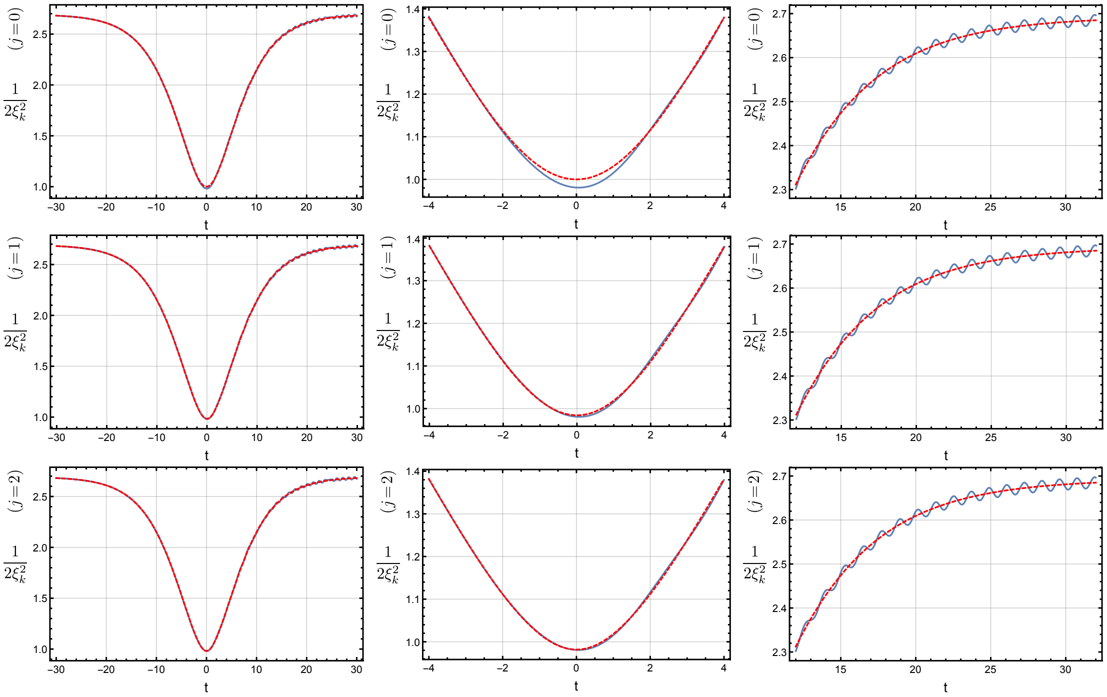

Fig. 2.20: The adiabatic approximation (2.131) of $1/(2\xi_k^2)$ (blue-solid line) compared to the adiabatic function $W_k^{(j)}$ (red-dashed line), for the first 3 orders of the adiabatic expansion, considering the single-pulse E-field (2.119) with $E_0 = 0.25$, $a = 0.1$, $k_\parallel = 0$, and $k_\perp = 0$, in units with $m = 1$. The central panels zoom in on time-scales near the pulse, while the right-hand panels zoom in on the late-time behavior. The deviations of the approximation from the exact form are typically very small, capturing well the averaged time dependence except near the the peak of the pulse, and except for tiny oscillations about the average value at late times.

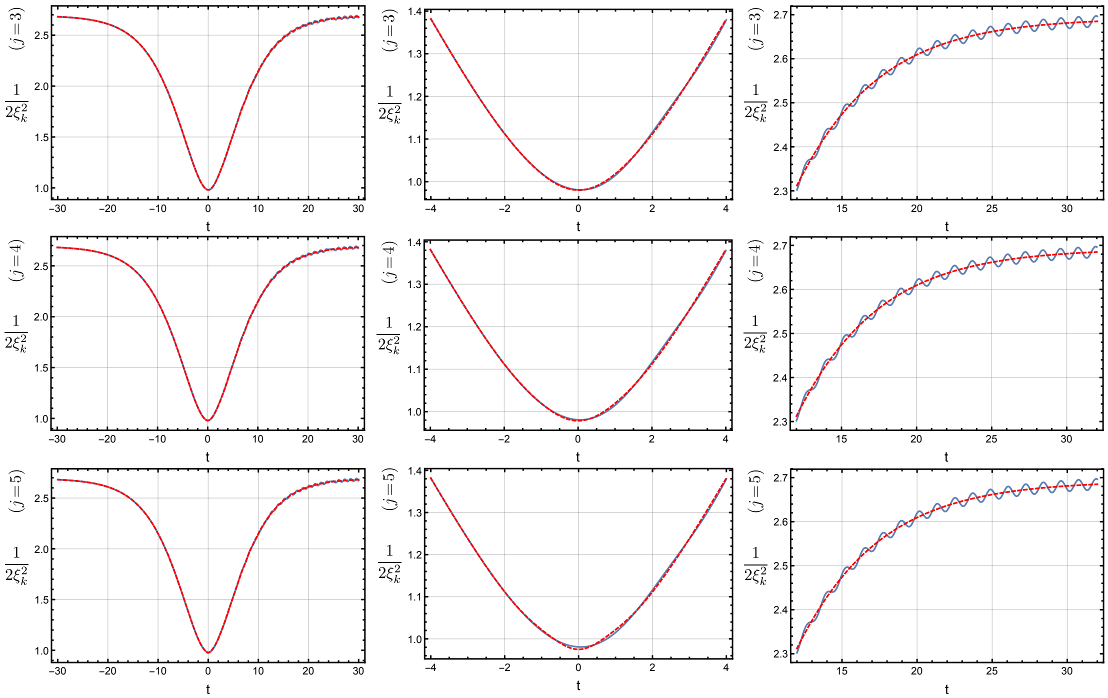

Fig. 2.21: As in Figure 2.20 but with plots of the next three adiabatic orders, $j = 3, 4, 5$ for the adiabatic approximation (2.131) of $1/(2\xi_k^2)$ (blue-solid line) compared to the adiabatic function $W_k^{(j)}$ (red-dashed line), considering the single-pulse E-field (2.119) with $E_0 = 0.25$, $a = 0.1$, $k_\parallel = k_\perp = 0$, in units with $m = 1$. The central panels zoom in on time-scales near the pulse, while the right-hand panels zoom in on the late-time behavior. The deviations of the approximation from the exact form are typically very small, capturing well the averaged time dependence except near the the peak of the pulse, and except for tiny oscillations about the average value at late times. The optimal order is reached at $j = 3$, after which the deviations begin to grow again.

2.13.1 Optimal Adiabatic Approximation of the Ermakov-Milne Equation

In Section 2.3, the adiabatic particle number was found to be determined by the projection of the solution $f_k(t)$ of the Klein-Gordon equation (2.16) against a basis set of approximate adiabatic states $\tilde{f}_k(t)$ defined in (2.27). The reference states $\tilde{f}_k(t)$ are chosen to be as good as possible approximations to the exact solution $f_k(t)$, with the appropriate particle production boundary conditions in (2.24). Therefore, the approximation is effectively characterized at j-th order of the adiabatic expansion by

$$\xi_k \sim \left(2W_k^{(j)}\right)^{-\frac{1}{2}} \tag{2.131}$$

and

$$\frac{\dot{\xi}_k}{\xi_k} \sim V_k^{(j)} \equiv -\frac{\dot{W}_k^{(j)}}{2W_k^{(j)}} \tag{2.132}$$

This last approximation can be equivalently seen as neglecting the exponentially small r_k^* in (2.73). Notice that the approximation (2.132) is the ratio form of the first derivative of approximation (2.131), and thus is consistent with the 'natural' basis choice (2.98).

The structure of the adiabatic particle number in (2.99) is explicitly composed of the differences of the adiabatic approximations (2.131, 2.132). We now examine how these approximations work in practice with the adiabatic expansion truncated at various adiabatic orders.

Single-pulse Electric Field

Figures 2.20 and 2.21 examine the adiabatic approximation (2.131) by directly comparing $1/(2\xi_k^2)$ with the adiabatic functions $W_k^{(j)}$ for various adiabatic orders,

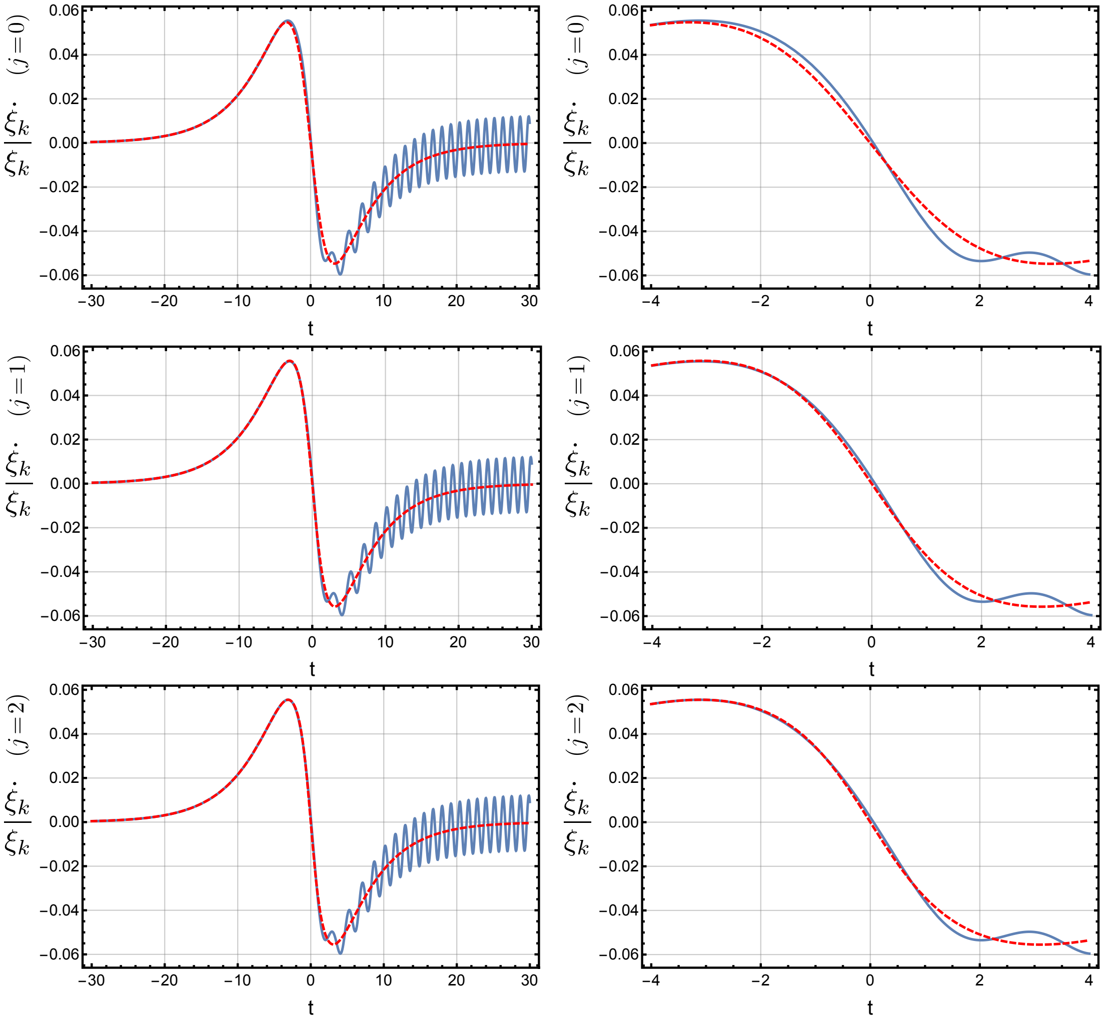

Fig. 2.22: Plots of approximation (2.132), the time derivative form of (2.131) as a ratio, by comparing $\dot{\xi}_k/\xi_k$ (blue-solid line) with the adiabatic function $V_k^{(j)} = -\dot{W}_k^{(j)}/(2W_k^{(j)})$ (red-dashed line), for the first three orders of the adiabatic expansion, considering the single-pulse E-field (2.119) with the same parameters as for Figure 2.20. The left-hand panels show the time-evolution over a wide time range, and the right-hand panels zoom in on the vicinity of the pulse. The approximate (red-dashed) curves accurately describe the averaged time evolution, but miss the late-time oscillations, which are more pronounced than those in Figures 2.20 and 2.21 because they are effectively the derivatives of those small oscillations.

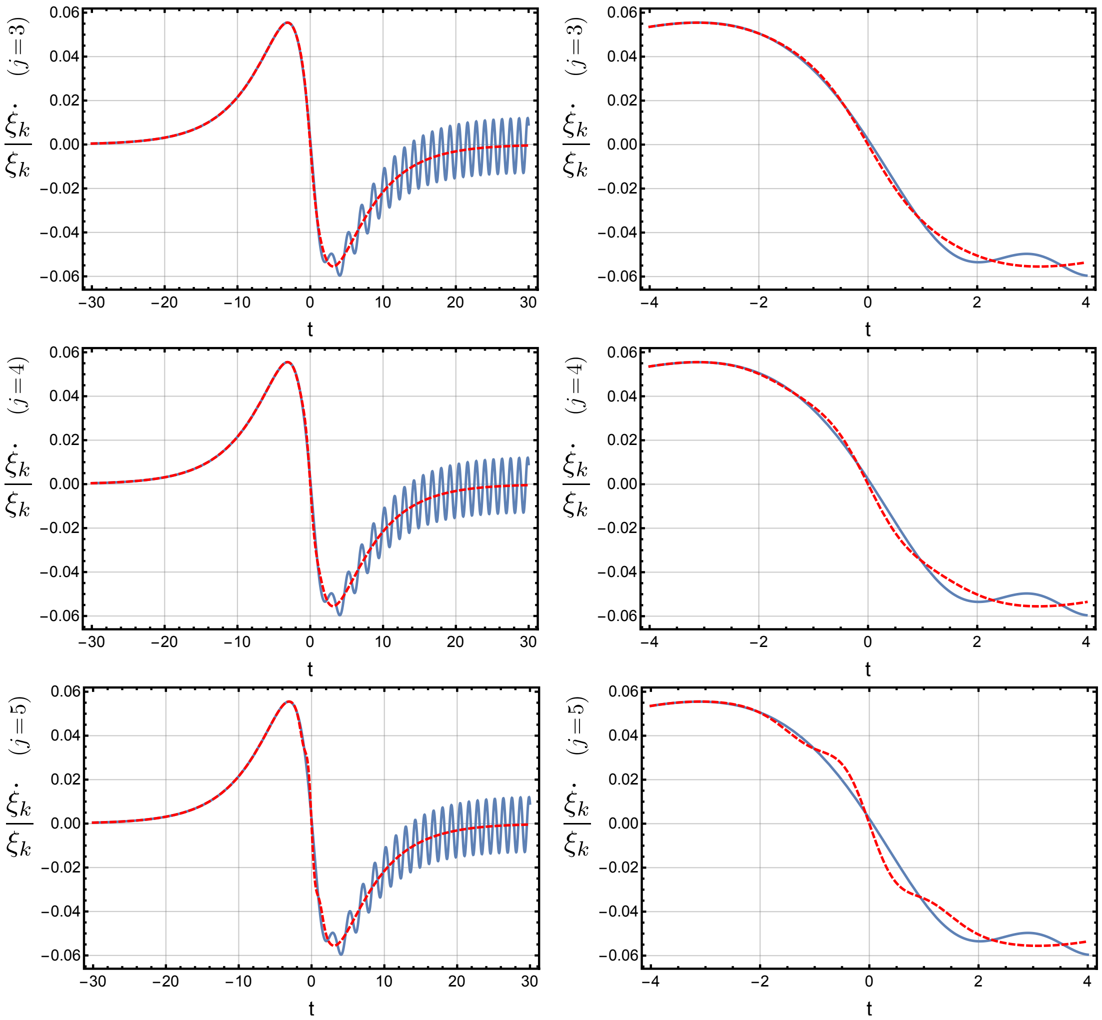

Fig. 2.23: As in Figure 2.22, but with plots of the next three adiabatic orders, $j = 3, 4, 5$, showing the approximation (2.132), the time derivative form of (2.131) as a ratio, by comparing $\dot{\xi}_k/\xi_k$ (blue-solid line) with the adiabatic function $V_k^{(j)} = -\dot{W}_k^{(j)}/(2W_k^{(j)})$ (red-dashed line), considering the single-pulse E-field (2.119) with the same parameters as for Figure 2.20. The left-hand panels show the time-evolution over a wide time range, and the right-hand panels zoom in on the vicinity of the pulse. The approximate (red-dashed) curves accurately describe the averaged time evolution, but miss the late-time oscillations, which are more pronounced than those in Figures 2.20 and 2.21 because they are effectively the derivatives of those small oscillations.

considering a single-pulse time-dependent electric field of the form (2.119) given by the vector potential (2.120).

Figure 2.20 considers the first three adiabatic orders, while Figure 2.21 considers the next three orders. The left-hand figures show the time-evolution over a wide range of t; the central panels zoom in on the vicinity of the pulse, and the right-hand panels zoom in on the late time behavior. Notice that the approximation (2.131) is extremely good, with only very small deviations between $W_k^{(j)}(t)$ and $1/(2\xi_k^2(t))$, which moreover do not change in any particularly dramatic fashion as the truncation order changes. Notice the tiny oscillations about an accurate time-averaged approximation at late times. There are small deviations near the time location of the pulse, which shrink until the optimal order and then begin to grow again. Again, this is typical of adiabatic expansions where the optimal order of truncation corresponds to a minimum error approximation, and results in $W_k^{(j)}$ corresponding to the optimal adiabatic approximation of $1/(2\xi_k^2)$. This optimal approximation represents a simple 'best possible' approximation.

Figures 2.22 and 2.23 examine the adiabatic approximation (2.132), the first derivative ratio form of approximation (2.131), by directly comparing $\dot{\xi}_k/\xi_k$ with the basis function $V_k^{(j)} = -\dot{W}_k^{(j)}/(2W_k^{(j)})$, evaluated at various orders j of the adiabatic expansion, using the same electric field configuration and parameters as used for Figures 2.20 and 2.21. Figure 2.22 considers the first three adiabatic orders, while Figure 2.23 considers the next three orders. In both Figures 2.22

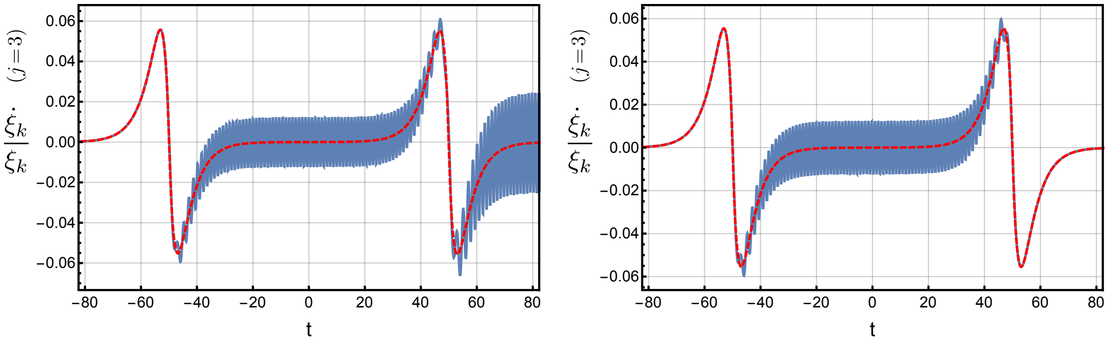

Fig. 2.24: Plots of the approximation (2.132) at the optimal truncation order ($j = 3$), for the time derivative form of (2.131) as a ratio, by comparing $\dot{\xi}_k/\xi_k$ (blue-solid line) and $V_k^{(j)} = -\dot{W}_k^{(j)}/2W_k^{(j)}$ (red-dashed line), for the double-pulse E-field (2.122) with $E_0 = 0.25$, $a = 0.1$, $b = 50$, and $k_\perp = 0$, in units with $m = 1$. $k_\parallel$ was selected to correspond to maximum constructive ($k_\parallel = 2.51555$, left subplot), and maximum destructive interference ($k_\parallel = 2.49887$, right subplot) in the particle number at future infinity. In the maximum constructive case, the oscillations introduced after each pulse interfere to double in magnitude. In the maximum destructive case, the oscillations introduced by the first and second pulse interfere to completely cancel.

and 2.23, $\dot{\xi}_k/\xi_k$ is plotted as a solid-blue curve, and $V_k^{(j)} = -\dot{W}_k^{(j)}/(2W_k^{(j)})$ is plotted as a dashed-red curve. The left-hand panels show the time-evolution over a wide range of t, and the right-hand panels zoom in on the vicinity of the pulse. Notice that there are once again oscillations about an accurate time-averaged approximation at late times, but that these oscillations are now larger than those seen at late times in Figures 2.20 and 2.21. This is because this is effectively measuring the *derivatives* of the tiny late-time oscillations in Figures 2.20 and 2.21. We also see that the changes from one order of truncation to the next are not particularly pronounced.

Alternating-sign Double-pulse Electric Field

We now examine the approximations by considering a time-dependent electric field with non-trivial temporal structure, to illustrate the phenomenon of quantum interference. Figures 2.24, 2.25 and 2.26 examine the adiabatic approximation (2.132) by considering the alternating sign double-pulse electric field of the form (2.122), given by the time-dependent vector potential (2.123).

Figure 2.24 compares the adiabatic approximation (2.132) at the optimal order of truncation, $j = 3$, for two different cases of constructive (left panel), and destructive (right panel) interference. At this optimal order, $V_k^{(3)}$ corresponds to the optimal adiabatic approximation of $\dot{\xi}_k/\xi_k$, accurately capturing the average of its amplitude at all times, but missing the oscillatory behavior, which encodes critical information regarding particle production. Figures 2.25 and 2.26 show zoomed-in views, near each of the pulses, for the left and right panels of Figure 2.24, respectively. Figures 2.25 and 2.26 are plotted with the same pulse parameters but with different longitudinal momentum to highlight the manifestation of quantum interference that are associated with electric fields having non-trivial temporal structure [43,67,68]. Specifically, the longitudinal momentum in Figure 2.25 corresponds to maximum *constructive* interference in the adiabatic particle number at asymptotic times, while the longitudinal momentum in Figure 2.26 corresponds to maximum *destructive* interference. A similar adiabatic order-by-order comparison of the adiabatic approximation shows the same trend observed

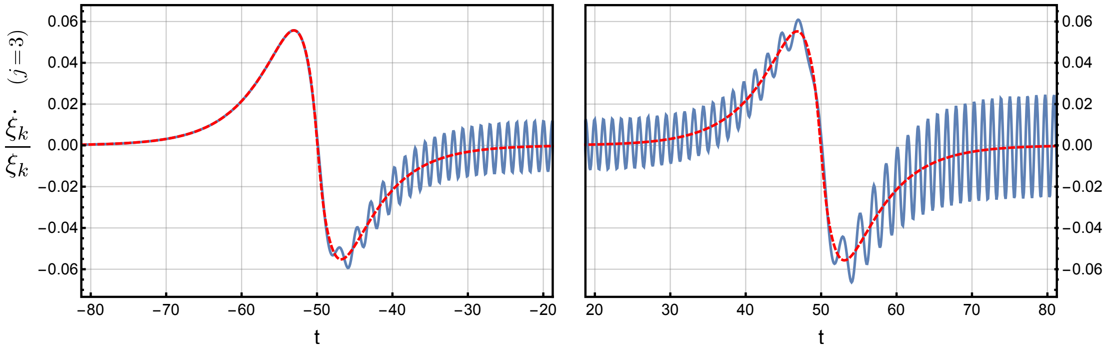

Fig. 2.25: Zoomed-in view of the left subplot of Figure 2.24, plotted for a closer examination of the approximation (2.132) in the vicinity of the pulse centers ($t = \pm 50$), for the case of maximum constructive interference.

in Figures 2.20, 2.21, 2.22, and 2.23: the matching of both sides of approximation (2.132) improve until the optimal order is achieved, and then grows more and more mismatched after this optimal order of truncation. The oscillations in $\dot{\xi}_k/\xi_k$ directly correspond to quantum interference: in Figure 2.25, we observe oscillations that increase in magnitude as a result of each pulse and constructively interfere with one another to double in magnitude; while in Figure 2.26 we observe oscillations that increase in magnitude as a result of the first pulse but then cancel completely as the oscillations introduced by the second pulse destructively interfere with the first. Note that the magnitude of the oscillations in between the two pulses in Figures 2.25 and 2.26, which are widely temporally separated, are equal to the magnitude of the oscillations at asymptotic times in the single-pulse case in Figures 2.22 and 2.23.

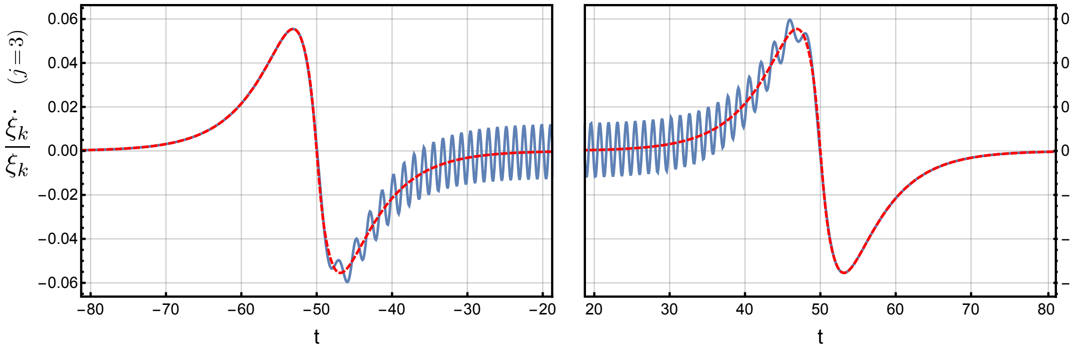

Fig. 2.26: Zoomed-in view of the right subplot of Figure 2.24, plotted for a closer examination of the approximation (2.132) in the vicinity of the pulse centers ($t = \pm 50$), for the case of maximum destructive interference.

2.13.2 Adiabatic Particle Number as a Measure of Small Deviations

In this subsection we examine how the small deviations from the adiabatic approximations (2.131, 2.132) determine the adiabatic particle number. We re-write the expression (2.99) as the sum of two terms, the first of which measures the deviations of the adiabatic approximation (2.131), and the second of which measures the deviations of the adiabatic approximation (2.132):

$$\tilde{\mathcal{N}}_k^{(j)}(t) = \frac{1}{4}\left(\sqrt{2W_k^{(j)}\xi_k^2} - \frac{1}{\sqrt{2W_k^{(j)}\xi_k^2}}\right)^2 + \frac{1}{4}\left(\frac{\frac{d}{dt}\left(\sqrt{2W_k^{(j)}\xi_k^2}\right)}{W_k^{(j)}}\right)^2 \tag{2.133}$$

As shown in the previous subsection, the relationship between the exact solution $\xi_k(t)$ to the Ermakov-Milne equation and the adiabatic expansion functions $W_k^{(j)}(t)$ are given by the approximations (2.131, 2.132). The structure of the adiabatic particle number (2.99) specifically extracts the very small changes introduced by truncating the adiabatic expansion at different orders and the small oscillations from the exact solution to the Ermakov-Milne equation that directly encode the particle production phenomenon. This yields a new perspective: particle production is characterized by the measure of these small deviations. The first

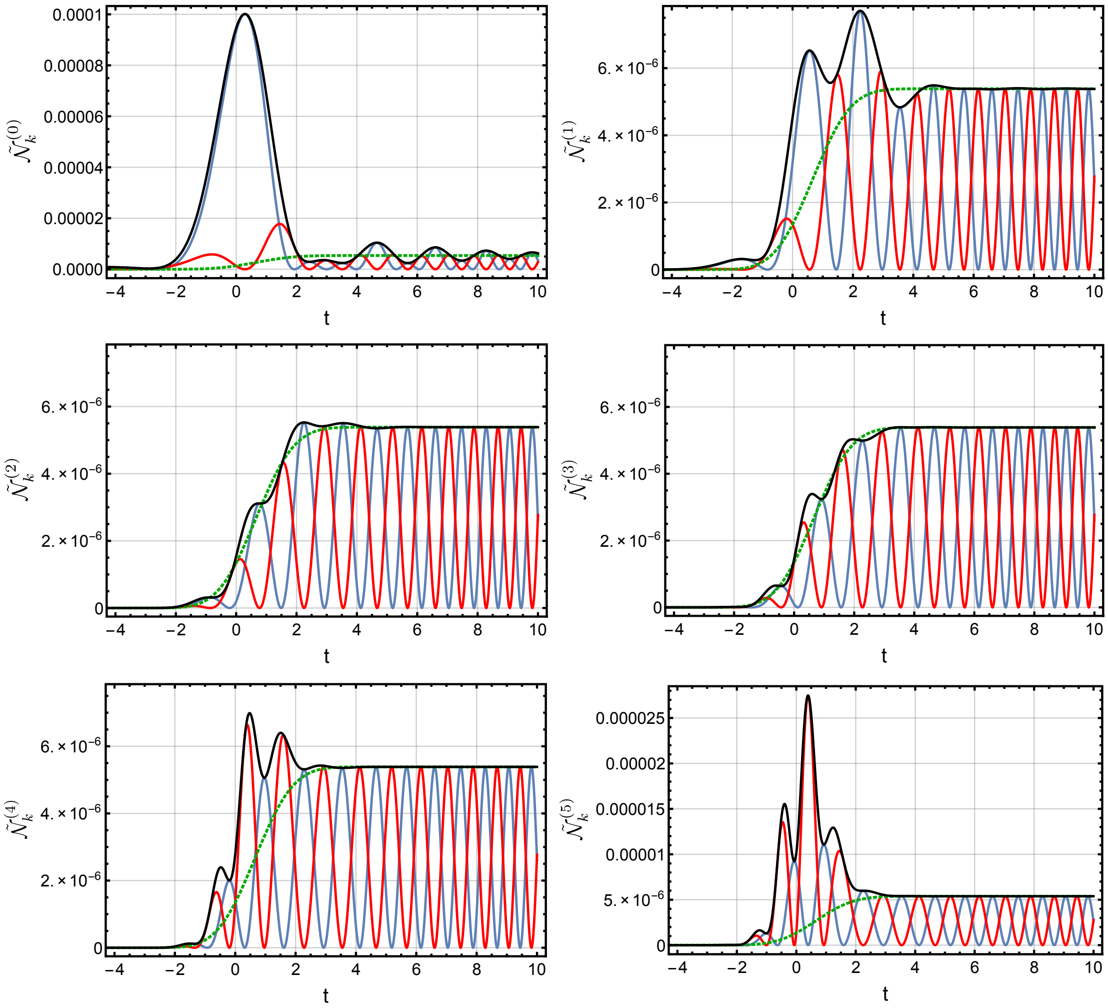

Fig. 2.27: $\tilde{\mathcal{N}}_k^{(j)}(t)$ (2.133) (black-solid line), and its components, the first (blue-solid line) and second (red-solid line) terms on the right-hand-side of (2.133), for the first 6 orders of the adiabatic expansion, considering a single-pulse E-field (2.119) with $E_0 = 0.25, a = 0.1$, $k_{\parallel} = 0$, and $k_{\perp} = 0$, in units with $m = 1$. Notice that each of the components (blue and red curves) is highly oscillatory, and out of phase, but the sum is smooth except in the vicinity of the pulse. Also note the difference in scales in the various sub-plots. The deviations decrease dramatically as the optimal order ($j_{\text{opt}} = 3$) is approached, and then grow again after this order. See text for additional details.

term on the right-hand-side of (2.133) measures the deviations of $2W_k^{(j)}(t)\xi_k^2(t)$ from 1, while the second term on the right-hand-side of (2.133) effectively measures the derivatives of this deviation.

In Figure 2.27 we see the results of these small deviations. The black solid line in Figure 2.27 shows the exact adiabatic particle number, for the first six orders of the adiabatic expansion. These are the curves plotted previously as solid blue lines in Figure 2.8. The blue and red curves in Figure 2.27 show, respectively, the first and second terms on the right-hand-side of (2.133). Notice that their combined envelope matches the adiabatic particle number (the black curve), but the blue and red curves oscillate out of phase with one another, since the latter effectively characterizes the time derivative of the former. Each component is highly oscillatory, especially at late times, but their envelope is smooth except in the vicinity of the pulse. Also notice the difference of scales in the various sub-plots. The deviations decrease significantly as the optimal order is approached, and then grow again as this order is passed. The green dashed line shows Berry's universal approximation, which matches the optimally truncated order of the adiabatic expansion (here $j = 3$). At the optimal order, we see the culmination of the optimal adiabatic approximation of the Ermakov-Milne equation in the final answer of the particle number: the scale of the oscillations of both components become comparable, they level off much more quickly, and sum to yield the smoothest time evolution of the adiabatic particle number.

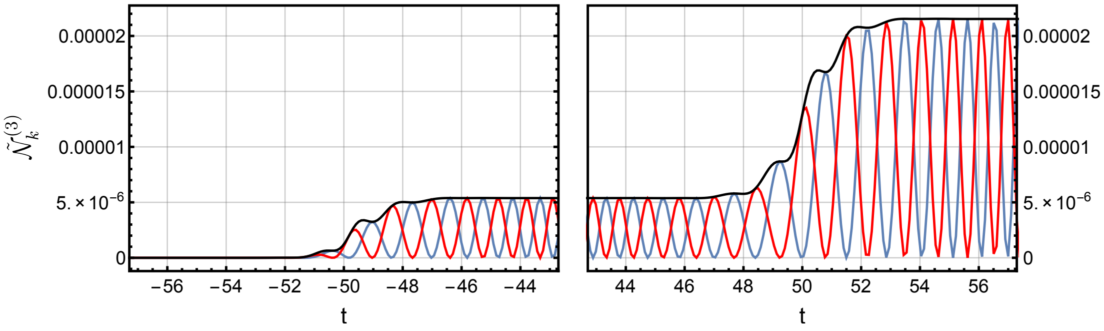

Fig. 2.28: $\tilde{\mathcal{N}}_k^{(j_{\rm opt})}(t)$ (2.133) (black-solid line), and its components, the first (blue-solid line) and second (red-solid line) terms on the right-hand-side of (2.133), for the double-pulse E-field (2.122) with $E_0 = 0.25, a = 0.1, b = 50$, $k_\parallel = 2.51555$, and $k_\perp = 0$, in units with $m = 1$. $k_\parallel$ was selected for maximum constructive interference, with the final value being 4 times the intermediate plateau value between the two pulses. At intermediate times, notice the phase difference of the oscillatory components of (2.133), which remarkably sum to a smooth evolution of $\tilde{\mathcal{N}}_k^{(j_{\rm opt})}$.

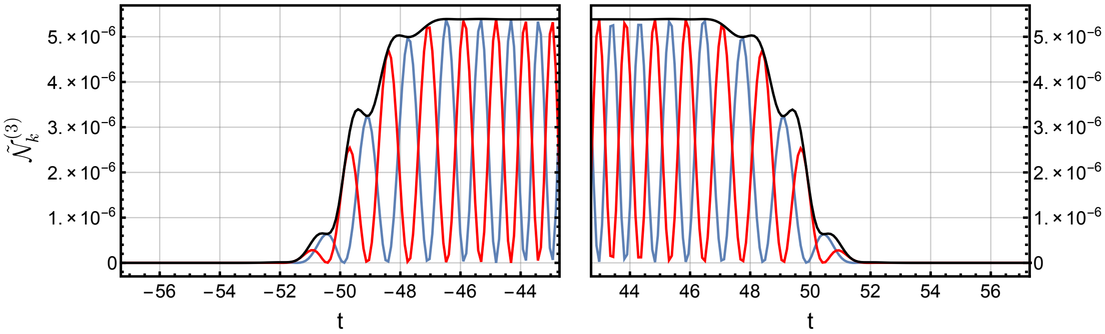

Fig. 2.29: $\tilde{\mathcal{N}}_k^{(j_{\rm opt})}(t)$ (2.133) (black-solid line), and its components, the first (blue-solid line) and second (red-solid line) terms on the right-hand-side of (2.133), for the double-pulse E-field (2.122) with $E_0 = 0.25, a = 0.1, b = 50$, $k_\parallel = 2.49887$, and $k_\perp = 0$, in units with $m = 1$. $k_\parallel$ was selected for maximum destructive interference, with vanishing final particle number at future infinity. At intermediate times, notice the phase difference of the oscillatory components of (2.133), which remarkably sum to a smooth evolution of $\tilde{\mathcal{N}}_k^{(j_{\rm opt})}(t)$.

In Figures 2.28 and 2.29 we plot in blue and red the same two components of the right-hand-side of the expression (2.133), but consider the alternating sign double-pulse electric field given by (2.122). Both Figures utilize the same pulse parameters, but with different longitudinal momentum that correspond to maximum constructive interference, Figure 2.28, and maximum destructive interference, Figure 2.29. The constructive interference can be seen in Figure 2.28 as the final value of the particle number at future infinity $\tilde{\mathcal{N}}_k(+\infty)$ is $4 = 2^2$ times the value at times in between the two pulses. The destructive interference can be seen in Figure 2.29 through the vanishing final value of the particle number at future infinity $\tilde{\mathcal{N}}_k(+\infty)$. Both figures show just the optimal order of truncation of the adiabatic expansion ($j = 3$ for these parameters), but we have confirmed that a similar adiabatic order-by-order comparison shows the same trend exhibited in the phase and scale of the oscillations, as seen in Figure 2.27. In Figure 2.28, the interference results in the components being out of phase in such a way to produce enhancement of particle production, which follow an n^2 coherence pattern (see Section 2.12), while in Figure 2.29 it leads to cancellation with no particles produced at the final time. Again, in each case, the two different components of (2.133) remarkably sum to produce a smooth evolution of the particle number at all times.

2.14 Extroduction

In this Chapter we have explored the structure of the time evolution of the adiabatic particle number for particle production in time-dependent electric fields (the Schwinger effect). Through the Ermakov-Milne equation (2.19), for the *amplitude* of the solution to the Klein-Gordon equation (2.16), an analytic expression (2.99) for the time-dependent adiabatic particle number was derived by projection of the exact solution $\xi_k(t)$ against a basis of approximate adiabatic reference states, characterized by the function $W_k(t)$ defined in (2.27), and its various orders of adiabatic approximation defined in (2.93). The form of expression (2.99) clearly illustrates the separation between the exact solution and the choice of adiabatic basis, and illustrates the role of the adiabatic approximation in defining the reference states. We showed that the Bogoliubov, Riccati, Spectral Function, and Schrödinger approaches to the adiabatic particle number each yield the same analytic expression for the particle number, indicating that this form of basis dependence is a universal feature of the definition of the adiabatic particle number at intermediate times.

In defining an optimal adiabatic particle number as that corresponding to the optimal truncation of the adiabatic expansion, we found very good agreement with Berry's universal error-function form of the time evolution (2.113) for a single pulse creation event, and with our generalization (2.130) for backgrounds with structure corresponding to multiple particle creation events. The universality of the approximate expression for the optimal adiabatic order means that in fact one does not need to make the explicit adiabatic expansion to the optimal order, which is complicated at high orders, and moreover for which the optimal order depends on the physical parameters. Instead, equations (2.113) and (2.130) express the universal time-evolution form that approximates well the optimal order in a simple and compact way. We have demonstrated the accuracy of the results in a variety of electric field configurations and demonstrated that the resulting time evolution reveals the quantum interference processes at work in the Stokes phenomenon, which is ultimately responsible for particle production. Depending on the phase accumulated by the Bogoliubov coefficients between successive turning points, the net particle number at future infinity can be understood in terms of quantum interference between different particle creation events. For the Schwinger effect we illustrated this for sequences of two and three alternating-sign electric field pulses, which can exhibit both constructive or destructive interference, depending on the momentum of the produced particles.

Finally the structure of (2.99) also shows that the adiabatic particle number may be characterized by the small deviations between the exact solution and its adiabatic approximations. These small deviations clearly show the manifestation of quantum interference effects, explicitly shown for the double-pulse sign-alternating electric field in (2.122), which exhibits both constructive and destructive interference, depending on the longitudinal momentum of the produced particles. At the optimal order of truncation of the adiabatic approximation, the deviations are the smallest and smoothest, and correspond to an optimal adiabatic approximation.

Chapter 3

Cosmological Particle Production

3.1 Overview

Particles can also be produced from the vacuum under the influence of gravitational curvature. A few well known examples include cosmological particle production due to expanding cosmologies [6–8,16,17,106] and de Sitter spacetime [13,14,18,19,22,23,107–109], Hawking radiation due to the gravitational horizon effects of black holes [10,110–116], and the Unruh effect [116], the particle number that an accelerating observer sees.

In this Chapter we examine de Sitter cosmological production of conformally coupled scalars in *Eternal* de Sitter spacetime where the mode decomposition of the equations of motion yield an analogous mode oscillator equation to that of sQED discussed in Chapter 2. It is known [13,14,107] that in even space-time dimensions there is particle production in de Sitter space, but that there is no particle production in odd space-time de Sitter space [108,117]. It has been argued in [118,119] that this difference between particle production in even and odd dimensional de Sitter space can also be understood in terms of quantum interference between two sets of complex turning points, and the associated Stokes phenomenon. Applying the techniques and results demonstrated in Chapter 2, we analyze this question for the full time evolution of the optimal adiabatic particle number for particles produced in an eternal de Sitter spacetime.

3.2 Scalar Fields conformally coupled to a de Sitter Spacetime

We consider a free scalar field in a d dimensional de Sitter gravitational background. The action of this coupled massive scalar is

$$S[\varphi] = \int dx^d \sqrt{-g} \left[\frac{1}{2} g^{\mu\nu} \varphi_{,\mu} \varphi_{,\nu} - \frac{\eta_d}{2} R \varphi^2 - \frac{m^2}{2} \varphi^2 \right] \tag{3.1}$$

where R is the Ricci Curvature Scalar, η_d is the gravitational Coupling Parameter, and m is the mass of the scalar field. Coupling the field to a d-dimensional de Sitter (dS_d) for a *Friedman-Robertson-Walker* (FRW) metric:

$$ds^2 = -dt^2 + a^2(t)\, d\Sigma^2_{d-1} \tag{3.2}$$

where $a(t)$ is the expansion parameter of the spacetime and $d\Omega^2_{d-1}$ denotes the infinitesimal surface area of a d-dimensional hypersphere. The FRW metric implies a conformally flat spacetime with a constant curvature given by

$$R = d(d-1)H^2 \tag{3.3}$$

where H is a scale parameter to the curvature. We specify that expansion parameter using *Eternal De Sitter Spacetime* global coordinates:

$$a(t) = \frac{1}{H}\cosh(Ht) \tag{3.4}$$

Upon extremizing the action (3.1), yields the equations of motion

$$g^{\mu\nu}\varphi_{,\mu\nu} + \frac{1}{\sqrt{-g}}\Big(g^{\mu\nu}\sqrt{-g}\Big)_{,\mu}\varphi_{,\nu} + \xi R\varphi + m^2\varphi = 0\ , \tag{3.5}$$

covariantly written as

$$\varphi_{;\mu}^{;\mu} + \left(\eta_d R + m^2\right)\varphi = 0 \tag{3.6}$$

where

$$\varphi_{;\mu}^{;\mu} = a^{-(d-1)}(t)\,\partial_t\Big(a^{d-1}(t)\partial_t\varphi\Big) - a^{-2}(t)\Delta_{S^{d-1}}\varphi \tag{3.7}$$

and $\Delta_{S^{d-1}}$ is the corresponding d-dimensional Spherical Laplacian.

Akin to the decomposition made in Section 2.3, the field can be decomposed to spherical mode functions by introducing time-independent bosonic creation/annihilation operators $a_{\mathbf{k}}, b_{-\mathbf{k}}$ and time-dependent, spatially homogenous, complex mode function $f_{klm_l}(t)$ as

$$\varphi_k = \frac{1}{a^{(d-1)/2}(t)}\sum_{k=1}^{\infty}\sum_{l=0}^{k}\sum_{m_l=-l}^{l}\Big[f_{klm_l}(t)\,a_{klm_l}Y_{klm_l}\big(\Sigma^{d-1}\big) + f^*_{klm_l}(t)\,a^\dagger_{klm_l}Y^*_{klm_l}\big(\Sigma^{d-1}\big)\Big] \tag{3.8}$$

The overall factor of $a^{-(d-1)/2}$, the bosonic equal-time commutation relations,

$$\Big[a_{klm_l}\ ,\ a^\dagger_{k'l'm'_l}\Big] = \delta_{kk'}\delta_{ll'}\delta_{m_l m'_l} \tag{3.9}$$

and the orthogonalization condition on the spherical harmonic functions for the unit radius d-dimensional hypersphere,

$$\int_{\mathbb{S}^{d-1}} d\Sigma^{d-1}\, Y_{klm_l}(\mathbb{S}^{d-1})\, Y_{k'l'm'_l}\big(\mathbb{S}^{d-1}\big) = \delta_{kk'}\delta_{ll'}\delta_{m_l m'_l} \quad , \tag{3.10}$$

impose the Wronskian condition on the mode function $f_{klm_l}(t)$ as

$$\mathrm{Wr}\big[f_{klm_l}(t), f^*_{klm_l}(t)\big] = f_{klm_l}(t)\dot{f}^*_{klm_l}(t) - \dot{f}_{klm_l}(t)f^*_{klm_l}(t) = i, \tag{3.11}$$

Substituting the spherical mode decomposition (3.8) into the equations of motion (3.6), where $\Delta_{S^{d-1}}Y_{klm_l} = -k(k+d-2)Y_{klm_l}$, yields an oscillator mode equation that is analogous to the sQED case:

$$\ddot{f}_k(t) + \omega_k^2(t) f_k(t) = 0 \tag{3.12}$$

such that [6–8,12–14,20,21]

$$\omega_k^2(t) = H^2\left(\gamma^2 + \left(\frac{2k+d-3}{2}\right)\left(\frac{2k+d-1}{2}\right)\mathrm{sech}^2(Ht)\right) \tag{3.13}$$

$$\gamma^2 = \frac{m^2}{H^2} + d(d-1)\left(\eta_d - \frac{d-2}{4(d-1)}\right) - \frac{1}{4} \tag{3.14}$$

for $d \geq 1$. A scalar field theory conformally coupled to gravity occurs under the condition:

$$\eta_d = \frac{d-2}{4(d-1)} \tag{3.15}$$

where, for example, $\eta_3 = \frac{1}{8}$ in $d = 3$, and $\eta_4 = \frac{1}{6}$ in $d = 4$.

3.3 Spacetime Implications for Cosmological Particle Production

In this section we illustrate how the adiabatic particle number for cosmological particle production can be viewed as coherent *constructive* interference in even dimensional de Sitter space and as coherent *destructive* interference in odd dimensional de Sitter space. We find that in even dimensions there is coherent constructive interference, while for odd dimensions destructive interference leads to the vanishing of the net particle number. The resulting behavior is similar to that of the two-pulse electric field example, with either constructive (even dimensions) or destructive (odd dimensions) interference.

3.3.1 Optimal Adiabatic Particle Number in 4d de Sitter space: Coherent Constructive Interference

We compute the adiabatic particle number numerically using (2.100, 2.101), for various orders j of the adiabatic expansion, starting with the time-dependent frequency for four dimensional de Sitter space, from (3.12, 3.14). We consider conformal coupling, so that $\eta_4 = \frac{1}{6}$ in 4 dimensions.

The results are shown in Figure 3.1. Note the strong similarity to the two-alternating-sign-pulse Schwinger effect, with particle momentum such that the interference is constructive, as shown in Figure 2.10. In the leading order of the adiabatic expansion, there are two large oscillatory peaks, several orders of magnitude larger than the final asymptotic particle number. As the order of the adiabatic expansion increases these oscillations become smaller, and at the optimal order ($j = 3$) the optimal adiabatic particle number evolves much more smoothly. Moreover, we clearly see the two-step structure, with the final plateau being 4 times the height of the intermediate plateau. This is indicative of coherent constructive interference. Note also that this is completely consistent with the analysis of [13,14]. See, for example, Figure 6 of [13], where two creation events can be clearly seen, again associated with the two towers of complex-conjugate turning points. Moreover, the first plateau is given in [13] by

$$\Delta N_1 = \frac{1}{e^{2\pi\,\gamma} - 1} \approx e^{-2\pi\gamma} \tag{3.16}$$

while the second plateau is given by

$$\Delta N_2 = \frac{1}{\sinh^2(\pi\,\gamma)} \approx 4\,e^{-2\pi\gamma} \tag{3.17}$$

which is 4 times as large. Furthermore, in Figure 8 of [13] one also sees an indication that higher orders of the adiabatic expansion lead to a smoother time evolution of the adiabatic particle number. As we see from our Figure 3.1, if the order of the adiabatic expansion increases beyond the optimal order, the large oscillations return. At the optimal order, the time evolution of the approximation of the optimal adiabatic particle number is given by Berry's universal error function form, generalized to two sets of turning points, as in (2.130).

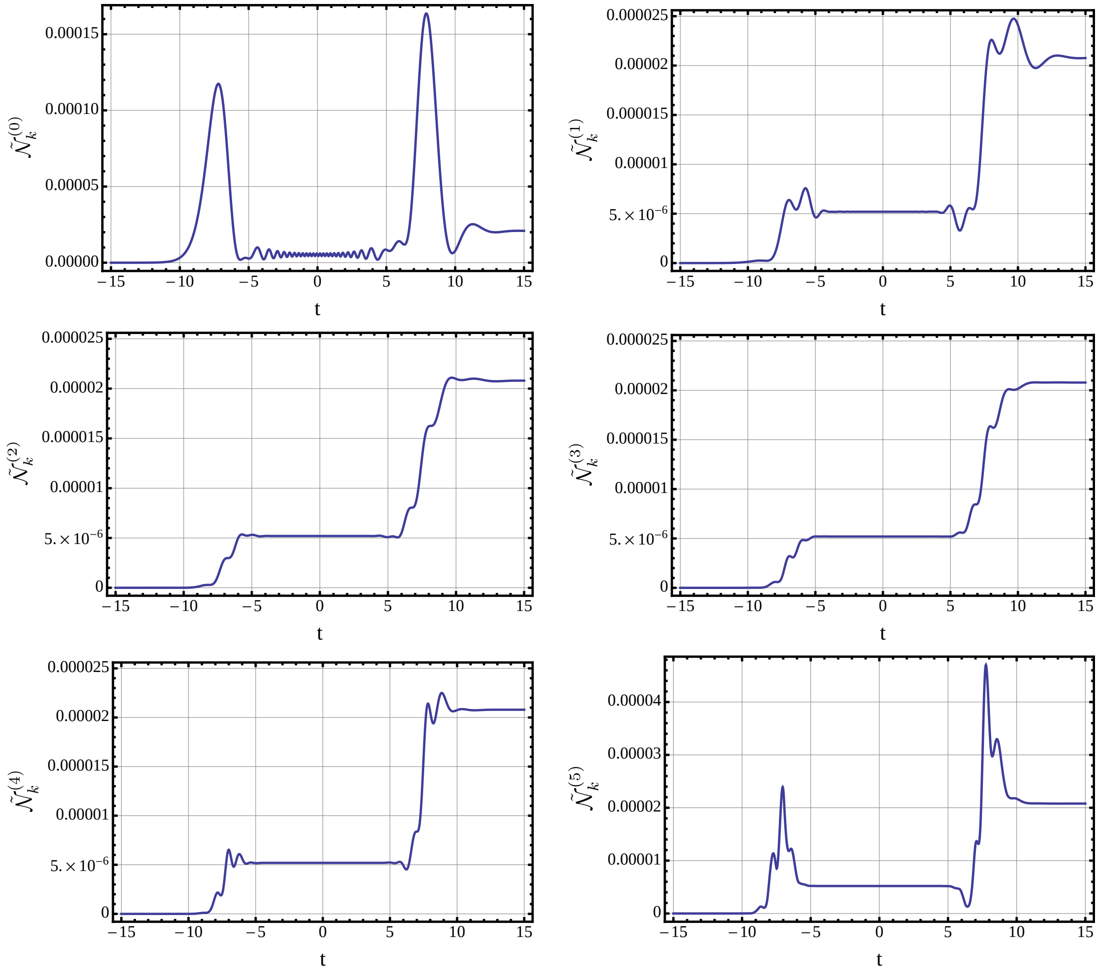

Fig. 3.1: $\tilde{\mathcal{N}}_k^{(j)}(t)$ for the first 6 orders of the adiabatic expansion, for particle production in four-dimensional de Sitter space (3.12, 3.14), with $k = 25$ and $H = 0.5$, in units with $m = 1$. Here, $\eta_4 = \frac{1}{6}$ in $d = 4$. Note the similarity with Figure 2.10, the coherent constructive interference case for a double-pulse E-field, in terms of the 4 fold enhancement of the final particle number and the smoothing of the particle number with optimal truncation of the adiabatic expansion.

3.3.2 Optimal Adiabatic Particle Number in 3d de Sitter space: Coherent Destructive Interference

We compute the adiabatic particle number numerically using (2.100, 2.101), for various orders j of the adiabatic expansion, starting with the time-dependent

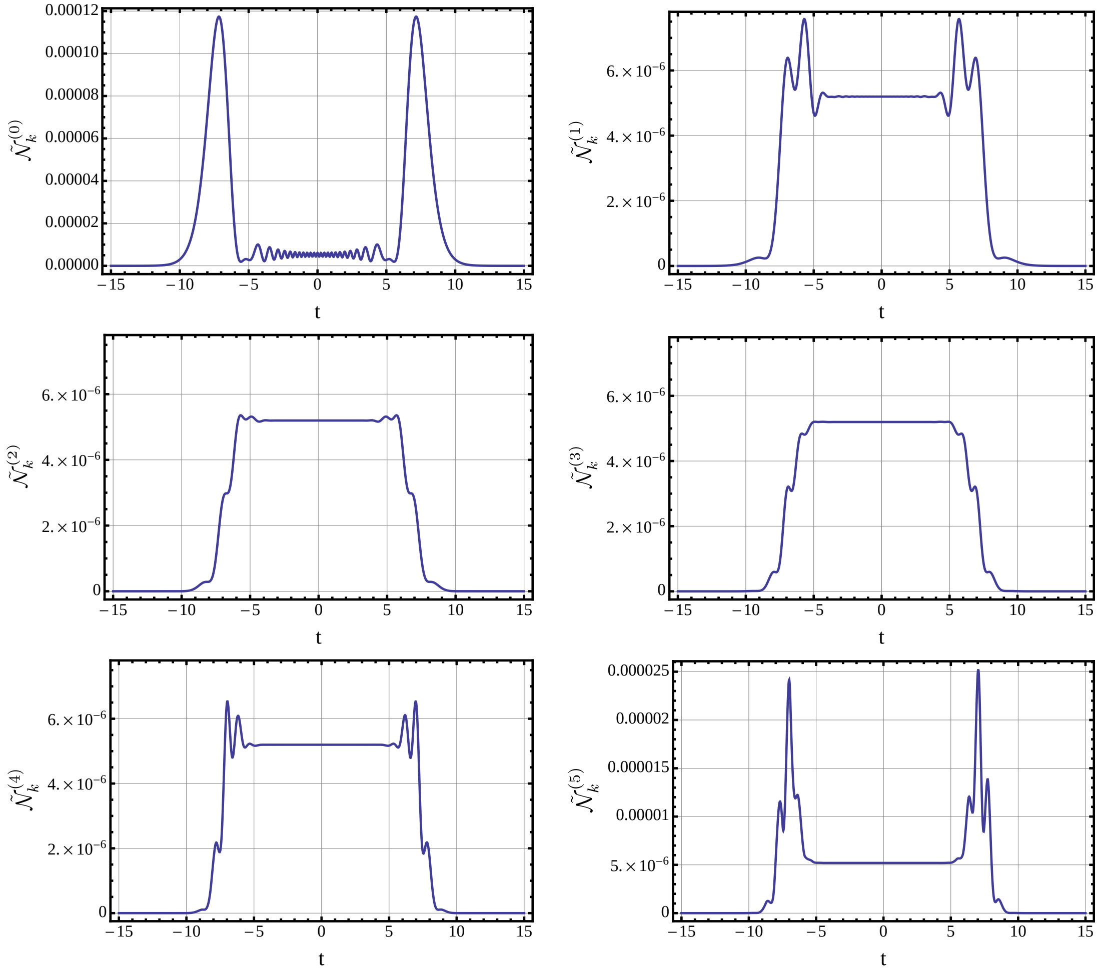

Fig. 3.2: $\tilde{\mathcal{N}}_k^{(j)}(t)$ for the first 6 orders of the adiabatic expansion, for particle production in four-dimensional de Sitter space (3.12, 3.14), with $k = 25$ and $H = 0.5$, in units with $m = 1$. Here, $\eta_3 = \frac{1}{8}$ in $d = 3$. Note the similarity with Figure 2.11, the coherent destructive interference case for a double-pulse E-field, in terms of a vanishing final particle number and the smoothing of the particle number with optimal truncation of the adiabatic expansion.

frequency for three dimensional de Sitter space, from (3.12, 3.14). We consider conformal coupling, so that $\eta_3 = \frac{1}{8}$ in 3 dimensions. The results are shown in Figure 3.2. Note the similarity to the two-alternating-sign-pulse Schwinger effect, with particle momentum such that the interference is destructive, as shown in

Figure 2.11. In the leading order of the adiabatic expansion, there are two large oscillatory peaks, several orders of magnitude larger than the final asymptotic particle number. As the order of the adiabatic expansion increases these oscillations become smaller, and at the optimal order ($j = 3$) the adiabatic particle number evolves much more smoothly. Moreover, we clearly see the two-step structure, with destructive interference leading to the final asymptotic result of zero net particle production. Also note that, as in the case of the Schwinger effect shown in Figure 2.11, the smooth evolution and interference is most evident at the optimal order, namely for the adiabatic particle number, with the large oscillations returning as one goes beyond the optimal order.

3.4 Extroduction

In this Chapter we have studied the time evolution of the adiabatic particle number for particle production in de Sitter space, motivated by the universality of Dingle and Berry's work. We examined various orders of the adiabatic expansion, noting the well-known fact that the time evolution at intermediate times is highly sensitive to the truncation order, even though the final particle number at future infinity is independent of this order. This optimal adiabatic particle number typically evolves in time much more smoothly than at low orders of the adiabatic expansion and demonstrates that the notion of an optimally truncated adiabatic particle number is a useful and well defined concept in the investigation of quantum interference. In addition, the resulting time evolution reveals that the Stokes phenomenon is ultimately responsible for particle production and the quantum interference that occurs in de Sitter particle production. Here, the distinction between constructive and destructive interference lies in the space-time dimensionality, with even dimensional de Sitter space producing a net particle number by coherent constructive interference, and odd dimensional de Sitter space producing zero net particle number, due to coherent destructive interference. We have verified the accuracy of this result in de Sitter particle production through numerical computations in even and odd spacetimes.

Chapter 4

The Back-reaction Problem

4.1 Overview

In Chapter 2 we addressed the question whether particle production under time-dependent driving could be understood during the duration of the time-dependent background perturbation. The ambiguity of identifying particle and anti-particles during this out-of-equilibrium period of evolution was addressed with a consistent universal definition to the particle number: an optimal particle number corresponding to the optimal truncation of the adiabatic expansion. This provides, a practical and well-defined concept for describing particle production during non-equilibrium evolution. However, the formulation used to determine this consistent definition for the particle number at intermediate times, obtained from neglecting the kinetic term of the gauge field A_μ and treating the field as classical, does not take into account the physically expected effect of pair recombination: a process, by which, particles and anti-particles oppositely accelerated by the applied external electric field could interact via back-reaction with one another to reduce the overall number of particles produced. This back-reaction manifests as a generated internal electric field that counteracts the applied external one, thus dynamically influencing the total electric field the pairs feel, and, in turn, affecting the number of pairs produced. It is expected that this effect should play a significant role for external electric fields near and beyond the Schwinger critical limit $E \sim E_c$. The back-reaction mechanism for Schwinger particle production raises interesting questions as to what experimental programs such as ELI and XFEL should expect to observe while probing this ultra-relativistic regime, and whether there is a maximally attainable electric field. These remain open questions due to the difficulty of addressing the back-reaction mechanism for particle production but have been extensively studied [53,61,120–124], to briefly mention a few, sparked also by its relevance for the quark-gluon plasma problem and inflationary cosmology.

Incorporating the back-reaction mechanism in Schwinger particle pair production requires taking into account the full equations of motion for sQED, to which the current density j^μ, arising in the context of sQED as

$$j^\mu = i\left[\left(D^\mu \Phi\right)^* \Phi - \Phi^* \left(D^\mu \Phi\right)\right] \tag{4.1}$$

then corresponds to the induced current of the produced particles. This quantity is unique and well-defined at intermediate times owing to the fact that is it observable, and thus measurable. As such, the expectation value of the current density (4.1) is of vital interest to a consistent formulation of back-reaction in Schwinger particle production. Another ingredient for a complete theory is the conservation of energy of the system, another observable and unambiguous quantity at intermediate times, in which the energy gained by the produced particles from the external electric field and the loss of energy of the resulting electric field doing work on the vacuum must be conserved.

Given a consistent definition for non-equilibrium evolution of the particle number presented in Chapter 2 and the understanding that the effect of back-reaction between the produced pair occurs during the non-equilibrium evolution, leads us to consider possible implications on the back-reaction mechanism for Schwinger particle production with the formalism developed in the previous chapters. Presented in this chapter is a summary of calculations, observations and comments on the back-reaction problem for Schwinger particle production in the formalism used in Chapter 2.

4.2 Formalism

4.2.1 Induced Local Current

Incorporating a back-reaction mechanism to Schwinger particle production requires taking into account the full equations of motion for sQED. In Section 2.2.1 we derived these classical equations in which complex scalar field $\Phi(x,t)$ satisfies the Klein-Gordon equation

$$\left(D_\mu D^\mu + m^2\right)\Phi(x,t) = 0 \tag{4.2}$$

and the gauge field A_μ satisfies the semiclassical Maxwell equations

$$\partial_\mu F^{\mu\nu} = \langle 0|j^\nu|0\rangle \tag{4.3}$$

with the conserved local current j^μ is defined as in (4.1). Accounting for back-reaction implies that the Maxwell equations (4.3) and the Klein-Gordon equation (2.2) are now coupled. Spatial homogeneity of the time-dependent external electric field, of the form $A^\mu = \delta_3^\mu A_\parallel(t)$, reduces the Maxwell equations to a single semi-classical equation

$$\ddot{\mathbf{A}}(t) = \langle 0|\mathbf{j}(t)|0\rangle \tag{4.4}$$

in which the gauge condition $A_0 = 0$ was used.

4.2.2 Mode Decomposition Conserved Current

Recalling Section 2.2.2, the assumption of a spatially homogeneous classical electric field allows the decomposition of the scalar field into spatial Fourier modes as (2.5,2.12). Assuming no particles are initially present, the expectation value of the mode decomposed current with respect to the asymptotic vacua yields the induced current $\mathbf{j}_{\text{ind}}(t)$:

$$\ddot{\mathbf{A}} = \mathbf{j}_{\text{ind}}(t) = \langle \mathbf{j}(t)\rangle = 2\int \frac{d^3k}{(2\pi)^3}\,[\mathbf{k} - \mathbf{A}]\,|f_k(t)|^2 \tag{4.5}$$

Notice that the induced current is integrated over all momenta k, and is well-defined at asymptotic and intermediate times. The components of the mode decomposed expression for the current in (4.5) further reduce as a result of the polarization of the external electric field. Along the parallel direction with respect to the field

$$\ddot{A}_{\parallel}(t) = j_{\text{ind},\parallel}(t) = \int \frac{d^3k}{(2\pi)^3}\,(k_{\parallel} - A_{\parallel}(t))|f_k(t)|^2 \tag{4.6}$$

while the perpendicular component of equation (4.5) yields a zero current in the perpendicular direction, $j_{\text{ind},\perp}(t) = 0$. This component further implies the following property on the modulus of the mode function $f_k(t)$ when integrated over the momenta k:

$$0 = \int \frac{d^3k}{(2\pi)^3}\,k_{\perp}\,|f_k(t)|^2 \tag{4.7}$$

in which the quantity $|f_k(t)|^2$ is symmetric with respect to the perpendicular momentum $k_{\perp}$.

4.3 Back-reaction Mechanism

In principle, we have already developed the necessary expressions to incorporate back-reaction for sQED Schwinger pair production: simultaneously solve the decomposed Klein-Gordon equation (2.16) for the mode k (the oscillator equation for the complex mode function $f_k(t)$, or equivalently, the Ermakov-Milne equation (2.19) for the amplitude function $\xi_k(t)$) and the dynamical equation for the vector potential $A_{\parallel}(t)$ (4.6), after setting

$$A_{\parallel}(t) = A_{\text{ex},\parallel}(t) + A_{\text{int},\parallel}(t) \tag{4.8}$$

throughout the expressions. Here, $A_{\text{ex},\|}(t)$ corresponds to the original external electric field applied to the vacuum, and $A_{\text{int},\|}(t)$ corresponds to the the developed internal electric field generated in response as pairs back-react with the applied field. Following the program, a solution for the complex mode function $f_k(t)$ (or its amplitude $\xi_k(t)$) and the evolution of the internal field $A_{\text{int},\|}(t)$ is obtained, which then can be used to calculate the particle number using the existing formalism in Chapter 2. With this particle number that includes back-reaction, one can calculate the distribution of particles produced with the momenta k, and, in principle, study the effects of a maximally attainable electric field where particle production becomes saturated after a critical magnitude of the electric field. However, we are confronted with the technical difficulty of not only solving the coupled expressions (2.16,4.6) but also addressing a complicated integral in (4.6) that involves integrating the modulus $|f_k(t)|^2$ across all momenta k. This is a numerically challenging evaluation.

4.4 Energy Conservation

4.4.1 Energy of the Produced Scalar Field and Electromagnetic Field

The produced particles gain energy from the applied external electric field. Thus the dynamical relationship between the energy of the produced scalar fields $\mathcal{H}_{\text{sQED}}(t)$ and the energy of the electromagnetic field $\mathcal{H}_{EM}(t)$ is relevant for energy conservation for all times of the process.

In the usual way, the scalar field Hamiltonian $\mathcal{H}_{\text{sQED}}(t)$ can be mode decomposed where its diagonal and off-diagonal components, respectively, are

$$\mathcal{H}^{\text{diag}}_{\text{sQED}} = \int \frac{d^3k}{(2\pi)^3} \left(\left| \dot{f}_{\mathbf{k}}(t) \right|^2 + \omega_k^2(t) \left| f_{\mathbf{k}}(t) \right|^2 \right) \left(a^\dagger_{\mathbf{k}} a_{\mathbf{k}} + b_{-\mathbf{k}} b^\dagger_{-\mathbf{k}} \right) \tag{4.9}$$

$$\mathcal{H}^{\text{off}}_{\text{sQED}} = \int \frac{d^3k}{(2\pi)^3} \left\{ \left[\dot{f}^2_{\mathbf{k}}(t) + \omega^2_{\mathbf{k}}(t)\, f^2_{\mathbf{k}}(t) \right] a_{\mathbf{k}} b_{-\mathbf{k}} + \text{h.c} \right\} \tag{4.10}$$

Here, the time-dependent effective frequency $\omega_k(t)$ for sQED is defined as in (2.17). Assuming no particles are initially present, the expectation value of the energy for the produced scalar field with respect to the asymptotic vacua is

$$\langle \mathcal{H}_{\text{sQED}} \rangle = \langle 0 | \left(\mathcal{H}^{\text{diag}}_{\text{sQED}} + \mathcal{H}^{\text{off}}_{\text{sQED}} \right) | 0 \rangle \tag{4.11}$$

$$= \int \frac{d^3k}{(2\pi)^3} H_k(t) = \int \frac{d^3k}{(2\pi)^3} \left(\left| \dot{f}_{\mathbf{k}}(t) \right|^2 + \omega^2_{\mathbf{k}}(t) \left| f_{\mathbf{k}}(t) \right|^2 \right) \tag{4.12}$$

The Hamiltonian for the mode k can be rewritten using $\xi_k(t)$-representation (2.18) as

$$H_k(t) = \dot{\xi}^2_k(t) + \omega^2_{\mathbf{k}}(t) \xi^2_k(t) + \frac{1}{4\xi^2_k(t)} \tag{4.13}$$

which is solved by evolving the Ermakov-Milne equation (2.19) with the initial conditions (2.26). Notice that the energy of the produced scalar field is unique and well-defined at intermediate times.

In the usual way, the energy of the dynamical background electromagnetic field $\mathcal{H}_{\text{EM}}(t)$ in the system is

$$\mathcal{H}_{\text{EM}}(t) = \frac{1}{2} E^2_{\parallel}(t) \tag{4.14}$$

Once again, the energy of the electric field is unique and well-defined at intermediate times.

4.4.2 Implications of Energy Conservation

The total energy of the particle production process is a dynamical exchange between the energy gained by the produced particles from the applied external electric field and the loss of energy of the resulting electromagnetic field doing work on the vacuum. This transfer mechanism of the energy of the system, $\mathcal{H}_{\text{tot}} = \mathcal{H}_{\text{sQED}}(t) + \mathcal{H}_{\text{EM}}(t)$, must be conserved which implies

$$\langle \dot{\mathcal{H}}_{\text{sQED}}(t) \rangle = -\dot{\mathcal{H}}_{\text{EM}}(t) \tag{4.15}$$

for all time t.

The rate by which the produced particle gains energy is obtained by taking the time-derivative of (4.12):

$$\langle \dot{\mathcal{H}}_{\text{sQED}}(t) \rangle = \int \frac{d^3k}{(2\pi)^3}\, \delta \dot{h}_k(t) \tag{4.16}$$

noting that the time-derivative of the energy (4.13) simplifies to $\delta\dot{h}_k(t) \equiv \dot{H}_k(t) = \partial_0 \left(\omega_k^2(t)\right) \xi_k^2(t)$ by using the Ermakov-Milne equation (2.19) for the amplitude function $\xi_k(t)$. The total energy gained up to the time t follows as

$$\delta_k h(t) = \int_{-\infty}^{t} dt'\, \partial_{t'} \left(\omega_k^2(t')\right) \xi_k^2(t') = -\int_{-\infty}^{t} dt' \, \left(k_\parallel - A_\parallel(t')\right) \dot{A}_\parallel(t') \xi_k^2(t') \tag{4.17}$$

Thus, from energy conservation of the total system, the energy of the electromagnetic field (4.14) may be written in terms of the total energy gained by the scalar field in (4.17) as

$$\mathcal{H}_{\text{EM}}(t) = \frac{1}{2}E_{\parallel}^2(t) = -\int \frac{d^3k}{(2\pi)^3}\,\delta h_k(t) \tag{4.18}$$

We briefly note that another equivalent and straightforward method to deriving the induced current (4.6) comes from differentiating the above expression with respect to time, and simplifying. The expression for the energy (4.18), in principle, can be used to determine how the electric field changes in response to the produced particles but we are again confronted with the analytical and numerical issue of evaluating the integral across all phase space. However, we can avoid the difficulties of evaluating this expression by rephrasing the total energy of the system $\mathcal{H}_{\text{tot}}$ exclusively in terms of $\xi_k(t)$. Utilizing the scalar field energy (4.13) and the rephrased expression for the electromagnetic field energy (4.18), we find a more tractable form for the total energy of the system as

$$\begin{aligned}\mathcal{E} = \mathcal{H}_{\text{tot}} = \int \frac{d^3k}{(2\pi)^3} \Bigg[\dot{\xi}_k^2(t) + \omega_k^2(t)\xi_k^2(t) + \frac{1}{4\xi_k^2(t)} + \\ + \int_{-\infty}^{t} dt'\,(k_{\parallel} - eA_{\parallel}(t'))\dot{A}_{\parallel}(t')\xi_k^2(t') \Bigg]\end{aligned} \tag{4.19}$$

where $\mathcal{E}$ is a conserved quantity of the system. The rewritten expression for the total energy of the system (4.19) demonstrates that energy is conserved for particle production at intermediate times, which is straightforward to confirm by a time-derivative.

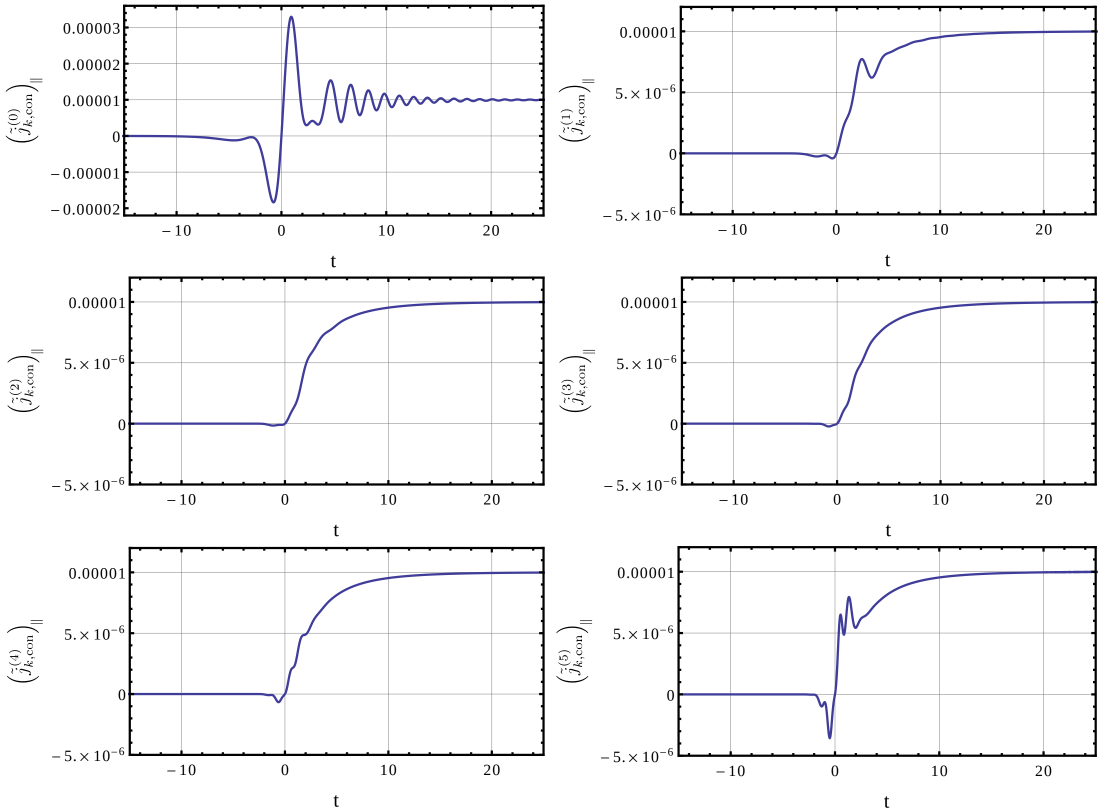

Fig. 4.1: The conduction current plotted for the first 6 orders of the adiabatic expansion, for Schwinger pair production in a single-pulse E-field (2.119, given by (2.120), with $E_0 = 0.25, a = 0.1, k_\perp = k_\parallel = 0$, in units of $m = 1$. As like Figure 2.8, the final value of the conduction current is same for all orders of truncation, but the oscillations differ significantly with the smoothest evolution occurring at the optimal order, here, $j_{\mathrm{opt}} = 3$.

4.5 Components of the Current

The mode reduced induced current $j_{\mathrm{ind},\parallel}(t)$ (4.6) is composed of three distinct parts that carry different physical meaning. Using the linear transformation to the adiabatic basis (2.31)

$$f_k(t) = \alpha_k(t)\tilde{f}_k(t) + \beta_k(t)\tilde{f}^*_k(t) \quad , \tag{4.20}$$

we may express the induced current (4.6) as

$$j^{(j)}_{\text{ind},\|}(t) = 2\int \frac{d^3k}{(2\pi)^3}\left(1 + 2\mathcal{N}_k(t) + \alpha_k(t)\beta_k^*(t)\tilde{f}_k^2(t) + \alpha_k^*(t)\beta_k(t)\left[\tilde{f}_k^*(t)\right]^2\right) \tag{4.21}$$

Here we made use of the definition of the adiabatic particle number (2.35) and the unitary condition of the Bogoliubov coefficients: $|\alpha_k(t)|^2 - |\beta_k(t)|^2 = 1$, for scalars.

Defining the reference mode functions using (2.27) and truncating the adiabatic expansion at the j-th adiabatic order, the induced current (4.6) at j-th order reads

$$\begin{aligned} j^{(j)}_{\text{ind},\|}(t) = 2\int \frac{d^3k}{(2\pi)^3}\,\frac{\left[k_\| - A_\|(t)\right]}{W_k^{(j)}(t)}\Big(1 + 2\,\tilde{\mathcal{N}}_k^{(j)}(t) + \\ + e^{-2i\int^t W_k^{(j)}}\alpha_k^{(j)}(t)[\beta_k^{(j)}(t)]^* + e^{2i\int^t W_k^{(j)}}[\alpha_k^{(j)}(t)]^*\beta_k^{(j)}(t)\Big) \end{aligned} \tag{4.22}$$

Recall from Section 2.9 that a quantity truncated at the j-th adiabatic order is obtained by utilizing the preferred basis (2.98) and setting $W_k(t) = W_k^{(j)}(t)$ throughout the expression. By taking derivatives of the adiabatic particle number and using the Bogoliubov evolution equations (2.36) to simplify, one finds

$$\begin{aligned} \mathrm{Im}\left[e^{2i\int^t W_k^{(j)}}(\alpha_k^{(j)})^*\beta_k^{(j)}\right] &= \frac{\dot{\tilde{\mathcal{N}}}_k^{(j)}(t)}{2\Lambda_k^{(j)}} \\ \mathrm{Re}\left[e^{2i\int^t W_k^{(j)}}(\alpha_k^{(j)})^*\beta_k^{(j)}\right] &= \frac{\ddot{\tilde{\mathcal{N}}}_k^{(j)} - \dot{\tilde{\mathcal{N}}}_k^{(j)}\left(\frac{\dot{\Lambda}_k^{(j)}}{\Lambda_k^{(j)}}\right) - 2\left|\Lambda_k^{(j)}\right|^2\left(1 + 2\,\tilde{\mathcal{N}}_k^{(j)}\right)}{4\left(iW_k^{(j)}\Lambda_k^{(j)} + \left|\Lambda_k^{(j)}\right|^2\right)} \end{aligned} \tag{4.23}$$

with the time-dependent function $\Lambda_k^{(j)}(t)$ defined as in (2.101). Note that $\Lambda_k^{(j)}(t)$ is purely imaginary. The forms (4.23) then can be used to rewrite the induced current (4.5) as

$$\tilde{\mathbf{j}}^{(j)}_{\text{ind}}(t) = \int \frac{d^3k}{(2\pi)^3} \frac{[\mathbf{k} - \mathbf{A}]}{W^{(j)}_k} \left[1 + 2\tilde{\mathcal{N}}^{(j)}_k + \left(\frac{\ddot{\tilde{\mathcal{N}}}^{(j)}_k - \dot{\tilde{\mathcal{N}}}^{(j)}_k \left(\frac{\dot{\Lambda}^{(j)}_k}{\Lambda^{(j)}_k} \right) - 2\left|\Lambda^{(j)}_k\right|^2 \left(1 + 2\tilde{\mathcal{N}}^{(j)}_k\right)}{2\left(iW^{(j)}_k \Lambda^{(j)}_k + \left|\Lambda^{(j)}_k\right|^2 \right)} \right) \right] \tag{4.24}$$

The induced current is composed of three physically distinct currents: one that pertains to the vacuum $\mathbf{j}^{(j)}_{\text{vac}}(t)$, and the conduction $\mathbf{j}^{(j)}_{\text{cond}}(t)$ and polarization currents $\mathbf{j}^{(j)}_{\text{pol}}(t)$ that are identified by comparison with the total current density that arises from electromagnetic fields classically interacting with a polarizable medium (the vacuum in this case). The individual components of the induced current, from simplify equation (4.24), are:

1. The Vacuum Term:

$$\left(\tilde{j}^{(j)}_{\text{vac}}(t)\right)_{\parallel} = \int \frac{d^3k}{(2\pi)^3} \left(\frac{k_{\parallel} - A_{\parallel}(t)}{W^{(j)}_k + i\Lambda^{(j)}_k} \right) \tag{4.25}$$

2. The Conduction Current:

$$\left(\tilde{j}^{(j)}_{\text{cond}}(t)\right)_{\parallel} = 2 \int \frac{d^3k}{(2\pi)^3} \tilde{\mathcal{N}}^{(j)}_k(t) \left(\frac{k_{\parallel} - A_{\parallel}(t)}{W^{(j)}_k + i\Lambda^{(j)}_k} \right) \tag{4.26}$$

   which corresponds to the terms that are proportional to $\tilde{\mathcal{N}}^{(j)}_k(t)$ in (4.24), the flow of produced particles from the vacuum.

3. The Polarization Current:

$$\left(\tilde{j}^{(j)}_{\text{pol}}(t)\right)_{\parallel} = \int \frac{d^3k}{(2\pi)^3} \left(\frac{k_{\parallel} - A_{\parallel}(t)}{W^{(j)}_k} \right) \left(\frac{\ddot{\tilde{\mathcal{N}}}^{(j)}_k - \dot{\tilde{\mathcal{N}}}^{(j)}_k \left(\frac{\dot{\Lambda}^{(j)}_k}{\Lambda^{(j)}_k} \right)}{2\left(iW^{(j)}_k \Lambda^{(j)}_k + \left|\Lambda^{(j)}_k\right|^2 \right)} \right) \tag{4.27}$$

which originates from the classical equation $\mathbf{J}_{\text{pol}} = \partial_0 \mathbf{P}$, where $\mathbf{P}$ is the Polarization Field Density, and hence is related to time derivatives of the adiabatic particle number.

We note that each of the quantities (4.25-4.27) is real.

We now demonstrate the universal behavior of the induced conduction current, corresponding to truncation of the adiabatic expansion at the optimal order, in Figures 4.1 and 4.2 for sQED Schwinger particle production. The results for the conduction current due to a single-pulse electric field given by (2.119), for the vector potential 2.120, are shown in Figure 4.2, and the results for the alternating-sign triple pulse electric field given by (2.124), for the vector potential (2.125), are shown in Figure 4.1. Both figures show the following trend observed for the smoothing of the adiabatic particle number at the optimal adiabatic order: there are large oscillations at intermediate times for low orders of the adiabatic expansion, that subside as the optimal order ($j_{\text{opt}} = 3$, in both figures) is reached, and then grow again as one goes to higher orders in the adiabatic expansion.

Lastly, the polarization component of the induced current (4.27) is typically highly oscillatory in time, and does not contribute to the final value of the current at future infinity.

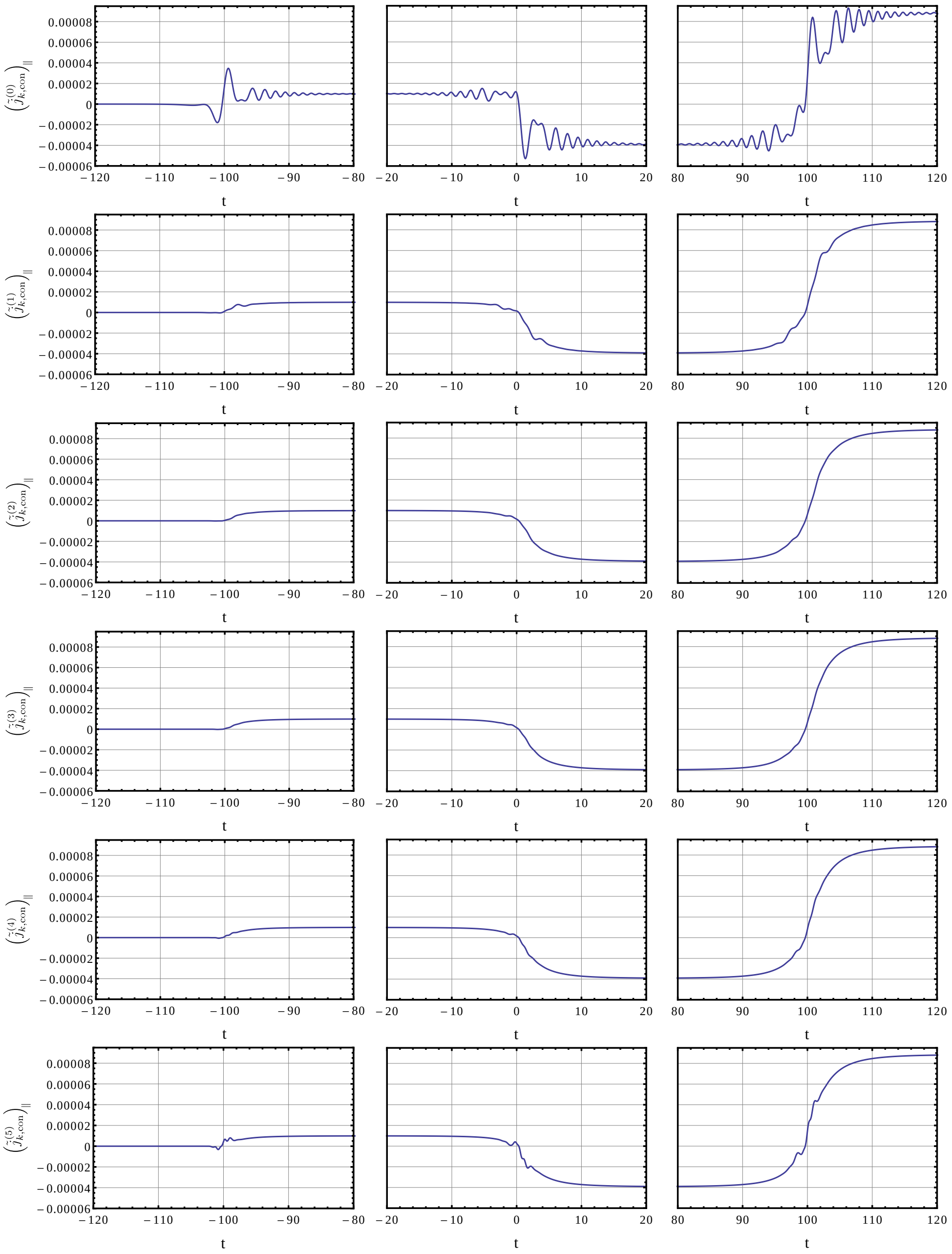

Fig. 4.2: The conduction current plotted for the first six orders of the adiabatic expansion, for Schwinger pair production in a triple-pulse E-field (2.124), given by (2.125), with $E_0 = 0.25, a = 0.1, b = 50, k_\perp = k_\parallel = 0$, in units of $m = 1$. As like the particle number in Figure 2.8, the final value of the conduction current is same for all orders of truncation, but the oscillations differ significantly. The smoothest evolution of the conduction current occurs at the optimal order, here, $j_{\mathrm{opt}} = 3$.

4.6 Extroduction

Motivated by a universal definition of the number of particles produced during out-of-equilibrium particle production, as developed in Chapter 2, we are led to consider possible implications for the back-reaction problem for sQED Schwinger particle production. Pairs produced from the vacuum back-react on one another leading to the possibility of pair recombination and a reduced particle number. As such, it is an effect expected to play an important role during non-equilibrium particle production, for which the formalism and results of Chapter 2 are well-suited. Presented in this chapter are calculations and comments on how to address the back-reaction problem in sQED pair production.

By considering the full equations of motion for sQED, expressions were developed to account for an internal electric field generated by the produced pairs by addressing the induced current. The incorporation of the internal field is realized by evolving the coupled dynamical equations (2.16,4.6) with $A_{\|}(t) = A_{\mathrm{ex},\|}(t)+A_{\mathrm{int},\|}(t)$. However, the program is challenging to execute in the formalism of Chapter 2 owing to the difficulties of not only solving the coupled equations simultaneously but also numerically evaluating an integral over the momentum k in equation (4.6). We also demonstrated how the problem of back-reaction can be addressed through energy conservation, and explicitly demonstrated energy conservation of the produced pairs and the dynamical background electric field, for all times t. This implies that the energy of the system will be conserved if a time-dependent internal electric field is included. Lastly, we also examined the induced current and expressed the result in terms of the time-dependent adiabatic particle number $\tilde{\mathcal{N}}_k(t)$ and its derivatives. In this way, it was shown that the time-dependent current is composed of three physically distinct parts that correspond to a vacuum term, a conduction current term, and a polarization current term. These currents were studied numerically for several examples of time-dependent external electric fields, see Figures 4.1 and 4.2.

Chapter 5

Time-dependent Quantum Excitations and the Non-equilibrium Work Theorem

5.1 Introduction

The *non-equilibrium work theorem* [125,126] is a work relation that allows the determination of an equilibrium free energy difference from the fluctuations of the work w done on the system as it undergoes non-equilibrium evolution. The theorem, also commonly referred to as the Jarzynski Equality, has been derived by a variety of means [127–136] and can be summarized in the following way. Suppose a physical system that lies in an initial (free) equilibrium configuration A, evolves in time under the influence of a dynamical background field, which then vanishes, and the system returns to a final (free) equilibrium configuration B at future infinity. The driving of the system in and out of equilibrium is characterized by the total work performed on the system as it evolves from configuration A to B. This work, which is not an observable [137], is influenced by the degrees of freedom of the actual system and the attached environment. However, by performing the process over a large number of configuration paths of the parametrized system from a similar starting initial configuration then the work performed on the system can be characterized by an averaging over the distribution of work values $p(w)$, observed over the entire set of work measurements. The non-equilibrium work theorem states that the total work performed on the system during its evolution through the time-dependent perturbation is related to the free energy difference ΔF_{AB} of the equilibrium configurations (A, B) by

$$\left\langle e^{-\beta w} \right\rangle = \int_A^B dw\, p(w) e^{\beta w} = e^{-\beta \Delta F_{AB}} \tag{5.1}$$

Importantly, this work relation is independent of how the system evolves from configuration A to B and insensitive to the behavior of the dynamical external field, whether it evolves adiabatically or diabatically. This remarkable feature implies that by studying its equilibrium configurations one can obtain information during the non-equilibrium evolution of the system, such as mean total work performed and the amount of work dissipated during the evolution of the system. The equality has been experimentally verified classically for mechanical torsion pendulums [138], for particles confined in an anharmonic trap [139] and demonstrated in biopolymer RNA unfolding experiments [140,141].

In this chapter we investigate the non-equilibrium work theorem for a thermodynamic system involving a quantum mechanical harmonic oscillator being driven by a time-dependent frequency using the results and out-of-equilibrium formalism of Chapter 2. The system initially lies in a thermal equilibrium configuration at past infinity, thermally equilibrated with respect to a heat bath of inverse temperature β. Contact with the bath is severed, and the system undergoes non-equilibrium evolution in the presence of the perturbation, until the system reaches a final equilibrium configuration at future infinity. Apart from the external influence, the time-dependent Hamiltonian is thermally isolated until future infinity is reached. In this way, the problem is conceptually and technically similar to the case Berry and, recently, we have investigated in the context of the quantum field theoretical problem of particle pair production in Chapters 2 and 3. Building on the work analyzing the quantum harmonic oscillator system in the context of the non-equilibrium work relation [137,142,143], we outline progress towards a time-dependent formulation of Jarzynski's work relation (5.1), applicable not only at asymptotic times, but for all times in the evolution of the system. Such a formulation could address the notion of work in a quantum system and provide information on the system during the interaction with an external field, with possible applications to particle production and related effects.

5.2 Formalism

5.2.1 Quantum Harmonic Oscillator Dynamics and Adiabatic Evolution

We consider a quantum-mechanical harmonic oscillator system that evolves in a time-dependent Hamiltonian of the form

$$\hat{H}(t) = \frac{1}{2}p^2 + \frac{1}{2}\omega^2(t)q^2 \tag{5.2}$$

A quantum system driven by the time-dependent frequency $\omega(t)$. As reviewed in Section 2.6, the dynamics of this quantum system are well known [89–94] and we re-emphasise the results here once again. The exact solution of the corresponding time-dependent Schrodinger equation is [89–94]

$$\psi(q,t) = \sum_n c_n \, \psi_n(q,t) \tag{5.3}$$

where

$$\psi_n(q,t) = \frac{1}{\sqrt{2^n n!}} \left(\frac{1}{2\pi\xi^2(t)} \right)^{1/4} e^{-\frac{1}{2}\Omega(t)q^2} H_n\left(\frac{q}{\sqrt{2}\xi(t)} \right) e^{-i(n+\frac{1}{2})\lambda(t)} \tag{5.4}$$

The Gaussian factor $\Omega(t)$ has the same form as (2.69), $\lambda(t)$ is defined by (2.20), and $\xi(t)$ is the exact solution to the Ermakov equation (2.19). These $\psi_n(q,t)$ are normalized eigenfunctions of the exact invariant operator (2.70) which satisfies equation (2.71) and the eigenvalue relation (2.72). The subscript k is omitted for clarity.

We may also define a basis set of adiabatically evolving eigenstates of the time-dependent Hamiltonian under the assumption of a slowly varying time-dependent frequency $\omega(t)$. Characterized by the adiabatic function $W_k(t)$, recall from (2.75), that the most general expression for these approximate slowly-varying eigenfunctions $\zeta_n(q,t)$ take the form

$$\zeta_n(q,t) = \frac{1}{\sqrt{2^n n!}} \left(\frac{W}{\pi}\right)^{1/4} e^{-\frac{1}{2}\left(W + i\frac{\dot{W}}{2W}\right)q^2} H_n\left(\sqrt{W}q\right) e^{-i(n+\frac{1}{2})\int^t W} \tag{5.5}$$

where it approximates the exact eigenfunctions (5.4) as: $\psi_n(q,t) \sim \zeta_n(q,t)$. Insisting that this basis of adiabatically evolving eigenstates be a solution to the time-dependent Schrodinger equation,

$$i\partial_0\zeta_n(q,t) - \hat{H}(t)\zeta_n(q,t) = \frac{1}{2}q^2\epsilon(t)\zeta_n(q,t)\ , \tag{5.6}$$

the adiabatic function $W(t)$ is related to the frequency $\omega(t)$ by

$$\epsilon(t) \equiv W^2(t) - \omega^2(t) + \left[\frac{\ddot{W}(t)}{2W(t)} - \frac{3}{4}\left(\frac{\dot{W}(t)}{W(t)}\right)^2\right] \tag{5.7}$$

Here, $\epsilon(t)$ characterizes the error of this approximate solution. The specification of adiabatically evolving eigenstates, which approximately satisfy the time-dependent Schrodinger equation, is equivalent to the specification of reference mode functions (2.27), which approximately satisfy the mode oscillator equation (2.16), in the Bogoliubov (Heisenberg Picture) approach. From setting equation (5.7) to zero, we obtain the same condition on the adiabatic function $W(t)$ as equation (5.7). [Note the subscript k is dropped.] This equation can be solved by an adiabatic expansion following the procedure in Section 2.8. Truncating the expansion at adiabatic order j, the adiabatically evolving eigenstates $\zeta_n(q,t)$ at j-th order is obtained by setting $W(t) = W^{(j)}(t)$, reading

$$\zeta_n^{(j)}(q,t) = \frac{1}{\sqrt{2^n n!}} \left(\frac{W^{(j)}}{\pi}\right)^{1/4} e^{-\frac{1}{2}\left(W^{(j)} + i\frac{\dot{W}^{(j)}}{2W^{(j)}}\right)q^2} H_n\left(\sqrt{W^{(j)}}q\right) e^{-i(n+\frac{1}{2})\int^t W^{(j)}} \tag{5.8}$$

For backgrounds that become constant at asymptotic times it follows that $W^{(j)}(\pm\infty) = \omega(\pm\infty)$, and $\dot{W}^{(j)}(\pm\infty) = 0$ for all truncated orders j of the adiabatic expansion (review Section 2.8 for additional details). As such, evolving the Ermakov-Milne equation (2.19) using the boundary conditions

$$\begin{aligned} \xi(t \to -\infty) &= \frac{1}{\sqrt{2\omega(-\infty)}} \\ \dot{\xi}(t \to -\infty) &= 0 \end{aligned} \tag{5.9}$$

sets the initial form of the wavefunction as it evolves between well-defined stationary harmonic oscillator eigenfunctions at past infinity and future infinity. The exact and adiabatically evolving eigenstates take the approximate form at asymptotic times as

$$\psi_n(q, t \to \pm\infty) = \zeta_n(q, t \to \pm\infty) \tag{5.10}$$

$$\begin{aligned} &\sim \frac{1}{\sqrt{2^n n!}} \left(\frac{\omega(\pm\infty)}{\pi}\right)^{1/4} e^{-\frac{1}{2}\omega(\pm\infty)q^2} H_n\left(\sqrt{\omega(\pm\infty)}q\right) \\ &\times e^{-i(n+\frac{1}{2})\omega(\pm\infty)t} \end{aligned} \tag{5.11}$$

We next examine transitions as the system evolves adiabatically in a time-dependent background given by the time-dependent frequency $\omega(t)$. A state initially prepared at a particular time can evolve to become a superposition of a variety of states at a later time t. For a system initially prepared in the m-th state at $t = -\infty$, the adiabatic transition probability of making a transition to the n-th state is obtained by projecting the adiabatically evolving eigenfunctions $\zeta_n(q,t)$ (5.5) onto the exact eigenfunctions (5.4). Taking the modulus of the amplitude of the transition (2.78), the probability (2.84), can be written as

$$\tilde{P}^{(j)}_{nm}(t) = \left|C^{(j)}_{nm}(t)\right|^2 \tag{5.12}$$

$$= \begin{cases} \dfrac{n!m!}{2^{n+m}\left[(\frac{n}{2})!(\frac{m}{2})!\right]^2}\sqrt{\dfrac{2}{\tilde{Q}^{(j)}+1}}\left(\dfrac{\tilde{Q}^{(j)}-1}{\tilde{Q}^{(j)}+1}\right)^{\frac{n+m}{2}} {}_2F_1\left[-\dfrac{m}{2}, -\dfrac{n}{2}, \dfrac{1}{2}, -\dfrac{2}{\tilde{Q}^{(j)}-1}\right]^2, \\ \qquad\qquad\qquad\qquad\qquad\qquad \text{for} \quad m,n = \text{even} \\ \dfrac{n!m!\left[(\frac{m-1}{2})!\right]^{-2}}{2^{n+m}\left[(\frac{n-1}{2})!\right]^2}\left(\dfrac{2}{\tilde{Q}^{(j)}+1}\right)^{\frac{3}{2}}\left(\dfrac{\tilde{Q}^{(j)}-1}{\tilde{Q}^{(j)}+1}\right)^{\frac{n+m-2}{2}} {}_2F_1\left[\dfrac{1-m}{2}, \dfrac{1-n}{2}, \dfrac{3}{2}, -\dfrac{2}{\tilde{Q}^{(j)}-1}\right]^2, \\ \qquad\qquad\qquad\qquad\qquad\qquad \text{for} \quad m,n = \text{odd} \\ 0\,, \qquad\qquad\qquad\qquad\qquad\quad\; \text{for} \quad m+n = \text{odd} \end{cases} \tag{5.13}$$

with

$$\tilde{Q}^{(j)}(t) = \frac{\xi^2(t)}{W^{(j)}(t)}\left[\frac{1}{4\xi^4(t)} + \left(W^{(j)}(t)\right)^2 + \left(\frac{\dot{\xi}(t)}{\xi(t)} + \frac{\dot{W}^{(j)}(t)}{2W^{(j)}(t)}\right)^2\right] \tag{5.14}$$

This quantity corresponds to the time-dependent form of the *adiabaticity parameter* identified in [142,143], and can be interpreted as the *measure of excitations* in the system [90,91].[1] Notice that this expression is completely characterized by the amplitude function $\xi(t)$ and the basis function $W^{(j)}(t)$, where the general procedure to evaluate (5.14) is the following: solve the Ermakov-Milne equation (2.19), to obtain $\xi(t)$, and compute $W^{(j)}(t)$ from the truncation of the adiabatic expansion at the desired order. The Ermakov-Milne equation is solved once and then repeatedly projected against different $W^{(j)}(t)$, truncated at different adiabatic orders j.

---

[1] Note that $\tilde{Q}^{(j)}$ (5.14) is commonly written in the literature as Q^*, where the star is a label,

In the next section we demonstrate the typical behavior of the adiabaticity parameter for different adiabatic orders in the context of Berry's universal smoothing in the Stokes Phenomenon and demonstrate its explicit appearance in other quantities used to describe the dynamics of the system.

5.2.2 On the Time-dependence of the Adiabaticity Parameter

In the previous sections we have shown the explicit dependence of the adiabatic approximation of the energy eigenvalues, the probability density of the total work via the adiabatic transition probability, and the characteristic function on the time-dependent adiabaticity parameter $\tilde{Q}^{(j)}(t)$. In this way, the adiabaticity parameter characterizes the dynamics of the system as it evolves in time.

The time-dependent adiabaticity parameter (5.14) is related to the adiabatic

---

not a complex conjugation.

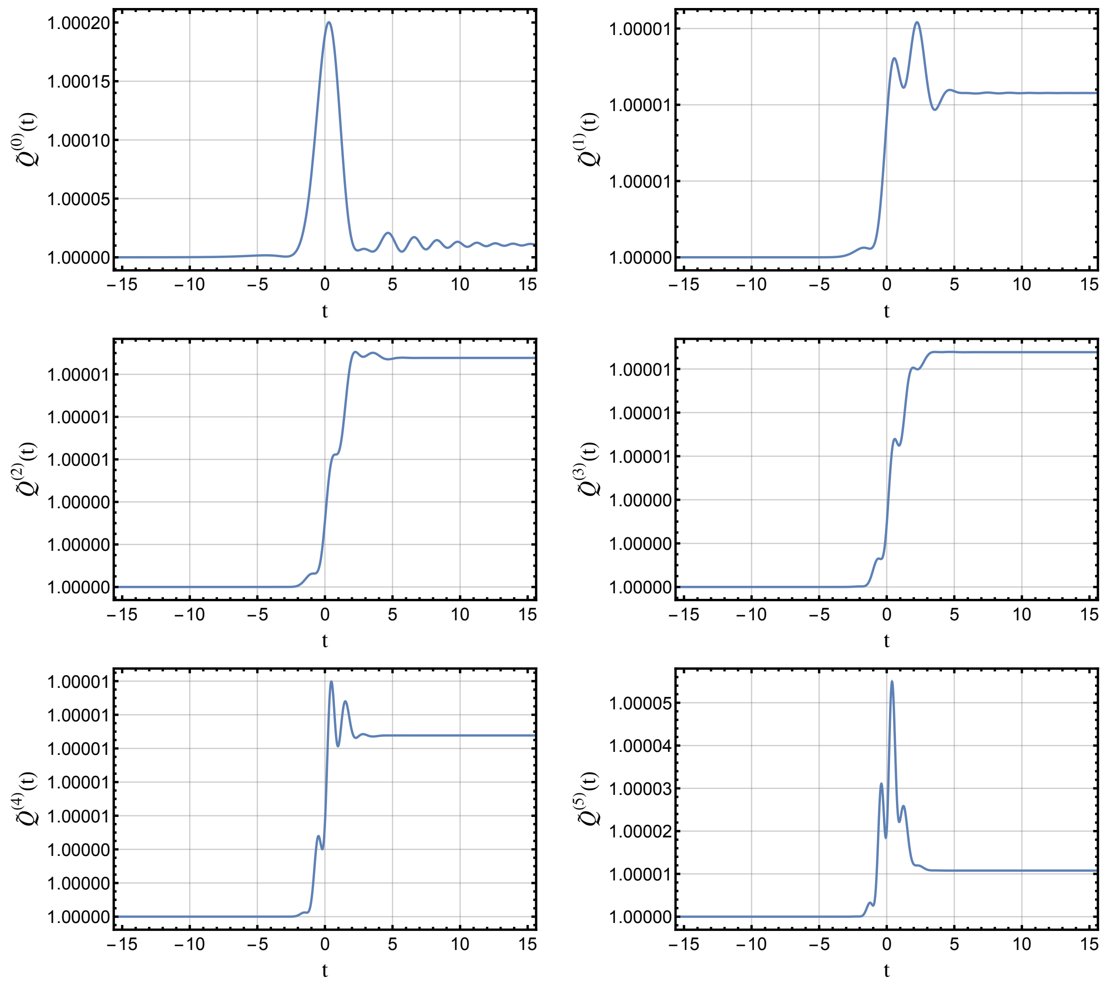

Fig. 5.1: Time evolution of $\tilde{Q}^{(j)}(t)$ (5.14) for the first six orders of the adiabatic expansion, considering an Schwinger particle production effective frequency (2.17), with parameters as in Figure 2.8. Note that $\tilde{Q}^{(j)}(t)$ has the same intermediate time behavior as the adiabatic particle number $\tilde{\mathcal{N}}^{(j)}(t)$ except shifted and twice the magnitude, as related by (5.15).

particle number (2.99) at j-th order by

$$\tilde{Q}^{(j)}(t) = 1 + 2\tilde{\mathcal{N}}^{(j)}(t) \tag{5.15}$$

Note that the various formalisms that can be used to determine $\tilde{\mathcal{N}}^{(j)}(t)$ in Chapter 2 can be equivalently used to determine $\tilde{Q}^{(j)}(t)$. Thus the typical behavior of the adiabaticity parameter truncated at different adiabatic orders is similar to the behavior of the adiabatic particle number demonstrated in Chapter 2:

1. Truncating the adiabatic expansion at different adiabatic orders does not affect the final $t = +\infty$ value of the adiabaticity parameter.

2. Truncating the adiabatic expansion at different adiabatic orders does significantly affect the adiabaticity parameter at intermediate times, in particular during the time of the background perturbation.

3. Truncating the adiabatic expansion at the optimal order j_{opt} leads to the smoothest time evolution, which agrees well with the universal form (2.113) found by Berry [64–66], applied to the adiabaticity parameter as

   $$\tilde{Q}^{(j_{\text{opt}})}(t) \approx 1 + \frac{1}{2}\text{Erfc}[-\sigma(t)]^2 e^{-2\text{Re}\left[F^{(0)}\right]} \tag{5.16}$$

   where the local action $\sigma(t)$ is defined as (2.111), and evaluated with respect to the Stokes Line between a dominant pair of complex conjugate turning points. See Section 2.10 for additional information.

4. Going beyond the optimal order again leads to large oscillations in the time vicinity of the applied background perturbation. This behavior is characteristic of an asymptotic expansion.

From the specified past infinity boundary conditions (5.9) and its relation to the adiabatic particle number in (5.15), the adiabaticity parameter evolves from

$\tilde{Q}^{(j)}(-\infty) = 1$ to the final value $\tilde{Q}(+\infty) = 1 + 2\tilde{\mathcal{N}}(+\infty)$, such that $\tilde{Q}^{(j)}(t) \geq 1$, for all time t and all truncated adiabatic orders j. In this way, the adiabaticity parameter measures the *amount of excitations* in the system due to the perturbation $\omega(t)$, and characterizes how '*adiabatic*' the evolution of the time-dependent Hamiltonian (5.2) is. Figure 5.1 plots the time evolution of the adiabaticity parameter for the first six orders of the adiabatic expansion using, as the time-dependent frequency $\omega(t)$, the sQED Schwinger effective frequency (2.17) for a time-dependent single-pulse electric field given by (2.119) with the parameters: $E_0 = 0.25, a = 0.1, k_\perp = k_\parallel = 0$, in units of $m = 1$. The final asymptotic value of the adiabaticity parameter, at future infinity, is the same for all orders of truncation j. At low orders of the adiabatic expansion we see large oscillations in the adiabaticity parameter at intermediate times. The magnitude of the oscillations decreases as we approach the optimal order, $j_{\text{opt}} = 3$, and then rapidly grow again if we continue beyond the optimal order. Recall that such behavior is characteristic of asymptotic expansions, where the order of truncation depends crucially on the size of the expansion parameter, and going beyond this optimal order typically yields increasingly worse results.

5.2.3 Adiabatic Approximation of the Energy

It is also useful to study the energy eigenvalues of the exact and adiabatically evolving Hamiltonian (5.2), with respect to the exact eigenstates (5.4) and its

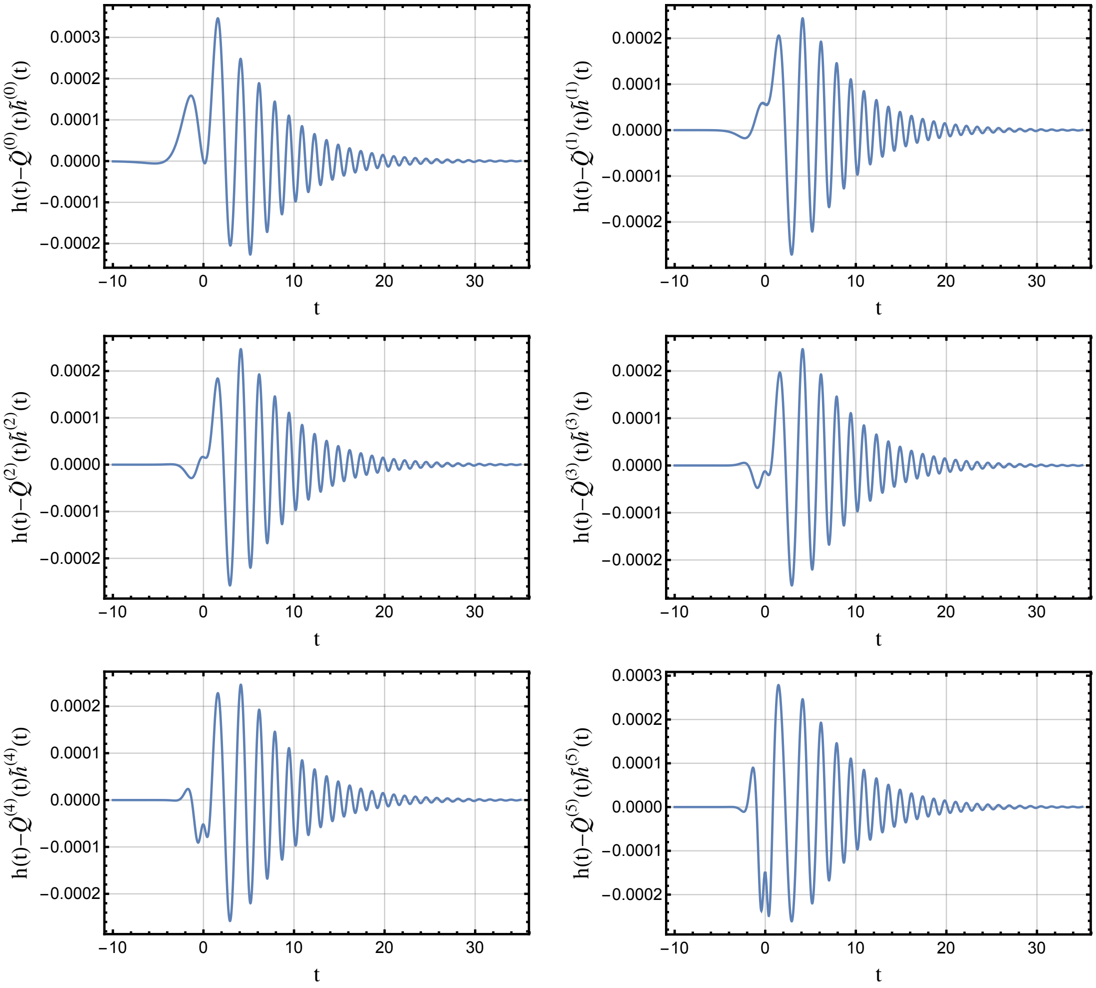

Fig. 5.2: The residual of $h(t)$ (5.18) and its approximation by (5.21) for the first six orders of the adiabatic expansion, considering the sQED particle production effective frequency (2.17) with the same pulse parameters as used in Figure 2.8. Here, $j_{\text{opt}} = 3$, which is consistent with Figure 2.8. The adiabatic order-by-order residual of both quantities show minor differences at intermediate times but agreement at asymptotically late times.

adiabatically evolving form (5.5). In the usual way, the corresponding energy eigenvalue of the eigenstate $\psi_n(q,t)$ is determined by

$$E_n(t) = \int_{-\infty}^{\infty} dq\, \psi_n^*(q,t) \hat{H} \psi_n(q,t) = h(t) \left(n + \frac{1}{2} \right) \tag{5.17}$$

with the energy gap between neighboring energy levels defined as

$$h(t) = \dot{\xi}^2(t) + \omega^2(t)\xi^2(t) + \frac{1}{4\xi^2(t)} \tag{5.18}$$

Notice that this energy $h(t)$ is determined by exactly solving the Ermakov-Milne equation (2.19) for $\xi(t)$ and is completely independent of the choice of basis. Following the initial conditions (5.9) used to evolve the Ermakov-Milne equation, the energy $h(t)$, given by (5.18), evolves between stationary states for a quantum harmonic oscillator from an initial past infinity with $h(-\infty) = \omega(-\infty)$ to the final value $h(+\infty) = \omega(+\infty)\tilde{Q}(+\infty)$. Here, $\tilde{Q}(t)$ accounts for the final form of the evolution of the system after interaction with the background, understood in Chapter 2 as the final "particle number."

In the same way, we may also identify the energy eigenvalues of the Hamiltonian (5.2) evolving adiabatically. The corresponding energy eigenvalue of the n-th eigenstate $\zeta_n(q,t)$ (5.5) defined as

$$\tilde{E}_n(t) = \tilde{h}(t)\left(n + \frac{1}{2}\right) \tag{5.19}$$

with the corresponding energy gap

$$\tilde{h}^{(j)}(t) = \frac{1}{2W^{(j)}(t)}\left(\left(W^{(j)}(t)\right)^2 + \omega^2(t) + \frac{1}{4}\left(\frac{\dot{W}^{(j)}(t)}{W^{(j)}(t)}\right)^2\right)\ , \tag{5.20}$$

The energy $\tilde{h}^{(j)}(t)$ is completely characterized by the adiabatic function $W^{(j)}(t)$, and thus its asymptotic behavior is $\tilde{h}^{(j)}(\pm\infty) = \omega(\pm\infty)$. While the asymptotic behavior of $\tilde{h}(-\infty)$ matches that of $h(-\infty)$ (5.18), ensured in $h(t)$ by the initial conditions (5.9), its asymptotic behavior at future infinity critically misses post-interaction contributions captured by $\tilde{Q}(t)$. This final time contribution is a crucial feature necessary for an expression to be used as an effective approximation of $h(t)$.

Thus, we propose the following adiabatic approximation of the energy $h(t)$:

$$h(t) \simeq \tilde{h}^{(j)}(t)\tilde{Q}^{(j)}(t) \tag{5.21}$$

to approximate the intermediate and asymptotically late time behavior of $h(t)$. From rewriting $h(t)$ (5.18) in terms of the adiabaticity parameter $\tilde{Q}^{(j)}(t)$ and the adiabatic error function $\epsilon^{(j)}(t)$, and their derivatives, the dominant term in the expression is (5.21). The other terms are composed of various products of $\epsilon^{(j)}(t)$ and $\tilde{Q}^{(j)}(t)$, and their derivatives, and are comparatively small to (5.21). In addition, their contributions are made even smaller as the adiabatic expansion is truncated at the optimal order. In Figure 5.2, we plot the residual of $h(t)$ and its approximation by (5.21) for the first six orders of the adiabatic expansion using, as the potential $\omega(t)$, the sQED Schwinger effective frequency (2.17) for a time-dependent single-pulse electric field given by (2.119) with the parameters: $E_0 = 0.25, a = 0.1, k_\perp = k_\parallel = 0$, in units of $m = 1$. The figure demonstrates the validity of the approximation both at intermediate and, critically, at asymptotically late times. Also note that the amplitude of the oscillations in Figure 5.21, especially near the vicinity of the applied pulse, grow smaller as the optimal order $j_{\text{opt}} = 3$ is reached and then increase after. This behavior is typical of asymptotic expansions, see Section 2.10. Lastly, we note that the asymptotic behavior of (5.21) matches that found in [143], given for asymptotically late times.

Later, we employ (5.21) as the adiabatic approximation of the eigenvalues for the adiabatically evolving Hamiltonian (5.2) where the adiabaticity parameter specifies its evolution.

5.3 Work Characteristic Function

The statistical properties of the system can be determined from the probability density of the work done on the system $p(w)$, or equivalently, from the corresponding characteristic function $G(\mu)$ [137,142]. Recent work regarding the non-equilibrium work theorem has focused on describing the time evolution of the system by a leading-order WKB approximation and has emphasized studying the properties of the system long after the interaction. Here, we seek to extend these results by investigating the full time evolution of the system, not just at asymptotic times, but also at intermediate times to study out-of-equilibrium properties. To this end, we study the system as it slowly varies in time and investigate the dependence on the truncation of the adiabatic expansion. We introduce a time-dependent probability density of the work done on the system, the work from $t = -\infty$ to time t, $p^{(j)}(w,t)$ and a time-dependent form for the characteristic function $G^{(j)}(\mu,t)$, truncated at adiabatic order j, as

$$G^{(j)}(\mu,t) = \int dw \; e^{i\mu w} p^{(j)}(w,t) \tag{5.22}$$

For adiabatic evolution of the time-dependent Hamiltonian, we employ the result in [137] and extend its interpretation in time at the j-th adiabatic order, as

$$p^{(j)}(w,t) = \sum_{n,m} \delta[w - \Delta\tilde{E}^{(j)}_{mn}(t)]\, \tilde{P}^{(j)}_{nm}(t)\, P_m(-\infty) \tag{5.23}$$

Here $\tilde{P}^{(j)}_{nm}(t)$, defined in (5.13), is the time-dependent probability of finding the system (at the j-th order) in the n-th state after adiabatically evolving from the initially prepared m-th state, and $P_m(-\infty)$ represents the initial thermal equilibrium state of the system

$$P_m(-\infty) = \frac{e^{-\beta E_m(-\infty)}}{Z(-\infty)} = \frac{e^{-\beta\,\omega(-\infty)(m+\frac{1}{2})}}{Z(-\infty)}\ , \tag{5.24}$$

Here $Z(-\infty)$ is the usual partition function for the QHO with the constant asymptotic frequency $\omega(-\infty)$. Also in (5.23), w represents the work done on the system up to time t, and $\Delta\tilde{E}^{(j)}_{mn}(t)$ represents the difference in the energy for the time-dependent transition from the m-th to n-th state, making use of the approximate intermediate time energy relation (5.21). It is defined as

$$\Delta E^{(j)}_{nm}(t) = \tilde{h}^{(j)}\tilde{Q}^{(j)}\left(\frac{1}{2}+n\right) - h_0\left(m+\frac{1}{2}\right) \tag{5.25}$$

Note the dependence on the adiabatic order j. We denote $h_0 \equiv h(-\infty) = \omega(-\infty)$ for convenience from now on.

Due to the form of (5.23), it is straightforward to obtain an expression for the characteristic function $G^{(j)}(\mu,t)$ by using the generating functions for the adiabatic transition probability [90,91,142]. Utilizing the adiabatic approximation for the energy eigenvalues of the system (5.21) and explicitly evaluating the integral in (5.22) using (5.23), the characteristic function, at j-th adiabatic order, can be expressed as

$$G^{(j)}(\mu,t) = \frac{e^{\frac{i}{2}\mu\tilde{h}^{(j)}\tilde{Q}^{(j)}}e^{-\frac{1}{2}h_0[i\mu+\beta]}}{Z(-\infty)}\sum_{mn}\left(e^{i\mu\tilde{h}^{(j)}\tilde{Q}^{(j)}}\right)^n\left(e^{-h_0[i\mu+\beta]}\right)^m\tilde{P}^{(j)}_{mn}(t) \tag{5.26}$$

In this form, we can exploit the equal-time bilinear generating functions involving products of exact (5.4) and adiabatically evolving eigenfunctions (5.5), see Appendix D. The bilinear function for the exactly evolving eigenfunction (5.4) is

$$\sum_{m=0}u^m\psi^*_m(x,t)\psi_m(y,t) = \left(\frac{1}{2\pi\xi^2(t)}\right)^{1/2}\frac{1}{\sqrt{1-u^2}}\cdot$$
$$\cdot\exp\left[\left(-\frac{i}{2}\frac{\dot{\xi}}{\xi}-\frac{1}{4\xi^2}\left[\frac{1+u^2}{1-u^2}\right]\right)x^2+\frac{1}{\xi^2}\left[\frac{u}{1-u^2}\right]xy+\left(\frac{i}{2}\frac{\dot{\xi}}{\xi}-\frac{1}{4\xi^2}\left[\frac{1+u^2}{1-u^2}\right]\right)y^2\right] \tag{5.27}$$

while the bilinear form for the adiabatically evolving eigenfunction (5.5) is

$$\sum_{n=0}v^n\zeta^*_n(y,t)\zeta_n(x,t) = \left(\frac{W^{(j)}}{\pi}\right)^{1/2}\frac{1}{\sqrt{1-v^2}}\cdot$$
$$\cdot\exp\left[\left(\frac{i}{2}\frac{\dot{W}^{(j)}}{W^{(j)}}-\frac{W^{(j)}}{2}\left[\frac{1+v^2}{1-v^2}\right]\right)y^2+2W^{(j)}\left[\frac{v}{1-v^2}\right]xy-\right.$$
$$\left.+\left(\frac{i}{2}\frac{\dot{W}^{(j)}}{W^{(j)}}+\frac{W^{(j)}}{2}\left[\frac{1+v^2}{1-v^2}\right]\right)x^2\right] \tag{5.28}$$

Applying the bilinear forms (5.27,5.28) to the form of characteristic function in (5.26), then simplifies the result to

$$G^{(j)}(\mu,t) = \frac{e^{\frac{1}{2}\beta h_0}\left(1-e^{\beta h_0}\right)}{2\sqrt{\eta[\tilde{Q}^{(j)}(t)]}} \tag{5.29}$$

with the denominator having the form

$$\begin{aligned}\eta[\tilde{Q}^{(j)}(t)] = &- i\tilde{Q}^{(j)}(t)\sinh\left[h_0\left(\beta + i\mu\right)\right]\sin\left[\mu\tilde{h}^{(j)}\tilde{Q}^{(j)}(t)\right] \\ &+ \cosh\left[h_0\left(\beta+i\mu\right)\right]\cos\left[\mu\tilde{h}^{(j)}(t)\tilde{Q}^{(j)}(t)\right] - 1 \end{aligned} \tag{5.30}$$

with the adiabaticity parameter $\tilde{Q}^{(j)}(t)$ defined as (5.14). Notice that the time dependence of this expression enters through its explicit characterization by the adiabaticity parameter $\tilde{Q}^{(j)}(t)$ and the energy $\tilde{h}^{(j)}(t)$. We note that equations (5.29) and (5.30) were obtained without making an approximation and fully describe the work distribution of the time-dependent quantum harmonic oscillator (5.2) for arbitrary parameterizations of the frequency $\omega(t)$.

5.4 Recovering Jarzynski's Equality

We now demonstrate how useful statistical properties of the system can be directly obtained from the characteristic function by solely manipulating the transform (5.22) and utilizing the probability density of the work truncated at j-th order, defined in (5.23). As a result, we also determine a time-dependent formulation of the non-equilibrium theorem that not only describes the relation at asymptotic times but also at intermediate times. The mean work probability distribution at j-th order, across the equivalent forms, follows from

$$-i\partial_\mu G^{(j)}(0,t) = \langle w\rangle^{(j)} = \int dw\, w\, p^{(j)}(w,t) = \sum_{n,m}\Delta\tilde{E}^{(j)}_{nm}(t)\tilde{P}^{(j)}_{nm}(t)\, P_m(-\infty)\ , \tag{5.31}$$

and, by setting $\mu = i\beta$ in (5.22),

$$G^{(j)}(i\beta,t) = \left\langle e^{-w(t)\beta}\right\rangle^{(j)}(t) \equiv \int dw\, e^{-w(t)\beta} p^{(j)}(w,t) \tag{5.32}$$

$$= \sum_{n,m} e^{-\Delta E^{(j)}_{nm}(t)\beta}\, \tilde{P}^{(j)}_{nm}(t)\, P_m(-\infty)\ , \tag{5.33}$$

the left-side of the non-equilibrium work theorem (5.1) is obtained for the j-th adiabatic order. Note the appearance of $w(t)$ in (5.33), which is interpreted at the total work that was performed on the system from $t = -\infty$ to time t.

Utilizing the characteristic function obtained previously, equation (5.29,5.30), the forms for $\langle w\rangle^{(j)}$ and the ensemble average $\langle e^{-w(t)\beta}\rangle^{(j)}(t)$ remarkably simplify. The time-dependent mean of the work probability distribution is then

$$\langle w\rangle^{(j)}(t) = \frac{1}{2}\left[\tilde{h}^{(j)}(t)\left(\tilde{Q}^{(j)}(t)\right)^2 - h_0\right]\coth\left[\frac{\beta h_0}{2}\right] \tag{5.34}$$

while the substitution for $\mu = i\beta$ into the characteristic function (5.29,5.30) yields an explicit time-dependent form to the left-hand-side of the non-equilibrium theorem as

$$\langle e^{-w(t)\beta}\rangle^{(j)}(t) = \frac{\sinh\left[\frac{1}{2}\beta h_0\right]}{\sinh\left[\frac{1}{2}\beta\tilde{h}^{(j)}(t)\tilde{Q}^{(j)}(t)\right]} \tag{5.35}$$

Following how the non-equilibrium theorem relates the work performed on the system to the difference of the Free Energies of the the configuration at $t = -\infty$ and at time t, this is readily identified as the ratio of the partition functions for the time-dependent oscillator at $t = -\infty$ and at time t. Using the approximate form for the energy, the partition function describing the adiabatically evolving time-dependent Hamiltonian (5.2) takes the form

$$Z^{(j)}(t) = \sum_n e^{-n\beta \tilde{E}_n^{(j)}(t)} = \frac{1}{2\sinh\left[\frac{1}{2}\beta\tilde{h}^{(j)}(t)\tilde{Q}^{(j)}(t)\right]} \tag{5.36}$$

and the time-dependent free energy $F^{(j)}(t)$, at j-th order, follows in the usual way as

$$F^{(j)}(t) = -\frac{1}{\beta}\ln\left[Z^{(j)}(t)\right] \tag{5.37}$$

The free energy of the system at past infinity is $F^{(j)}(-\infty) = F(-\infty)$, for all orders j.

We deduce that the time-dependent form for the non-equilibrium work theorem with the time-dependent work $w(t)$ and Free energy $F(t)$ is

$$\langle e^{-w(t)\beta}\rangle^{(j)}(t) = e^{-\beta\left(F^{(j)}(t)-F(-\infty)\right)} \tag{5.38}$$

in which the relation becomes an equality at asymptotically late times. Behind the scenes, the relation is fundamentally determined by the adiabaticity parameter $\tilde{Q}^{(j)}$ truncated at j-th order.

5.5 Time-Dependent Work Probability Distribution

As discussed in Section 5.2.2, the measure of how adiabatically a system evolves in time is determined by the time-dependent adiabaticity parameter $\tilde{Q}^{(j)}(t)$. Truncation at the optimal order provides a universal form to the evolution, with a universal approximate form (5.16), but different parameterizations of the frequency

$\omega(t)$ determine which adiabatic order corresponds to the optimal order and the scale of the adiabaticity parameter (see Section 5.2.2). In this section we explore the consequence on the form of the adiabaticity parameter in relation to the time-dependent work probability.

5.5.1 Work Probability Distribution for $\tilde{Q}^{(j)}(t) \approx 1$

For the evolution of the adiabaticity parameter which is approximately close to unity at all times, we may perform an expansion of the characteristic function:

$$G(\mu, t) \approx \frac{\sinh\left[h_0\beta/2\right]}{\sinh\left[\left(h_0\beta - i\mu\Delta h^{(j)}(t)\right)/2\right]} + \mathcal{O}\left(\tilde{Q}^{(j)}(t) - 1\right) \tag{5.39}$$

where $\Delta h^{(j)}(t) \equiv h_0 - \tilde{h}^{(j)}(t)$. The leading term of this expansion corresponds to the dominant contribution to the characteristic function and further simplifies in the limits of low and high temperature. In the classical (high-T) limit $\beta \ll 1$, we find

$$G^{(j)}(\mu, t) = \frac{\beta h_0}{\beta h_0 - i\mu\Delta h^{(j)}(t)} \tag{5.40}$$

with the corresponding inverse Fourier transform yielding the work distribution

$$p^{(j)}(w, t) = \frac{\beta h_0}{|\Delta h^{(j)}|}\mathrm{Exp}\left[-\frac{w\beta h_0}{\Delta h^{(j)}(t)}\right]\Theta\left[\frac{w\beta h_0}{\Delta h^{(j)}}\right] \tag{5.41}$$

where Θ denotes the Heaviside function. This is the time-dependent form of the time-independent work probability distribution derived by Jarzynski in [125].

In the opposite (low-T limit), $\beta \gg 1$, we find

$$G^{(j)}(\mu, t) = \mathrm{Exp}\left[i\mu\Delta h^{(j)}(t)/2\right] \tag{5.42}$$

with the corresponding inverse Fourier transform yielding the work distribution given by the Delta-Dirac distribution

$$p^{(j)}(w,t) = \delta\left[w - \frac{\Delta h^{(j)}(t)}{2}\right] \tag{5.43}$$

This is the time-dependent generalization of the time-independent result in [142].

5.5.2 Work Probability Distribution for $\tilde{Q}^{(j)}(t) > 1$

We next consider the time-evolution of the adiabaticity parameter for $\tilde{Q}^{(j)}(t) > 1$. The characteristic function in the classical limit $\beta \gg 1$ then simplifies to

$$G^{(j)}(\mu,t) = \frac{\beta h_0}{\sqrt{A[\tilde{Q}^{(j)}(t)]\mu^2 + B[\tilde{Q}^{(j)}(t)]\mu + C}} \tag{5.44}$$

where the coefficients are defined as

$$A[\tilde{Q}^{(j)}(t)] = \tilde{h}^{(j)}(t)\left[\tilde{Q}^{(j)}(t)\right]^2\left(2h_0 - \tilde{h}^{(j)}(t)\right) - h_0^2 \tag{5.45}$$

$$B[\tilde{Q}^{(j)}(t)] = 2i\beta h_0\left(h_0 - \tilde{h}^{(j)}(t)\left[\tilde{Q}^{(j)}(t)\right]^2\right) \tag{5.46}$$

and with $C = \beta^2 h_0^2$. The inverse Fourier transform of (5.44) is obtained with the solution to the integral found in Appendix E, and simplifies to

$$\begin{aligned} p^{(j)}(w,t) = &\sqrt{\frac{\beta^2 h_0^2}{\pi^2 A[\tilde{Q}^{(j)}(t)]}} \exp\left[\frac{B[\tilde{Q}^{(j)}(t)]}{2i\beta A[\tilde{Q}^{(j)}(t)]}\right] \\ &\times K_0\left[\frac{h_0 \tilde{h}^{(j)}(t)\tilde{Q}^{(j)}(t)\sqrt{[\tilde{Q}^{(j)}(t)]^2 - 1}}{\left|A[\tilde{Q}^{(j)}(t)]\right|}\beta|w|\right] \end{aligned} \tag{5.47}$$

The low-temperature limit of the characteristic function (5.44) can be taken but under the restricting limit of small $\tilde{h}^{(j)}(t)$.

5.6 Statistical Properties of the System: Mean Work Probability and Dissipated Work

The time-dependent dissipated work up to time t for a quantum harmonic oscillator driven by the time-dependent frequency $\omega(t)$ is calculated by the difference of the mean work $\langle w\rangle^{(j)}$ in (5.34) and the change in the free energy at the time t, where the free energy is defined in (5.37) and $\Delta F^{(j)}(t) = F^{(j)}(t) - F(-\infty)$:

$$\langle w\rangle^{(j)}_{\text{diss}}(t) = \langle w\rangle^{(j)}(t) - \Delta F^{(j)}(t) \tag{5.48}$$

The time-dependent dissipated work for arbitrary inverse temperature simplifies to

$$\langle w\rangle^{(j)}_{\text{diss}}(t) = \frac{1}{2}\left[\tilde{h}^{(j)}(t)[\tilde{Q}^{(j)}(t)]^2 - h_0\right]\coth\left[\frac{\beta h_0}{2}\right] - \frac{1}{\beta}\ln\left[\frac{\sinh\left[\beta\tilde{h}^{(j)}(t)\tilde{Q}^{(j)}(t)/2\right]}{\sinh[\beta h_0/2]}\right] \tag{5.49}$$

with the smoothest evolution of dissipated work corresponding to truncation of the adiabatic expansion at the optimal order.

5.7 Extroduction

The non-equilibrium work theorem, developed by Jarzynski, is a remarkable relation, in which the work done on the system as it undergoes non-equilibrium evolution can be obtained directly from the free energy differences between initial and final equilibrium configurations of the system. With the universality of Berry's work to describe optimal adiabatic approximation of the evolution of dynamical quantum systems, we developed a time-dependent generalization of the non-equilibrium work relation (5.38) that is not only applicable at asymptotic times but also at intermediate times. This was achieved by modifying the probability work distribution in [137] to take into account a time-dependent probability of making a transitions under the time-dependent driving of the system by $\omega(t)$ and developing an adiabatic approximation of the energy of the system (5.21). Thus, we demonstrated that, behind the scenes of the modified work relation (5.38), the dynamics of the system is governed by a time evolution of the adiabaticity parameter, defined in (5.14). This is a quantity that measures the excitations of the system as it evolves in time. Also derived were various expressions for the statistical properties of the system, such as the time-dependent mean work probability and the mean dissipated work of the system. At optimal truncation of the adiabatic expansion, each of these developed quantities evolves the smoothest in time, as per the universal behavior of the asymptotic expansions. Despite the success of modifying the non-equilibrium work theorem to apply for all time, further considerations are necessary. For instance, for arbitrary inverse temperature β and adiabaticity parameter, a selection rule for the work done, due to the discrete starting expression for the probability work distribution in (5.23), may need to be addressed. Also, it would be interesting to study other forms of the time evolution, and in particular to study the effects of quantum interference on the generalized time-dependent non-equilibrium work theorem.

Chapter 6

Fractionalized Non-self-dual Solutions in the $\mathbb{CP}^{N-1}$ Model

6.1 Introduction

Recent work has emphasized the physical significance of "bions", topologically trivial vacuum configurations that are locally molecules of instantons and anti-instantons, for the study of confinement and chiral symmetry breaking in QCD and supersymmetric gauge theory [144–153]. These are extensions of important related early work by Yung [154], and Rubakov and Shevkov [155]. Using spatial compactification and the principle of continuity, in gauge theories and $\mathbb{CP}^{N-1}$ models a correspondence has been demonstrated between infrared renormalons and certain fractionalized non-perturbative bion (and bion-molecule) objects [156–159]. Motivated by these results, in this chapter we study non-self-dual classical solutions of the $\mathbb{CP}^{N-1}$ model with twisted boundary conditions on the spatially compactified cylinder. These non-self-dual solutions are solutions to the second-order classical equations of motion, but are not solutions to the first-order instanton equations. They have finite action, but are 'unstable' in the sense that the fluctuation operator around these classical solutions has negative modes, and so these solutions are saddle-points of the action rather than minima. They were found and classified by Din and Zakrzewski [160–162] for $\mathbb{CP}^{N-1}$ on $\mathbb{R}^2$ and $\mathbb{S}^2$. Here we investigate these solutions on the spatially compactified cylinder, $\mathbb{S}^1_L \times \mathbb{R}^1$, with $\mathbb{Z}_N$ twisted boundary conditions, and show that the non-self-dual solutions fractionalize with a rich pattern of actions and charges, that can be identified locally with fractionalized instantons that occur in twisted $\mathbb{CP}^{N-1}$ models [163–166].

Our motivation is to propose a new physical interpretation of these 'unstable' finite action classical solutions, in light of recent work on the $\mathbb{CP}^{N-1}$ model using resurgent asymptotic analysis [158,159], in which the perturbative infrared renormalons of $\mathbb{CP}^{N-1}$ were identified with fractionalized multi-instanton configurations [instanton–anti-instanton bions and bion-molecules] in the non-perturbative sector. This identification relies crucially on the spatial compactification, which regularizes the otherwise-ill-defined (due to the instanton scale modulus problem) non-perturbative instanton gas description, and generates $\mathbb{Z}_N$ twisted boundary conditions, which in turn lead to the appearance of fractionalized instanton configurations. Certain multi-instanton amplitudes produce imaginary non-perturbative contributions which were shown to cancel against terms produced by the analysis of the non-Borel-summable (due to infrared renormalons) perturbative sector. Taken together, as a resurgent semi-classical expansion, the imaginary ambiguities in the perturbative and non-perturbative sectors cancel, rendering the theory fully self-consistent. This is a concrete field theoretic realization of the Bogomolny-Zinn-Justin (BZJ) cancellation mechanism of quantum mechanics [167,168,170,169,171,172].

The analysis of $\mathbb{CP}^{N-1}$ bion amplitudes in [158,159], and in the related Yang-Mills studies in [156,157], was based on the standard instanton calculus approach that considers the interactions amongst the constituents of classical configurations consisting of far-separated instantons and anti-instantons [173,154,174–176]. These bions and bion-molecules are *approximate* classical solutions, and for certain alignments and fermion content, the bions or bion-molecules have unstable negative modes leading to imaginary non-perturbative contributions [156–159]. However, we point out here that in precisely these two asymptotically free quantum field theories, 4d Yang-Mills theory and 2d $\mathbb{CP}^{N-1}$, there exist *exact* non-self-dual solutions, consisting locally of combinations of instantons and anti-instantons. These classical solutions have finite action, but have negative fluctuation modes. For 4d Yang-Mills theory, there is a mathematical existence proof for these non-self-dual solutions in $su(2)$ [177], explicit ansatz forms [178–181], and simple embedding constructions for $su(N)$ with $N \geq 4$ [176], but these Yang-Mills solutions are somewhat unwieldy. On the other hand, for $\mathbb{CP}^{N-1}$ there is a simple construction for generating these solutions on $\mathbb{R}^2$ and $\mathbb{S}^2$ [160–162], which makes them easy to analyze. While a number of mathematical properties of these non-self-dual solutions have been studied [160,162,182], no concrete physical interpretation has been proposed. Motivated by the above discussion of resurgent analysis of 4d Yang-Mills theory and 2d $\mathbb{CP}^{N-1}$ [156–159], where spatial compactification and $\mathbb{Z}_N$ twisted boundary conditions play key roles, in this chapter we study the unstable non-self-dual classical solutions in $\mathbb{CP}^{N-1}$ with twisted boundary conditions. The effect of twisted boundary conditions on self-dual instanton solutions has been studied in detail previously, for $\mathbb{CP}^{N-1}$ [163,164] and Yang-Mills [183–185]. While the physical interpretation of these caloron solutions is quite different [158,159], many technical details are similar.

In this chapter we generalize the work of Din and Zakrzewski on non-self-dual solutions to incorporate twisted boundary conditions, and show that the solutions persist, and lead to a rich structure of fractionalized topological charges. Our ultimate motivation is to identify these exact saddle-point solutions with a resurgent trans-series expansion of the field theoretic path integral at weak coupling:

$$\int \mathcal{D}n \, e^{-\frac{1}{g^2}S[n]} = \sum_k \sum_l \sum_p c_{k,l,p} \, e^{-k/g^2} \, g^{2l} \left(\ln \left(-\frac{1}{g^2} \right) \right)^p \tag{6.1}$$

Here the sum over k covers all multi-instanton sectors, the sum over l covers perturbation theory and all perturbative fluctuations about each multi-instanton sector, and the log sum encapsulates quasi-zero mode contributions. This trans-series structure arises generically from a full semi-classical expansion around all critical points, both minima (instantons) and saddle points (non-self-dual classical solutions). While the dominant non-perturbative contributions for a given topological charge come from instantons, the non-self-dual classical solutions are saddle points, so they produce higher-order contributions. Nevertheless, the results of [158,159] show that these saddle point contributions should be included for the semi-classical trans-series expansion (6.1) to be fully self-consistent. This is because, due to the appearance of negative fluctuation modes, these contributions will generically be complex, and for consistency of the theory they must be canceled by imaginary non-perturbative contributions arising from the non-Borel-summable nature of the perturbative expansions about the vacuum and each instanton sector. "Resurgence" is the statement that these cancellations occur to all orders in the expansion (6.1), and this has been demonstrated explicitly for low orders in $\mathbb{CP}^{N-1}$ models [158,159].

Lastly, we note that the work presented here has recently been addressed by Jarzynski and Bolognesi [186].

6.2 Formalism: Classical solutions of $\mathbb{CP}^{N-1}$

We begin with a brief review of notation and previous results [160–162].

6.2.1 Action and Topological Charge

The $\mathbb{CP}^{N-1}$ model has classical action

$$S[n] = \int d^2x \, (D_\mu n)^\dagger (D_\mu n) \tag{6.2}$$

where n is a complex N-component vector satisfying $n^\dagger n = 1$. The $\mathbb{CP}^{N-1}$ model has a global $U(N)$ symmetry and a local $U(1)$ gauge symmetry, for which the covariant derivative is $D_\mu = \partial_\mu - iA_\mu$, with $A_\mu = -i\, n^\dagger \partial_\mu n$. The 2d manifold over which the integral in (6.2) is taken, and associated boundary conditions, will be specified below. The cases of interest here are $\mathbb{R}^2$, $\mathbb{S}^2$ and $\mathbb{S}^1_L \times \mathbb{R}^1$. With a Bogomolny factorization, the action can be re-written

$$S = \int d^2x \left[\frac{1}{2} \Big| D_\mu n \pm i\epsilon_{\mu\nu} D_\nu n \Big|^2 \mp i\epsilon_{\mu\nu} \left(D_\nu n\right)^\dagger D_\mu n \right] \tag{6.3}$$

from which we identify the topological charge

$$Q = \int d^2x\, i\epsilon_{\mu\nu} \left(D_\nu n\right)^\dagger D_\mu n = \int d^2x\, \epsilon_{\mu\nu} \partial_\mu A_\nu \tag{6.4}$$

Thus, $S \geq |Q|$, and we note that for finite action solutions on $\mathbb{R}^2$ and $\mathbb{S}^2$, Q is an integer multiple of 2π.

Another useful representation of the $\mathbb{CP}^{N-1}$ model is in terms of the $N \times N$ holomorphic projector field, $\mathbb{P} \equiv n\, n^\dagger$, which satisfies $\mathbb{P}^2 = \mathbb{P} = \mathbb{P}^\dagger$, and $\mathrm{Tr}\, \mathbb{P} = 1$. The action (6.2) and topological charge (6.4) take the simple form

$$S = 2 \int d^2x\, \mathrm{Tr} \left[\partial_z \mathbb{P}\, \partial_{\bar z} \mathbb{P} \right] \tag{6.5}$$

$$Q = 2 \int d^2x\, \mathrm{Tr} \Big[\mathbb{P}\, \partial_{\bar z} \mathbb{P}\, \partial_z \mathbb{P} - \mathbb{P}\, \partial_z \mathbb{P}\, \partial_{\bar z} \mathbb{P} \Big] \tag{6.6}$$

where $z = x_1 + ix_2$. This projector representation is particularly convenient for analyzing non-self-dual solutions.

6.2.2 Self-dual (instanton) solutions

From the Bogomolny factorization (6.3), we deduce the first-order instanton (self-duality) equations:

$$D_\mu n = \pm i \epsilon_{\mu\nu} D_\nu n \tag{6.7}$$

Explicit instanton solutions are simple to construct using the homogeneous field ω, where $n \equiv \omega/|\omega|$, in terms of which the first-order instanton equations reduce to the Cauchy-Riemann equations, so that instantons correspond to holomorphic vectors, $\omega = \omega(z)$, and anti-instantons correspond to anti-holomorphic vectors, $\omega = \omega(\bar{z})$. In the projector representation, the instanton equations are:

$$\partial_{\bar{z}}\mathbb{P}\,\mathbb{P} = 0 \quad \text{(instanton)} \quad , \quad \partial_z\mathbb{P}\,\mathbb{P} = 0 \quad \text{(anti-instanton)} \tag{6.8}$$

The instanton equations are solved by the $N \times N$ holomorphic projectors, $\mathbb{P} = \frac{\omega\,\omega^\dagger}{\omega^\dagger\omega}$, with $\omega = \omega(z)$.

6.2.3 Non-self-dual solutions

The critical points of the action (6.2) are solutions to the full (second-order) classical equations of motion:

$$D_\mu D_\mu n - (n^\dagger \cdot D_\mu D_\mu n)\, n = 0 \qquad \text{or} \qquad [\partial_z \partial_{\bar{z}}\mathbb{P}\,,\, \mathbb{P}] = 0 \tag{6.9}$$

Note that solutions to the instanton equations (6.7) or (6.8) are automatically solutions to (6.9), but not vice versa.

Explicit non-self-dual solutions can be generated from an initial self-dual (instanton) solution by the following procedure of projection operations [160–162]. We define the projection operator Z_+ acting on a classical solution $\omega(z, \bar{z})$ as:

$$Z_+ : \omega \to Z_+\omega \equiv \partial_z \omega - \frac{\left(\omega^\dagger \partial_z \omega\right)}{\omega^\dagger \omega} \omega \quad , \quad Z_+ : n \to Z_+ n \equiv \frac{Z_+\omega}{|Z_+\omega|} \tag{6.10}$$

It is straightforward to verify using elementary identities that if ω is a classical solution, then $Z_+\omega$ is also a classical solution [160–162]. We can therefore generate a tower of classical solutions by starting with an initial instanton configuration, $\omega = \omega_{(0)}(z)$, and repeatedly acting with Z_+:

$$\omega_{(k)}(z, \bar{z}) \equiv Z_+^k \omega_{(0)}(z) \tag{6.11}$$

Notice that the projection operation (6.10) introduces dependence on $\bar{z}$, due to the adjoint operation, so the projected solutions are no longer instantons. Nevertheless, they satisfy the second-order classical equations of motion. Moreover, the tower of projection operations eventually truncates, after at most $(N-1)$ steps in $\mathbb{CP}^{N-1}$, because eventually the classical solution becomes an anti-instanton, for which $Z_+\omega(\bar{z}) = 0$. (Indeed, we could have begun with an anti-instanton and projected up the ladder in the other direction; this is equivalent.) Din and Zakrzewski proved that on $\mathbb{R}^2$ and $\mathbb{S}^2$, this repeated projection operation (6.11) produces *all* finite action non-self-dual classical solutions [160–162]:

$$\omega_{(0)} \xrightarrow{Z_+} \omega_{(1)} \xrightarrow{Z_+} \cdots \xrightarrow{Z_+} \omega_{(k)} \xrightarrow{Z_+} \cdots \xrightarrow{Z_+} \omega_{(N-1)} \xrightarrow{Z_+} 0 \tag{6.12}$$

In the tower (6.12), the initial solution $\omega_{(0)}$ is an instanton, while the final solution $\omega_{(N-1)}$ is an anti-instanton. Note in particular that for $\mathbb{CP}^1$ we do not generate any non-self-dual solutions, as the initial instanton maps directly to an anti-instanton. Thus, we need to consider at least the $N = 3$ case: $\mathbb{CP}^2$. Explicit examples are presented below.

6.2.4 Action and Topological Charge of Non-Self-Dual Classical Solutions

The projector representation is particularly convenient for describing the action and topological charge of the non-self-dual solutions. The solution $\omega_{(k)}$ has action $S_{(k)}$ and topological charge $Q_{(k)}$ given by expressions (6.5, 6.6) evaluated on the projector

$$\mathbb{P}_{(k)} \equiv \frac{\omega_{(k)}\,\omega_{(k)}^\dagger}{\omega_{(k)}^\dagger \omega_{(k)}} \tag{6.13}$$

Using basic algebraic identities and the result [162] that for all k:

$$\mathbb{P}_{(k)}\bar{\partial}\mathbb{P}_{(k)} = \sum_{j=0}^{k} \bar{\partial}\mathbb{P}_{(j)} \tag{6.14}$$

one can show that:

$$S_{(k)} = Q_{(k)} + 2\sum_{j=0}^{k-1} Q_{(j)} \tag{6.15}$$

Some useful related identities are listed in the Appendix. Since the final solution is an anti-instanton, $S_{(N-1)} = -Q_{(N-1)}$, and therefore we see that $S_{(N-1)} =$

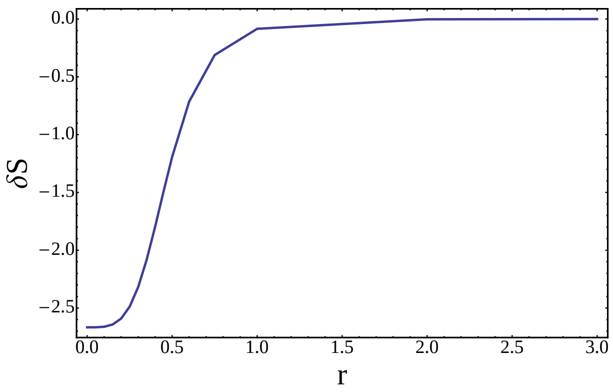

Fig. 6.1: The change (6.18) in the action under the fluctuation (6.17), for the $Q = 0$ non-self-dual configuration plotted in the second row of Figure 6.2. The horizontal axis denotes the (symmetric) distance of each object from the center. At large separation this fluctuation is a zero mode, while at finite separation it becomes a negative mode.

$\sum_{j=0}^{N-2} Q_{(j)}$. For example, for $\mathbb{CP}^2$ ($N = 3$) we have

$$S_{(0)} = Q_{(0)} \quad , \quad S_{(1)} = 2Q_{(0)} + Q_{(1)} \quad , \quad S_{(2)} = Q_{(0)} + Q_{(1)} \tag{6.16}$$

In particular, if the intermediate non-self-dual solution has $Q_{(1)} = 0$, then $S_{(1)} = 2Q_{(0)}$, and $Q_{(2)} = -Q_{(0)}$. For $\mathbb{CP}^{N-1}$ on $\mathbb{R}^2$ and $\mathbb{S}^2$, all $S_{(k)}$ and $Q_{(k)}$ are integer multiples of 2π. We show below that with twisted boundary conditions on the spatially compactified cylinder, $\mathbb{S}^1_L \times \mathbb{R}^1$, there is a much richer set of actions and charges.

6.2.5 Fluctuation Modes

The non-self-dual classical solutions are 'unstable' in the sense that the fluctuation operator about the solution has at least one negative mode. A systematic characterization of the negative modes, and even their number, has not yet been fully performed (see comments in [160–162,182]), but the following physical argument illustrates the point. Consider for example a non-self-dual solution with zero net topological charge, $Q = 0$, consisting locally of 2 instantons and 2 anti-instantons. This is the simplest such non-self-dual configuration. In $\mathbb{CP}^{N-1}$ a single instanton is characterized by $2N$ parameters, and so has $2N$ zero modes. Therefore, this non-self-dual configuration would have a total of $8N$ zero modes in the infinite separation limit. However, the exact solution at finite separation is constructed by applying projection operators to an initial $Q = 2$ instanton, which has just $4N$ zero modes. Thus, the exact non-self-dual solution only has $4N$ zero modes. So, half the zero modes at infinite separation become non-zero-modes, either positive or negative, at finite separation. Depending on the parameters, such as orientations, the lifted zero modes may become negative modes or positive modes. As an example, consider the fluctuation

$$n \to \tilde{n} = n\sqrt{1 - \phi^\dagger \phi} + \phi \qquad , \qquad \phi = D_z n \;\; ; \;\; \phi^\dagger \cdot n = 0 \tag{6.17}$$

for which the change in the action is manifestly negative [160,161]:

$$\delta S = -\int d^2x \left(\mathrm{Tr}\left[(D_z n)^\dagger \, D_z n \, (D_{\bar{z}} n)^\dagger \, D_{\bar{z}} n \right] + \mathrm{Tr}\left[(D_{\bar{z}} n)^\dagger \, D_z n \, (D_z n)^\dagger \, D_{\bar{z}} n \right] \right) \tag{6.18}$$

In Figure 6.1 we plot the change in the action as a function of separation, showing how a zero mode at large separation becomes a negative mode at finite separation. This example is for $\mathbb{CP}^2$ ($N = 3$). The action and charge of the corresponding configuration is shown in the second row of Figure 6.2.

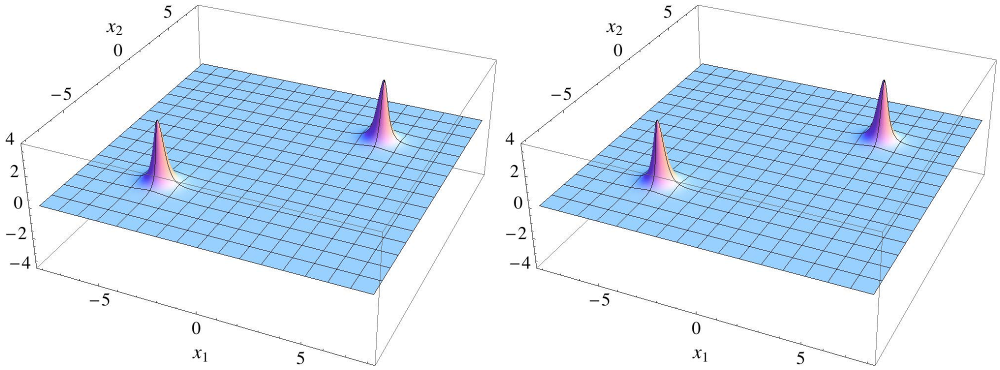

Action Density of $\omega_{(0)}$: $(S_{(0)} = 2)$ Charge Density of $\omega_{(0)}$: $(Q_{(0)} = 2)$

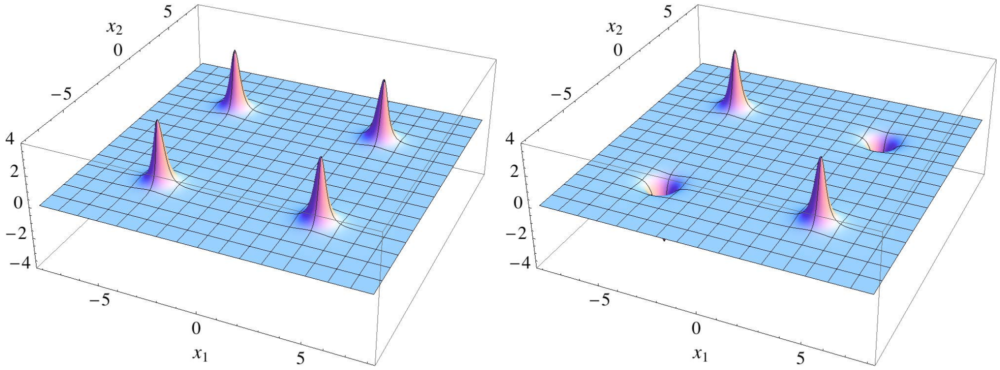

Action Density of $\omega_{(1)}$: $(S_{(1)} = 4)$ Charge Density of $\omega_{(1)}$: $(Q_{(1)} = 0)$

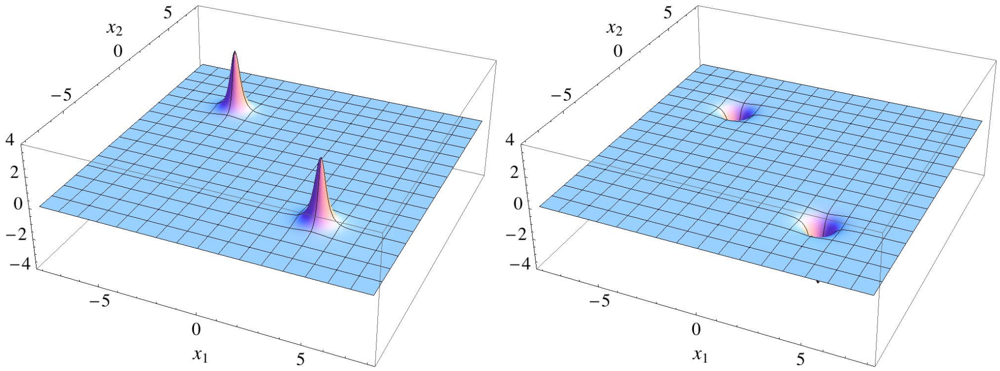

Action Density of $\omega_{(1)}$: $(S_{(2)} = 2)$ Charge Density of $\omega_{(2)}$: $(Q_{(2)} = -2)$

Fig. 6.2: The Action and Charge Density configurations due to successive mappings from the ansatz solution (6.19) in $\mathbb{CP}^2$ on $\mathbb{R}^2$, where $a = a_1 + i\,a_2$ and $b = b_1 + i\,b_2$, with $\lambda, \mu = 2$, $a_1, a_2 = 0$, $b_1, b_2 = 4$, $\forall\ \theta_1, \theta_2 \in [0, 2\pi)$. $\omega_{(0)}$ corresponds to two instantons, while $\omega_{(1)}$ corresponds to two instantons and two anti-instantons, and $\omega_{(2)}$ corresponds to two anti-instantons. All are exact solutions to (6.7) but $\omega_{(1)}$ is non-self-dual.

6.3 Explicit Examples on $\mathbb{R}^2$ and $\mathbb{S}^2$

As Zakrzewski and Din have shown, non-self-dual solutions exist on $\mathbb{R}^2$ (and correspondingly on compactified $\mathbb{S}^2$) for the $\mathbb{CP}^{N-1}$ model when $N \geq 3$. These solutions are characterized by a number of parameters that dictate the location, orientation and profile of the configurations and their sub-components. The simplest example occurs for $\mathbb{CP}^2$ ($N = 3$) on $\mathbb{R}^2$, beginning with a two-instanton. This is illustrated in Figure (6.2), using the two-instanton ansatz

$$\omega_{(0)} = \big(1,\, \lambda\, e^{i\theta_1}\,(z - a)\,,\, \mu\, e^{i\theta_2}(z^2 - b^2)\big) \tag{6.19}$$

This self-dual configuration $\omega_{(0)}$ has total action $S_{(0)} = 2$, and total topological charge $Q_{(0)} = 2$ (as multiples of 2π), and the parameters $\lambda, \mu > 0$, $a, b \in \mathbb{C}$ and $\theta_1, \theta_2 \in [0, 2\pi)$ govern the size, location, and phase orientation of each component single-instanton. After one step, the mapping (6.10) produces a non-self-dual configuration $\omega_{(1)}$, whose action and topological charge densities are shown in the second row of Figure 6.2. A second projection produces a configuration $\omega_{(2)}$ which is anti-self-dual, comprising two anti-instantons, as shown in the third row of Figure 6.2. When $a = 0$, the original solution $\omega_{(0)}$ and mapped solutions, $\omega_{(1)}$ and $\omega_{(2)}$, correspond to symmetric configurations whose individual components are equally spaced, as seen in Figure 6.2. The non-self-dual configuration $\omega_{(1)}$ in the second line of Figure 6.2 consists of two instantons and two anti-instantons, each of action one, leading to a total action of $S_{(1)} = 4$, and zero total topological charge, $Q_{(1)} = 0$. The final mapping generates a configuration that consists of two anti-instantons of charge-(-1). So we can summarize the action and topological charge values of the tower of solutions as:

$$\left(S_{(0)}, Q_{(0)}\right) = (2,2) \xrightarrow{Z_+} \left(S_{(1)}, Q_{(1)}\right) = (4,0) \xrightarrow{Z_+} \left(S_{(2)}, Q_{(2)}\right) = (2,-2) \tag{6.20}$$

Note the consistency with the relations in (6.16).

6.4 Explicit Examples on $\mathbb{S}^1_L \times \mathbb{R}^1$

As in [158,159], we impose $\mathbb{Z}_N$ twisted boundary conditions in the compactified spatial direction:

$$n(x_1, x_2 + L) = \Omega\, n(x_1, x_2) \quad , \quad \Omega = \text{diag}\left(1, e^{-2\pi i/N}, \ldots, e^{-2\pi i(N-1)/N}\right) \tag{6.21}$$

This corresponds to the same condition on the homogeneous field $\omega(x_1, x_2)$, and we see from (6.10) that if the initial instanton solution $\omega_{(0)}$ satisfies $\mathbb{Z}_N$ twisted boundary conditions, then all subsequent projected solutions in (6.10), (in particular, the non-self-dual ones), also satisfy $\mathbb{Z}_N$ twisted boundary conditions.

For self-dual solutions, the fractionalization arises because of an interplay between the twisted boundary condition, which could be imposed by phase factors in the compactified x_2 direction, and the holomorphicity condition for an instanton. Thus for an instanton, the twists must arise from factors expressed in terms of the holomorphic variable $z = x_1 + ix_2$, and so the twists in the compact

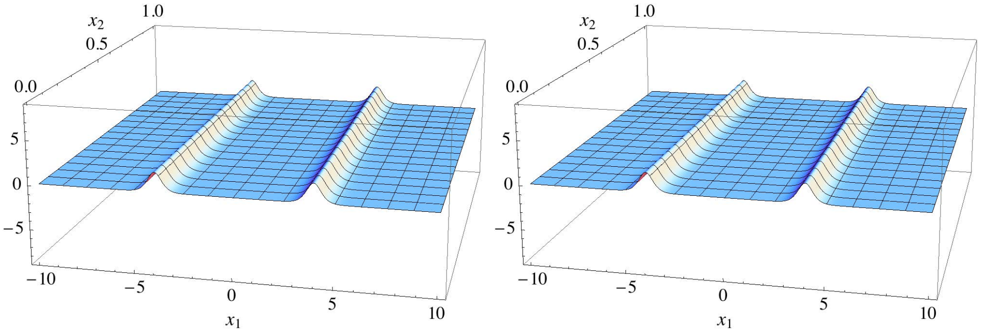

Action Density of $\omega_{(0)}$: $(S_{(0)} = \frac{2}{3})$

Charge Density of $\omega_{(0)}$: $(Q_{(0)} = \frac{2}{3})$

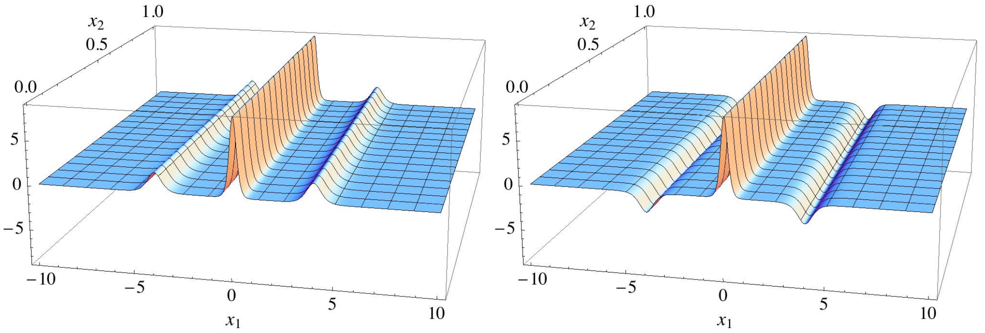

Action Density of $\omega_{(1)}$: $(S_{(1)} = \frac{4}{3})$

Charge Density of $\omega_{(1)}$: $(Q_{(1)} = 0)$

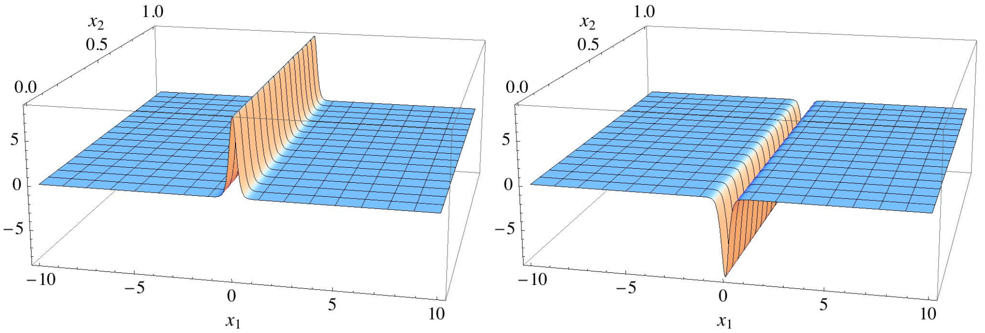

Action Density of $\omega_{(2)}$: $(S_{(2)} = \frac{2}{3})$

Charge Density of $\omega_{(2)}$: $(Q_{(2)} = -\frac{2}{3})$

Fig. 6.3: The Action and Charge Density configurations due to successive mappings from the ansatz solution (6.22) in $\mathbb{CP}^2$ on $\mathbb{S}^1_L \times \mathbb{R}^1$, with $\lambda = 4000, \mu = 1, \forall\ \theta_1, \theta_2 \in [0, 2\pi)$. $\omega_{(0)}$ corresponds to two fractionalized instantons, while $\omega_{(1)}$ corresponds to a single fractionalized instanton and two anti-instantons, and $\omega_{(2)}$ corresponds to a single fractionalized anti-instanton. All are exact solutions to (6.7) but $\omega_{(1)}$ is non-self-dual.

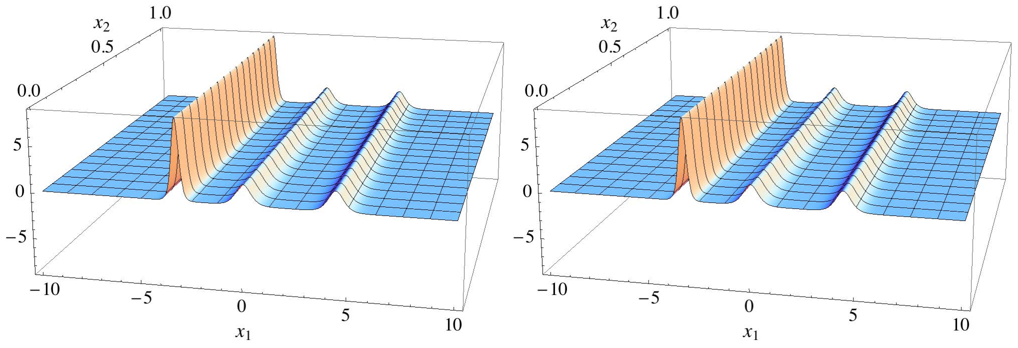

Action Density of $\omega_{(0)}$: $(S_{(0)} = \frac{4}{3})$ Charge Density of $\omega_{(0)}$: $(Q_{(0)} = \frac{4}{3})$

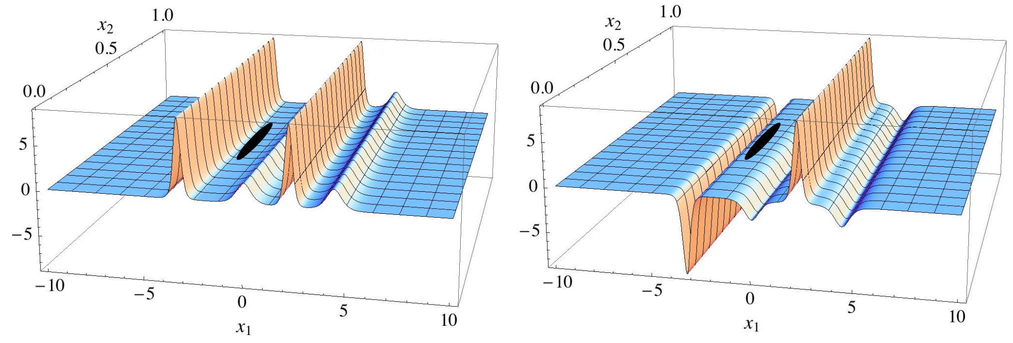

Action Density of $\omega_{(1)}$: $(S_{(1)} = 3)$ Charge Density of $\omega_{(1)}$: $(Q_{(1)} = \frac{1}{3})$

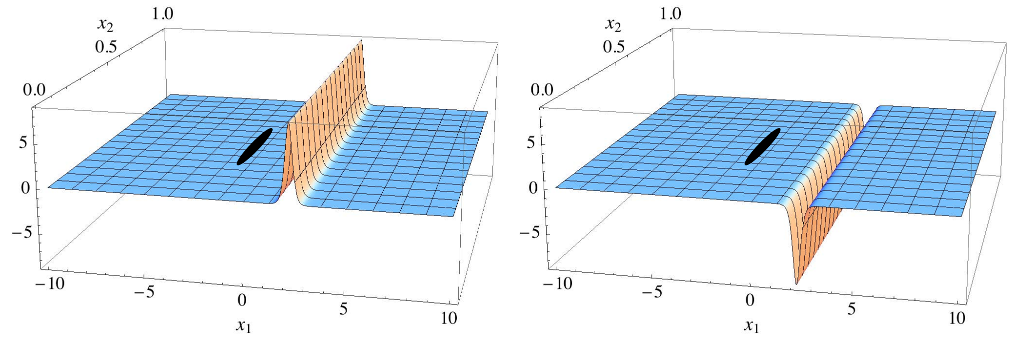

Action Density of $\omega_{(2)}$: $(S_{(2)} = \frac{5}{3})$ Charge Density of $\omega_{(2)}$: $(Q_{(2)} = -\frac{5}{3})$

Fig. 6.4: The Action and Charge Density configurations due to successive mapping from an ansatz solution with more structure (6.24) in $\mathbb{CP}^2$ on $\mathbb{S}^1_L \times \mathbb{R}^1$, with $\lambda = 10^4, \mu = 10^{-2}, \nu = 10^4$, $\theta_1 = \pi, \theta_2 = 0, \forall\, \theta_3 \in [0, 2\pi)$. See text for quantitative details on the mapping. $\omega_{(0)}$, $\omega_{(1)}$ and $\omega_{(2)}$ are all exact solutions to (6.7), but $\omega_{(1)}$ is non-self-dual.

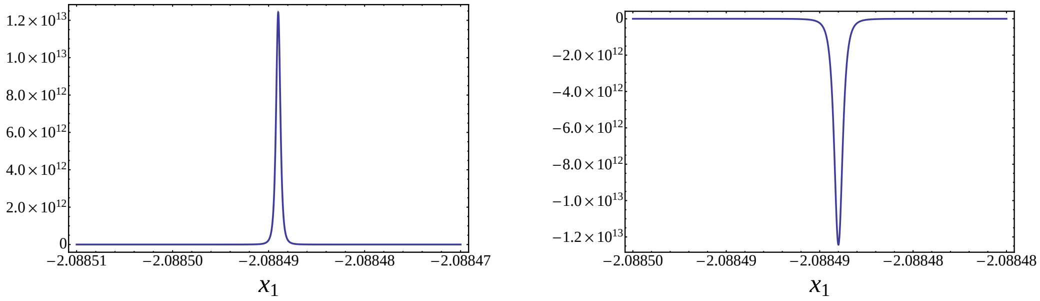

Fig. 6.5: A magnified cross section of the charge density of the highly localized charge-1 instanton and anti-instanton that appear in the fourth and sixth plots in Figure 6.4. Both are plotted with the same parameters used in Figure 6.4.

x_2 direction necessarily also affect the form of the solution in the non-compact x_1 direction [163,164,158,159]. For non-self-dual solutions, the fractionalization is inherited from the fractionalization of the initial self-dual solution $\omega_{(0)}$.

We illustrate the effect of twisted boundary conditions on some non-self-dual configurations in $\mathbb{CP}^2$, for which $N = 3$. The first example demonstrates a configuration analogous to that in Figure 6.2 on $\mathbb{R}^2$, while the second demonstrates a new effect not seen on $\mathbb{R}^2$. These examples also serve to demonstrate the diversity of non-self-dual solutions that are possible with twisted boundary conditions in $\mathbb{CP}^2$ on $\mathbb{S}^1_L \times \mathbb{R}^1$.

Example 1: Figure 6.3 shows the simplest non-self-dual solution, manifest in $\mathbb{CP}^2$, on $\mathbb{S}^1_L \times \mathbb{R}^1$ with $\mathbb{Z}_3$ twisted boundary conditions. We take an initial two-instanton ansatz

$$\omega_{(0)} = \left(1,\, \lambda\, e^{i\theta_1} e^{-2\pi z/3},\, \mu\, e^{i\theta_2} e^{-4\pi z/3}\right), \tag{6.22}$$

where $\lambda, \mu > 0$, $\theta_1, \theta_2 \in [0, 2\pi)$. This solution is self-dual, with action and charge

$S_{(0)} = Q_{(0)} = 2/3$, consisting of two separate fractionalized instantons of charge 1/3. After one application of the mapping (6.10) we obtain a non-self-dual configuration $\omega_{(1)}$ with zero net topological charge $Q_{(1)} = 0$, and action $S_{(1)} = 4/3$, as shown in the second row of Figure 6.3. We can identify this configuration as consisting of a double-instanton of charge 2/3 at the midpoint of the original instanton components, with two anti-instantons each of charge $-1/3$, located near the positions of the original instanton components. Note the difference from the example on $\mathbb{R}^2$ in Figure 6.2. After one further application of the mapping (6.10) we obtain an anti-self-dual configuration $\omega_{(2)}$, which for this choice of parameters looks like a double (fractionalized) anti-instanton configuration, with total charge $-2/3$. So we can summarize the action and topological charge values of the tower of solutions as:

$$\left(S_{(0)}, Q_{(0)}\right) = \left(\frac{2}{3}, \frac{2}{3}\right) \xrightarrow{Z_+} \left(S_{(1)}, Q_{(1)}\right) = \left(\frac{4}{3}, 0\right) \xrightarrow{Z_+} \left(S_{(2)}, Q_{(2)}\right) = \left(\frac{2}{3}, -\frac{2}{3}\right) \tag{6.23}$$

Note the consistency with the relations in (6.16).

Example 2: Figure 6.4 shows a non-trivial non-self-dual solution in $\mathbb{CP}^2$ on $\mathbb{S}^1_L \times \mathbb{R}^1$ with $\mathbb{Z}_3$ twisted boundary conditions. We begin with the initial instanton ansatz

$$\omega_{(0)} = \left(1,\, \lambda\, e^{i\theta_1} e^{-2\pi z/3} + \mu\, e^{i\theta_2} e^{-8\pi z/3},\, \nu\, e^{i\theta_3} e^{-4\pi z/3}\right), \tag{6.24}$$

where $\lambda, \mu, \nu > 0$, $\theta_1, \theta_2, \theta_3 \in [0, 2\pi)$. This starting configuration consists of three instantons of topological charge $2/3, 1/3$ and $1/3$, respectively, producing

$S_{(0)} = Q_{(0)} = 4/3$. On comparison with (6.22) and Figure 6.3, we note that the inclusion of the extra $\mathbb{Z}_3$ twist preserving term $\exp[-8\pi z/3]$ directly contributes the extra charge 2/3 instanton in the starting configuration, and imbues greater structure to the subsequent non-self-dual solution. At first sight, the non-self-dual configuration $\omega_{(1)}$ plotted in the second row of Figure 6.4 appears to consist of one instanton of charge 2/3, and three anti-instantons, two of charge $-1/3$, and one of charge $-2/3$. This would suggest a net charge of $-2/3$ and net action equal to 2. However, there is another instanton, of net charge $+1$, which for these parameters is not fractionalized, that is a very sharp peak that can not be seen on the scale of the figure. It is marked by the black oval in the plots in the second line of Figure 6.4. A magnified cross-section of this extra instanton is shown in Figure 6.5. Thus, the actual assignment of action and charge, which is easily verified by numerical integration, is $S_{(1)} = 3$, and $Q_{(1)} = 1/3$. It is interesting to see that for this non-self-dual configuration some sub-components are clearly fractionalized, while there is a distinct lump that is not. This demonstrates a richer structure when compared to the non-self-dual solutions on $\mathbb{R}^2$ (and $\mathbb{S}^2$). The unresolved sharp peaks in the configurations of Figure 6.4, marked by a black oval shape, correspond to this highly localized non-fractionalized instanton and anti-instanton, and have the resolved form shown in Figure 6.5. In addition, the extra twist preserving term also affects the final mapped configuration $\omega_{(2)}$, with further structure when compared to Figure 6.3. Thus, while at first sight, it looks like the final configuration $\omega_{(2)}$ has $S_{(2)} = -Q_{(2)} = 2/3$, in fact there is a very sharply peaked anti-instanton at the location marked by the black oval, leading to the net result: $S_{(2)} = -Q_{(2)} = 5/3$. Observe that, unlike the $\mathbb{R}^2$ examples, the total action and topological charge of the final solution $\omega_{(0)}$ need not be equal to those of the starting solution $\omega_{(2)}$. So we summarize the action and topological charge values of this tower of solutions as:

$$\left(S_{(0)}, Q_{(0)}\right) = \left(\frac{4}{3}, \frac{4}{3}\right) \xrightarrow{Z_+} \left(S_{(1)}, Q_{(1)}\right) = \left(3, \frac{1}{3}\right) \xrightarrow{Z_+} \left(S_{(2)}, Q_{(2)}\right) = \left(\frac{5}{3}, -\frac{5}{3}\right) \tag{6.25}$$

Note again the consistency with the relations in (6.16). With the inclusion of further twist preserving terms, an even richer set of solutions develop that are unique to twisted boundary conditions on $\mathbb{S}^1_L \times \mathbb{R}^1$, generating all multiples of 1/3 for the charge of the non-self-dual solution $\omega_{(1)}$.

Lastly, some important and useful projector identities can be found in Appendix F.

6.5 Conclusion

In this chapter we have shown that Din and Zakrzewski's construction of non-self-dual classical solutions in the $\mathbb{CP}^{N-1}$ model on $\mathbb{R}^2$ and $\mathbb{S}^2$ extends naturally to non-self-dual classical solutions on $\mathbb{S}^1_L \times \mathbb{R}^1$, with $\mathbb{Z}_N$ twisted boundary conditions. As occurs for the self-dual instantons, the non-self-dual solutions fractionalize into sub-component objects, which we can identity locally as fractionalized instantons and anti-instantons. This leads to a much richer spectrum of actions and charges, generically in integer units of $1/N$ for $\mathbb{CP}^{N-1}$. We furthermore propose that the physical significance of these ‘unstable’ non-self-dual solutions is not associated with unstable vacuum decay, but rather that in a semi-classical saddle point analysis of the path integral they produce imaginary non-perturbative terms that match (and cancel against) imaginary non-perturbative terms arising in the perturbative sector due to the infrared-renormalon-induced non-Borel-summability of perturbation theory for $\mathbb{CP}^{N-1}$. This suggests that it would be worthwhile to classify and analyze more systematically the negative modes corresponding to these exact non-self-dual solutions. Technically, in $\mathbb{CP}^{N-1}$ we see that these negative modes arise as some would-be zero-modes associated with an approximate non-self-dual configuration of infinitely-far-separated instantons and anti-instantons, become negative modes as these sub-components approach one another; the exact non-self-dual solution has fewer zero-modes than its sub-components would suggest, because it inherits these zero-modes from the parameters of the simpler initial self-dual configuration $\omega_{(0)}$. We expect similar behavior in twisted Yang-Mills theory, although the $\mathbb{CP}^{N-1}$ case is simpler and more explicit. Finally, we note that similar effects should also occur in other 2d sigma models.

Chapter 7

Conclusion

In this dissertation, I have studied semiclassical effects in QFT and made use of the universal behavior of the asymptotic adiabatic expansion to study quantum non-equilibrium dynamics for systems with time-dependent driving. The universality of optimal truncation of the divergent and asymptotic adiabatic expansion provides a well-defined concept for the adiabatic approximation of the far-from-evolution of dynamical systems. I have considered three applications: 1) particle production with time-dependent driving, where a consistent definition to time-dependent particle production was developed and the back-reaction problem was addressed, 2) Jarzynski's non-equilibrium work theorem was modified to incorporate optimal adiabatic evolution, for study of non-equilibrium quantum dynamics, and 3) the semi-classical (non-instanton) solutions in an asymptotically free $\mathbb{CP}^{N-1}$ model were classified. This work has been published in three papers in Physical Review D [187–189].

Appendices

A Schwinger Effect for Spinor QED

We now consider the production of fermionic particles in the Schwinger Effect and briefly outline the analogous decomposition of the equation of motion to a set of decoupled oscillators spanned by the momentum k, as seen in the scalar version of QED. Apart from opposite phase of interference effects, the physics is very similar to sQED but more notationally technical. Of physical importance to the Schwinger Effect is that the electron and positron mass is much smaller than that of any known charged scalar particle. Thus the Schwinger critical field is much smaller in QED and particle production is dominated by the production of e^+e^- pairs. Lastly, this section demonstrates that the results formulated in Chapter 2 to address a time-dependent particle number can be applied to fermionic QED.

The action of a charged massive fermion is given by the Dirac Lagrangian under a local $U(1)$ symmetry:

$$S = \int d^4x \, \bar{\psi} \left(i \not{D} - m \right) \psi \tag{7.1}$$

where $D_\mu = \partial_\mu + ieA_\mu$. Extremizing the action, the equations of motion for the spinor field $\psi(x,t)$ read

$$\left(i \not{D} - m \right) \psi = 0 \tag{7.2}$$

Considering a time-dependent, spatially homogeneous electric field given by the vector potential $A^\mu(x) = \delta^\mu_3 A(x^0)$, the equation of motion reduces to

$$\left(i\partial\!\!\!/ - e\gamma^3 A_3 - m\right)\psi = 0 \tag{7.3}$$

This equation can be conveniently rewritten by defining an auxiliary field χ defined as

$$\psi \equiv \left(i\partial\!\!\!/ - e\gamma^3 A_3 - m\right)\chi \tag{7.4}$$

which transforms equation (7.3) into a Klein-Gordon-like expression for the auxiliary field χ:

$$\left(\partial_\mu\partial^\mu + m^2(eA_3)^2 + e\gamma^0\gamma^3\dot{A}_3 - 2ieA_3\partial^3\right)\chi = 0 \tag{7.5}$$

This equation can now be solved via mode decomposition with the following ansatz for positive and negative solutions:

$$\chi_{k,1} \sim e^{i\mathbf{k}\cdot\mathbf{x}} g_k(t)\epsilon_1 \qquad\qquad \chi_{k,2} \sim e^{-i\mathbf{k}\cdot\mathbf{x}} g_k^*(t)\epsilon_2 \tag{7.6}$$

where $g_k(t)$ denotes the fermionic time-dependent complex mode functions and ϵ_s correspond to the positive eigenvalues of the matrix $\gamma^0\gamma^3$, thus fixing the degrees of freedom, which have the form

$$\epsilon_1 = (0,1,0,-1)^T \qquad\qquad \epsilon_2 = (1,0,1,0)^T \tag{7.7}$$

Requiring the ansatz (7.6) be a solution to equation (7.5), yields the fermionic set of decoupled linear time-dependent oscillator equations spanned by the momenta k:

$$\ddot{g}_k(t) + \omega_k^2(t) g_k(t) = 0 \tag{7.8}$$

Here, the effective frequency, with the field and momenta k written in terms of the polarization of the electric, is

$$\omega_k^2(t) = m^2 + k_\perp^2 + \big(k_\parallel - eA_\parallel(t)\big) + ie\dot{A}_\parallel(t) \tag{7.9}$$

Lastly, we note that because spinors satisfy anti-commutation relations, the corresponding Bogoliubov transformation from time-independent to time-dependent creation/annihilation operators must now be a $SU(2)$ transformation:

$$\begin{pmatrix} \tilde{a}_k(t) \\ \tilde{b}^\dagger_{-k}(t) \end{pmatrix} = \begin{pmatrix} \alpha_k(t) & \beta_k^*(t) \\ \beta_k(t) & \alpha_k^*(t) \end{pmatrix} \begin{pmatrix} a_k \\ b^\dagger_{-k} \end{pmatrix} \tag{7.10}$$

such that unitarity requires $|\alpha_k(t)|^2 + \beta_k(t)|^2 = 1$ for fermions, for all time t.

B Single-pulse Analytical Example

An analytic example that is commonly used in the literature [190] in connection with the adiabatic particle number is the single-pulse electric field given by (2.119) with the vector potential (2.120). The solution of the Klein-Gordon equation (2.16) with this electric field case is a hypergeometric solution of the form

$$f_k(t) = \frac{(-x)^{-i\mu_k}(1-x)^\epsilon}{\sqrt{2\omega_k(-\infty)}}\, {}_2F_1\left[\epsilon - i(\mu_k+\nu_k), \epsilon - i(\mu_k-\nu_k), 1-2i\mu_k, x\right] \tag{7.11}$$

where $x \equiv -e^{2at}$, and

$$\epsilon = \frac{1}{2}\left(1+\sqrt{1-\frac{4E_0^2}{a^4}}\right) \qquad \mu_k = \frac{\omega_k(-\infty)}{2a} \qquad \nu_k = \frac{\omega_k(+\infty)}{2a} \tag{7.12}$$

which satisfies the Wronskian condition (2.15) and matches the rightward scattering scenario (2.24). From (2.18), then the absolute magnitude of (7.11) is the analytic solution to the Ermakov-Milne equation (2.19). The scattering coefficients in equation (2.24) with (7.11) are

$$A_k = \sqrt{\frac{\nu_k}{\mu_k}} \frac{\Gamma\left(1 - 2i\mu_k\right)\Gamma\left(-2i\nu_k\right)}{\Gamma\left(\epsilon - i(\mu_k + \nu_k)\right)\Gamma\left(1 - \epsilon - i(\mu_k + \nu_k)\right)} \tag{7.13}$$

$$B_k = \sqrt{\frac{\nu_k}{\mu_k}} \frac{\Gamma\left(1 - 2i\mu_k\right)\Gamma\left(2i\nu_k\right)}{\Gamma\left(\epsilon - i(\mu_k - \nu_k)\right)\Gamma\left(1 - \epsilon - i(\mu_k - \nu_k)\right)} \tag{7.14}$$

where the coefficients satisfy unitarity, $|A_k|^2 - |B_k|^2 = 1$, and are related to the final-time Bogoliubov coefficients by $A_k = \alpha_k(+\infty)$ and $B_k = \beta_k(+\infty)$. Thus, the final particle number at future infinity for the single-pulse case is precisely $\tilde{\mathcal{N}}_k(+\infty) = |B_k|^2$.

C Transition Amplitude Evaluation: Double Hermite Integral Solution

Determining the adiabatic transition amplitude of a generalized quantum harmonic system evolving to the n-th state at a later time t from being initially prepared in the m-th state requires evaluating an integral composed of a product of two Hermite polynomials (2.78). The solution of the integral for arbitrary

Hermite polynomial orders and arguments is presented:

$$\frac{1}{\sqrt{2\pi}}\int_{-\infty}^{\infty} dy\, e^{-\frac{1}{2}y^2} H_n(ay)H_m(by) =$$
$$= \begin{cases} \frac{n!m!}{(\frac{n}{2})!(\frac{n}{2})!}\left(2a^2-1\right)^{\frac{n}{2}}\left(2b^2-1\right)^{\frac{m}{2}} {}_2F_1\left[-\frac{m}{2}, -\frac{n}{2}, \frac{1}{2}, \rho^2\right], & \text{for}\, m,n = \text{even} \\ \frac{2n!m!\,ab}{(\frac{n-1}{2})!(\frac{m-1}{2})!}\left(2a^2-1\right)^{\frac{n-1}{2}}\left(2b^2-1\right)^{\frac{m-1}{2}} {}_2F_1\left[\frac{1-m}{2}, \frac{1-n}{2}, \frac{3}{2}, \rho^2\right], & \text{for}\, m,n = \text{odd} \\ 0, & \text{for}\, m+n = \text{odd} \end{cases} \tag{7.15}$$

for $a, b \in \mathbb{C}$ and

$$\rho = \frac{2ab}{\sqrt{(2a^2-1)(2b^2-1)}} \tag{7.16}$$

D Hermite Bilinear Forms

The bilinear generating function (Mehler Formula) for the product of two Hermite Polynomials with equal indices but different arguments:

$$\sum_{n=0} \frac{\theta^n}{2^n n!} H_n(x)H_n(y) = \frac{1}{\sqrt{1-\theta^2}}\exp\left[\frac{2\theta xy - \theta^2(x^2+y^2)}{1-\theta^2}\right] \tag{7.17}$$
$$= \frac{1}{\sqrt{1+\theta}}\exp\left[\frac{\theta\,(x+y)^2}{2\,(1+\theta)}\right]\frac{1}{\sqrt{1-\theta}}\exp\left[-\frac{\theta\,(x-y)^2}{2\,(1-\theta)}\right]$$

E A Useful Integral

The following integral has the solution [191]:

$$\int_{-\infty}^{+\infty} dx\,\frac{e^{i\lambda x}}{(x^2+z^2)^{\rho}} = \frac{2^{3/2-\rho}\sqrt{\pi}}{\Gamma[\rho]} K_{\rho-1/2}\left(z|\lambda|\right) \tag{7.18}$$

where $K_\nu(x)$ is the MacDonald Function.

F $\mathbb{CP}^{N-1}$ Projector Identities

We list some useful identities concerning the non-self-dual configurations generated by the mapping (6.11). For all classical solutions generated by (6.11), we have:

$$\omega^\dagger_{(k)}\,\omega_{(l)} = 0 \quad \text{if } \; k \neq l \tag{7.19a}$$

$$\partial_{\bar z}\,\omega_{(k)} = -\,\omega_{(k-1)}\,\frac{|\omega_{(k)}|^2}{|\omega_{(k-1)}|^2} \tag{7.19b}$$

$$\partial_z\left(\frac{\omega_{(k-1)}}{|\omega_{(k-1)}|^2}\right) = \frac{\omega_{(k)}}{|\omega_{(k-1)}|^2} \tag{7.19c}$$

$$\omega_{(N)} = Z_+\omega_{(N-1)} = 0 \tag{7.19d}$$

In terms of the projectors:

$$\omega_{(k+1)} \propto \partial_z \mathbb{P}_{(k)}\omega_{(k)} \qquad , \qquad \omega_{(k-1)} \propto \partial_{\bar z}\mathbb{P}_{(k)}\omega_{(k)} \tag{7.20}$$

The following projector identities are useful in determining (6.15), and are general for all Grassmanians:

$$\mathbb{P}_{(i)}\,\mathbb{P}_{(j)} = \mathbb{P}_{(i)}\delta_{ij} \tag{7.21a}$$

$$\mathbb{P}_{(i)}\,\partial_z\mathbb{P}_{(i)}\,\mathbb{P}_{(i)} = 0 \quad \forall\, i \tag{7.21b}$$

$$\mathbb{P}_{(i)}\,\partial_z\mathbb{P}_{(j)} = 0 \quad \text{if} \quad j = i+1 \quad \text{or} \quad |i-j| \geq 2 \tag{7.21c}$$

$$\partial_z\mathbb{P}_{(i)}\,\mathbb{P}_{(j)} = 0 \quad \text{if} \quad j = i+1 \quad \text{or} \quad |i-j| \geq 2 \tag{7.21d}$$

$$\partial_z\mathbb{P}_{(i)}\,\partial_z\mathbb{P}_{(j)} = 0 \quad \text{if} \quad j = i+1 \quad \text{or} \quad j = i+2 \quad \text{or} \quad |i-j| \geq 3 \tag{7.21e}$$

$$\partial_z\mathbb{P}_{(i)}\,\partial_{\bar z}\mathbb{P}_{(j)} = 0 \quad \text{if} \quad |i-j| \geq 2 \tag{7.21f}$$

Additional identities are found by taking the Hermitian conjugate since $\left(\partial_z \mathbb{P}_{(i)}\right)^\dagger = \partial_{\bar{z}} \mathbb{P}_{(i)}$.

Bibliography

[1] W. Heisenberg and H. Euler, "Consequences of Dirac's Theory of Positrons," Z. Phys. **98**, 714 (1936).

[2] J. Schwinger, "On gauge invariance and vacuum polarization," Phys. Rev. **82** (1951) 664.

[3] A. Ringwald, "Pair production from vacuum at the focus of an X-ray free electron laser," Phys. Lett. **B510**, 107 (2001).

[4] G. V. Dunne, "Heisenberg-Euler effective Lagrangians: Basics and extensions," Ian Kogan Memorial Collection, *'From Fields to Strings: Circumnavigating Theoretical Physics,'* M. Shifman et al (ed.), vol. 1, pp 445, (World Scientific, 2005).

[5] W. Greiner, B. Müller and J. Rfelski, *Quantum Electrodynamics of Strong Fields*, (Springer, Berlin, 1985).

[6] L. Parker, "Particle creation in expanding universes," Phys. Rev. Lett. **21**, 562 (1968).

[7] L. Parker, "Quantized fields and particle creation in expanding universes. 1.," Phys. Rev. **183**, 1057 (1969).

[8] L. Parker, "Quantized fields and particle creation in expanding universes. 2.," Phys. Rev. D **3**, 346 (1971). [Erratum-ibid. D **3**, 2546 (1971)].

[9] S. A. Fulling, *Aspects of Quantum Field Theory in Curved Space-time*, London Math. Soc. Student Texts **17**, 1 (1989).

[10] N. D. Birrell and P. C. W. Davies, *Quantum Fields in Curved Space*, (Cambridge Univ Press, 1983).

[11] E. Mottola, "Particle Creation in de Sitter Space," Phys. Rev. D **31**, 754 (1985).

[12] E. Greenwood D. C Dai and D. Stojkovic, “Time dependent fluctuations and particle production in cosmological de Sitter,” Phys. Rev. Lett. B **692**, 226 (2010).

[13] P. R. Anderson and E. Mottola, “On the Instability of Global de Sitter Space to Particle Creation,” Phys. Rev. D **89**, 104038 (2014).

[14] P. R. Anderson and E. Mottola, “Quantum Vacuum Instability of ’Eternal’ de Sitter Space,” Phys. Rev. D **89**, 104039 (2014).

[15] R. Bousso, A. Maloney, and A. Strominger, “Conformal vacua and entropy in de Sitter space,” Phys. Rev. D **65**, 104039 (2002).

[16] Y. B. Zeldovich, “Particle Creation in cosmology,” Pisma Zh. Eksp. Teor. Fiz. **12**, 443 (1970).

[17] Y. .B. Zeldovich and A. A. Starobinsky, “Particle production and vacuum polarization in an anisotropic gravitational field,” Sov. Phys. JETP **34**, 1159 (1972).

[18] A. M. Polyakov, “De Sitter space and eternity,” Nucl. Phys. B **797**, 199 (2008).

[19] A. M. Polyakov, “Decay of Vacuum Energy,” Nucl. Phys. B **834**, 316 (2010).

[20] T. Vachaspati, D. Stojkovic and L. Krauss, “Observation of Incipient Black Holes and the Information Loss Problem,” Phys. Rev. D, **76**, 024005 (2007).

[21] M. Kolopanis and T. Vachaspati, “Quantum Excitations in Time-dependent Backgrounds,” Phys. Rev. D **87**, 085041 (2013).

[22] G. Mahajan and T. Padmanabhan, “Particle Creation, Classicality, and Related Issues in Quantum Field Theory: I. Formalism and Toy Models,” Gen. Rel. Grav. **40**, 661 (2007).

[23] G. Mahajan and T. Padmanabhan, “Particle Creation, Classicality, and Related Issues in Quantum Field Theory: II. Examples From Field Theory,” Gen. Rel. Grav. **40**, 709 (2007).

[24] L. H. Ford, “Gravitational Particle Production and Inflation,” Phys. Rev. D **35**, 2955 (1987).

[25] G. W. Gibbons and S. W. Hawking, “Cosmological Event Horizons, Thermodynamics, and Particle Creation,” Phys. Rev. D **15**, 2738 (1977).

[26] W. G. Unruh, “Notes on blackhole evaporation,” Phys. Rev. D **14**, 870 (1976).

[27] R. Schutzhold, G. Schaller and D. Habs, “Signatures of the Unruh effect from electrons accelerated by ultra-strong laser fields,” Phys. Rev. Lett. **97**, 121302 (2006), Erratum: [Phys. Rev. Lett. **97**, 139902 (2006)].

[28] F. Gelis and R. Venugopalan, “Particle production in field theories coupled to strong external sources, I: Formalism and main Results,” Nucl. Phys. A **776**, 135 (2006).

[29] F. Gelis and R. Venugopalan, “Particle production in field theories coupled to strong external sources, II: Generating Functions,” Nucl. Phys. A **779**, 177 (2006).

[30] D. Kharzeev and K. Tuchin, “From color glass condensate to quark gluon plasma through the event horizon,” Nucl. Phys. A **753**, 316 (2005).

[31] D. Kharzeev, E. Levin and K. Tuchin, “Multi-particle production and thermalization in high-energy QCD,” Phys. Rev. C **75**, 044903 (2007).

[32] F. Gelis, E. Iancu, J. Jalilian-Marian and R. Venugopalan, “The Color Glass Condensate,” Ann. Rev. Nucl. Part. Sci. **60**, 463 (2010).

[33] R. Ruffini, G. Vereshchagin and S. Xue, “Electron-positron pairs in physics and astrophysics: From heavy nuclei to black holes,” J. Phys. Rep. **407**, 1 (2010).

[34] G. Mourou, T. Tajima and S. Bulanov, “Optics in the relativistic regime,” Rev. Mod. Phys. **78**, 309 (2006).

[35] M. Marklund and P. Shukla, “Nonlinear collective effects in photon photon and photon plasma interactions,” Rev. Mod. Phys. **78**, 591 (2006).

[36] G. V. Dunne, “New Strong-Field QED Effects at ELI: Nonperturbative Vacuum Pair Production,” Eur. Phys. J. D **55**, 327 (2009).

[37] A. Di Piazza, C. Muller, K. Z. Hatsagortsyan and C. H. Keitel, “Extremely high-intensity laser interactions with fundamental quantum systems,” Rev. Mod. Phys. **84**, 1177 (2012).

[38] T. Oka and H. Aoki, “Nonequilibrium Quantum Breakdown in a Strongly Correlated Electron System,” in *Quantum and Semi-classical Percolation and Breakdown in Disordered Solids*, Lecture Notes in Physics, Vol. 762, A. K. Sen , K. K. Bardhan and B. K. Chakrabarti (Eds), (Springer, 2009).

[39] P. D. Nation, J. R. Johansson, M. P. Blencowe and F. Nori, “Colloquium: Stimulating uncertainty: Amplifying the quantum vacuum with superconducting circuits,” Rev. Mod. Phys. 84, 1 (2012).

[40] S. N. Shevchenko, S. Ashhab and F. Nori, "Landau-Zener-Stuckelberg interferometry," Phys. Rept. **492**, 1 (2010).

[41] V. V. Dodonov, "Current status of the dynamical Casimir effect," Phys. Scripta **82**, 038105 (2010).

[42] C. M. Wilson, G. Johansson, A. Pourkabirian, M. Simoen, J. R. Johansson, T. Duty, F. Nori and P. Delsing, "Observation of the dynamical Casimir effect in a superconducting circuit," Nature **479**, 376 (2011).

[43] E. Akkermans and G. V. Dunne, "Ramsey Fringes and Time-domain Multiple-Slit Interference from Vacuum," Phys. Rev. Lett. **108**, 030401 (2012).

[44] J. Gabelli and B. Reulet, "Shaping a time-dependent excitation to minimize shot noise in a tunnel junction," Phys. Rev. B **87**, 075403 (2013).

[45] V. F. Mukhanov and S. Winitzki, *Introduction to Quantum Effects in Gravity*, (Cambridge University Press, 2007).

[46] E. A. Calzetta and B. L. Hu, *Nonequilibrium Quantum Field Theory*, (Cambridge University Press, 2008).

[47] E. Brezin and C. Itzykson, "Pair Production In Vacuum By An Alternating Field," Phys. Rev. D **2**, 1191 (1970).

[48] V. S. Popov, "Pair Production in a Variable External Field (Quasiclassical approximation)," Sov. Phys. JETP **34**, 709 (1972).

[49] V. S. Popov, "Pair production in a variable and homogeneous electric fields as an oscillator problem," Sov. Phys. JETP **35**, 659 (1972).

[50] V. G. Bagrov, D. M. Gitman, S. P. Gavrilov and S. M. Shvartsman, "Creation Of Boson Pairs In A Vacuum," Izv. Vuz. Fiz. **3**, 71 (1975).

[51] D. Gitman and S. Gavrilov, "Quantum Processes In A Strong Electromagnetic Field. Creating Pairs," Izv. Vuz. Fiz. **1**, 94 (1977).

[52] S. P. Gavrilov and D. M. Gitman, "Vacuum instability in external fields," Phys. Rev. D **53**, 7162 (1996).

[53] Y. Kluger, E. Mottola and J. Eisenberg, "The quantum Vlasov equation and its Markov limit," Phys. Rev. D **58**, 125015 (1998).

[54] S. Habib, C. Molina-Paris and E. Mottola, "Energy momentum tensor of particles created in an expanding universe," Phys. Rev. D **61**, 024010 (2000).

[55] S. P. Kim and D. Page, “Schwinger pair production via instantons in a strong electric field,” Phys. Rev. D **65**, 105002 (2002).

[56] S. P. Kim and D. Page, “Schwinger pair production in electric and magnetic fields,” Phys. Rev. D **73**, 065020 (2006).

[57] S. P. Kim and D. Page, “Improved approximations for fermion pair production in inhomogeneous electric fields,” Phys. Rev. D **75**, 045013 (2007).

[58] S. Winitzki, “Cosmological particle production and the precision of the WKB approximation,” Phys. Rev. D 72, 104011 (2005).

[59] S. P. Kim and C. Schubert, “Non-adiabatic Quantum Vlasov Equation for Schwinger Pair Production,” Phys. Rev. D **84**, 125028 (2011).

[60] F. Gelis and N. Tanji, “Schwinger mechanism revisited,” Prog. Part. Nucl. Phys. **87**, 1 (2016).

[61] J. Zahn, “The current density in quantum electrodynamics in time-dependent external potentials and the Schwinger effect,” J. Phys. A **48**, 475402 (2015).

[62] L. Parker and S. A. Fulling, “Adiabatic regularization of the energy momentum tensor of a quantized field in homogeneous spaces,” Phys. Rev. D **9**, 341 (1974).

[63] R. B. Dingle, *Asymptotic expansions: their derivation and interpretation*, (Academic Press, London, 1973).

[64] M. V. Berry, “Uniform asymptotic smoothing of Stoke’s discontinuities,” Proc. R. Soc. A **422**, 7 (1989).

[65] M. V. Berry, “Waves near Stokes lines,” Proc. R. Soc. A **427**, 265 (1990).

[66] M. V. Berry, “Semiclassically weak reflections above analytic and non-analytic potential barriers,” J. Phys. A **15**, 3693 (1982).

[67] C. K. Dumlu and G. V. Dunne, “The Stokes Phenomenon and Schwinger Vacuum Pair Production in Time-Dependent Laser Pulses,” Phys. Rev. Lett. **104**, 250402 (2010).

[68] C. K. Dumlu and G. V. Dunne, “Interference Effects in Schwinger Vacuum Pair Production for Time-Dependent Laser Pulses,” Phys. Rev. D **83**, 065028 (2011).

[69] K. Fukushima and T. Hayata, “Schwinger Mechanism with Stochastic Quantization,” Phys. Lett. B **30** (2014).

[70] K. Fukushima, "Spectral Representation of the Particle Production Out of Equilibrium - Schwinger Mechanism in Pulsed Electric Fields," New J. Phys. **16** (2014).

[71] J. Rau, "Pair production in the quantum Boltzmann equation," Phys. Rev. D **50**, 6911 (1994).

[72] J. Rau and B. Müller, "From reversible quantum microdynamics to irreversible quantum transport," Phys. Rept. **272**, 1-59 (1996).

[73] S. A. Smolyansky, G. Ropke, S. M. Schmidt, D. Blaschke, V. D. Toneev, A. V. Prozorkevich, "Dynamical derivation of a quantum kinetic equation for particle production in the Schwinger mechanism," [arXiv:hep-ph/9712377].

[74] S. M. Schmidt, D. Blaschke, G. Ropke, S. A. Smolyansky, A. V. Prozorkevich, V. D. Toneev, "A Quantum kinetic equation for particle production in the Schwinger mechanism," Int. J. Mod. Phys. **E7**, 709 (1998).

[75] A. Huet, S. P. Kim and C. Schubert, "Vlasov equation for Schwinger pair production in a time-dependent electric field," Phys. Rev. D **90**, no. 12, 125033 (2014).

[76] F. Hebenstreit, R. Alkofer and H. Gies, "Schwinger pair production in space and time-dependent electric fields: Relating the Wigner formalism to quantum kinetic theory," Phys. Rev. D **82**, 105026 (2010).

[77] F. Hebenstreit, A. Ilderton, M. Marklund and J. Zamanian, "Strong field effects in laser pulses: the Wigner formalism," Phys. Rev. D **83**, 065007 (2011).

[78] A. Steen, "Om Formen for Integralet af den lineaere Differentialligning af anden Orden," Overs. over d. K. Danske Vidensk. Selsk. Forh. (1874), 1-12.

[79] R. Redheffer and I. Redheffer, "Steen's 1874 paper: historical survey and translation," Appl. Anal. Discrete Math. **2** (2008), 146-157.

[80] V. P. Ermakov, "Second-order Differential Equations: Conditions of Complete Integrability," Univ. Izv. Kiev **20**, 1 (1880).

[81] W. E. Milne, "The Numerical Determination of Characteristic Numbers," Phys. Rev. **35**, 863 (1930).

[82] E. Pinney, "The Nonlinear Differential Equation $y'' + p(x)y + cy^{-3} = 0$," Proc. Am. Math. Soc. **1**, 681 (1950).

[83] I. M. Gel'fand and L. A. Dikii, "Asymptotic Behavior of the Resolvent of Sturm-Liouville Equations and the Algebra of the Korteweg-De Vries Equations," Russ. Math. Surv. **30**, 5 (1975).

[84] I. M. Gel'fand and L. A. Dikii, "The Resolvent and Hamiltonian Systems," Func. Anal. App. **11**, 2 (1977), 93-105.

[85] A. B. Balantekin, J. E. Seger and S. H. Fricke, "Dynamical effects in pair production by electric fields," Int. J. Mod. Phys. A **6**, 695 (1991).

[86] G. V. Dunne and T. Hall, "On the QED Effective Action in Time-Dependent Electric Backgrounds," Phys. Rev. D **58**, 105022 (1998).

[87] K. G. Budden, *Radio Waves in the Ionosphere: The Mathematical Theory of the Reflection of Radio Waves from Stratified Ionised Layers*, (Cambridge Univ. Press, 1961).

[88] M. V. Berry and K. E. Mount, "Semiclassical approximations in wave mechanics," Rept. Prog. Phys. **35**, 315 (1972).

[89] W. Dittrich and M. Reuter, *Classical and Quantum Dynamics*, (Springer, 2001).

[90] K. Husimi, "Miscellanea in elementary quantum mechanics: I," Prog. Theor. Phys. **9**, 238-244 (1953).

[91] K. Husimi, "Miscellanea in elementary quantum mechanics: II," Prog. Theor. Phys. **9**, 381-402 (1953).

[92] H. R. Lewis, "Classical and Quantum Systems with Time-Dependent Harmonic-Oscillator-Type Hamiltonians," Phys. Rev. Lett. **18**, 518 (1967).

[93] H. R. Lewis, "Class of Exact Invariants for Classical and Quantum Time-Dependent Harmonic Oscillators," J. Math. Phys. **9**, 1976 (1968).

[94] H. R. Lewis and W. B. Riesenfeld, "An Exact Quantum Theory of the Time-Dependent Harmonic Oscillator and of a Charged Particle in a Time-Dependent Electromagnetic Field," J. Math. Phys. **10**, 1458 (1969).

[95] NIST Digital Library of Mathematical Functions, [http://dlmf.nist.gov/].

[96] N. Fröman and P. O. Fröman, *Physical Problems Solved by the Phase-Integral Method*, (Cambridge Univ. Press, 2004).

[97] P. Szriftgiser, D. Guéry-Odelin, M. Arndt and J. Dalibard, "Atomic Wave Diffraction and Interference using Temporal Slits," Phys. Rev. Lett. **77**, 4 (1996).

[98] F. Lindner et al, “Attosecond Double-Slit Experiment,” Phys. Rev. Lett. **95**, 040401 (2005).

[99] G. G. Paulus and G. Stania, “Attosecond Quantum Stroboscope,” ChemPhysChem **10**, 875 (2009).

[100] T. Remetter et al, “Attosecond electron wave packet interferometry,” Nature Phys. **2**, 323 (2006).

[101] E. Mansten et al, “Spectral Signature of Short Attosecond Pulse Trains,” Phys. Rev. Lett. **102**, 083002 (2009).

[102] J. Gabelli and B. Reulet, “Shaping a time-dependent excitation to control the electron distribution function: noise minimization in a tunnel junction,” Phys. Rev. B **87**, 075403 (2013).

[103] F. Hebenstreit, R. Alkofer, G. V. Dunne and H. Gies, “Momentum signatures for Schwinger pair production in short laser pulses with sub-cycle structure,” Phys. Rev. Lett. **102**, 150404 (2009).

[104] R. Lim and M.V. Berry, “Superadiabatic Tracking of Quantum Evolution,” J.Phys.A **24**, 3255 (1991).

[105] R. Lim, “Overlapping Stokes smoothings in adiabatic quantum transitions,” J. Phys. A: Math. Gen. **26**, 7615 (1993).

[106] L. Parker, “Particle creation in isotropic cosmologies,” Phys. Rev. Lett. **28**, 705 (1972) [Erratum-ibid. **28**, 1497 (1972)].

[107] E. Mottola, “Particle Creation in de Sitter Space,” Phys. Rev. D **31**, 754 (1985).

[108] R. Bousso, A. Maloney and A. Strominger, “Conformal vacua and entropy in de Sitter space,” Phys. Rev. D **65**, 104039 (2002).

[109] E. Greenwood, D. C. Dai and D. Stojkovic, “Time dependent fluctuations and particle production in cosmological de Sitter and anti-de Sitter spaces,” Phys. Lett. B **692**, 226 (2010).

[110] S. W. Hawking and G. F. R. Ellis, *The Large Scale Structure of Space-Time*, (Cambridge Univ. Press, Cambridge 1973).

[111] G. W. Gibbons and S. W. Hawking, “Cosmological Event Horizons, Thermodynamics, and Particle Creation,” Phys. Rev. D **15**, 2738 (1977).

[112] S. A. Fulling, *Aspects of Quantum Field Theory in Curved Space-time*, London Math. Soc. Student Texts **17**, 1 (1989).

[113] L. H. Ford, “Gravitational Particle Creation and Inflation,” Phys. Rev. D **35**, 2955 (1987).

[114] M. K. Parikh and F. Wilczek, “Hawking radiation as tunneling,” Phys. Rev. Lett. **85**, 5042 (2000).

[115] R. Schutzhold and W. G. Unruh, “On Quantum Correlations across the Black Hole Horizon,” Phys. Rev. D **81**, 124033 (2010).

[116] W. G. Unruh, “Notes on black hole evaporation,” Phys. Rev. D **14**, 870 (1976).

[117] P. Lagogiannis, A. Maloney and Y. Wang, “Odd-dimensional de Sitter Space is Transparent,” [arxiv:1106.2846].

[118] S. P. Kim, “The Stokes Phenomenon and Quantum Tunneling for de Sitter Radiation in Nonstationary Coordinates,” JHEP **1009**, 054 (2010).

[119] S. P. Kim, “Geometric Origin of Stokes Phenomenon for de Sitter Radiation,” Phys. Rev. D **88**, 044027 (2013).

[120] Y. Kluger, J. M. Eisenberg, B. Svetitsky, “Pair production in a strong electric field: an initial value problem in quantum field theory,” Int. J. Mod. Phys. E **02** 333 (1993).

[121] J. M. Eisenberg, “Back-Reaction in the Presence of Thermalizing Collisions,” Found. Phys. **27**, 1213 (1997).

[122] S. S. Bulanov, A. M. Fedotov, and F. Pegoraro, ”Damping of electromagnetic waves due to electron-positron pair production,” Phys. Rev. **E** 71, 016404 (2005).

[123] J. Schlemmer, and J. Jahn, “The current density in quantum electrodynamics in external potentials,” Ann. Phys. **359** 31 (2015).

[124] F. Hebenstreit, J. Berges, and D. Gelfand, “Simulating fermion production in $1 + 1$ dimensional QED,” Phys. Rev. D 87, 105006 (2013).

[125] C. Jarzynski, “Nonequilibrium Equality for Free Energy Differences,” Phys. Rev. Lett. **78**, 2690 (1997).

[126] C. Jarzynski, “Equilibrium free-energy differences from nonequilibrium measurements: A master-equation approach,” Phys. Rev. E **56**, 5018 (1997).

[127] C. Jarzynski, “Nonequilibrium work theorem for a system strongly coupled to a thermal environment,” J. Stat. Mech: Theor. Exp. 2004 (2004).

[128] C. Jarzynski, “Rare events and the convergence of exponentially averaged work values,” Phys. Rev. E **73**, 046105 (2006).

[129] G.E. Crooks, “Nonequilibrium Measurements of Free Energy Differences for Microscopically Reversible Markovian Systems,” J. Stat. Phys. **90**, 1481 (1998).

[130] G.E. Crooks, “Entropy production fluctuation theorem and the nonequilibrium work relation for free energy differences,” Phys. Rev. E **60**, 2721 (1999).

[131] G.E. Crooks, “Path-ensemble averages in systems driven far from equilibrium,” Phys. Rev. E **61**, 2361 (2000).

[132] G. Hummer and A. Szabo, “Free energy reconstruction from nonequilibrium single-molecule pulling experiments,” Proc. Natl. Acad. Sci. (USA) **98**, 3658 (2001).

[133] P. Garbaczewski and R. Olkiewicz, *Dynamics of Dissipation*, eds. (Springer, Berlin 2002).

[134] S.X. Sun, “Equilibrium free energies from path sampling of nonequilibrium trajectories,” J. Chem. Phys. **118**, 5769 (2003).

[135] D.J. Evans, “A non-equilibrium free energy theorem for deterministic systems,” Mol. Phys. **101**, 1551 (2003).

[136] S. Mukamel, “Quantum Extension of the Jarzynski Relation: Analogy with Stochastic Dephasing,” Phys. Rev. Lett. **90**, 170604 (2003).

[137] P. Talkner, and E. Lutz, and P. Hänggi, “Fluctuation theorems: Work is not an observable,” Phys. Rev. E **75**, 050102(R) (2007).

[138] F. Douarche, S. Ciliberto, A. Petrosyan, and I. Rabbiosi, “An experimental test of the Jarzynski equality in a mechanical experiment,” Euro-phys. Lett. **70**, 593 (2005).

[139] V. Blickle, T. Speck, L. Helden, U. Seifert, and C. Bechinger, “Thermodynamics of a Colloidal Particle in a Time-Dependent Nonharmonic Potential,” Phys. Rev. Lett. **96**, 070603 (2006).

[140] J. Liphardt et al, “Equilibrium Information from Nonequilibrium Measurements in an Experimental Test of Jarzynski’s Equality,” Science **296**, 1832 (2002).

[141] J.M. Schurr, and B.S. Fujimoto, “Equalities for the Nonequilibrium Work Transferred from an External Potential to a Molecular System. Analysis of Single-Molecule Extension Experiments,” J. Phys. Chem. B **107**, 14007 (2003).

[142] S. Deffner, and E. Lutz, “Nonequilibrium work distribution of a quantum harmonic oscillator,” Phys. Rev. E **77**, 021128 (2008).

[143] S. Deffner, O. Abah, and E. Lutz, “Quantum work statistics of linear and non-linear parametric oscillators,” Chem. Phys. **375**, 200 (2010).

[144] M. Unsal, “Magnetic bion condensation: A New mechanism of confinement and mass gap in four dimensions,” Phys. Rev. D **80**, 065001 (2009).

[145] M. Shifman and M. Unsal, “QCD-like Theories on R(3) x S(1): A Smooth Journey from Small to Large r(S(1)) with Double-Trace Deformations,” Phys. Rev. D **78**, 065004 (2008).

[146] E. Poppitz and M. Unsal, “Conformality or confinement: (IR)relevance of topological excitations,” JHEP **0909**, 050 (2009).

[147] E. Poppitz and M. Unsal, “Seiberg-Witten and ’Polyakov-like’ magnetic bion confinements are continuously connected,” JHEP **1107**, 082 (2011).

[148] E. Poppitz, T. Schfer and M. Unsal, “Continuity, Deconfinement, and (Super) Yang-Mills Theory,” JHEP **1210**, 115 (2012).

[149] E. Poppitz, T. Schfer and M. Unsal, “Universal mechanism of (semi-classical) deconfinement and theta-dependence for all simple groups,” JHEP **1303**, 087 (2013).

[150] E. Shuryak and T. Sulejmanpasic, “The Chiral Symmetry Breaking/Restoration in Dyonic Vacuum,” Phys. Rev. D **86**, 036001 (2012).

[151] E. Shuryak and T. Sulejmanpasic, “Holonomy potential and confinement from a simple model of the gauge topology,” Phys. Lett. B **736**, 257 (2013).

[152] M. M. Anber and E. Poppitz, “Microscopic Structure of Magnetic Bions,” JHEP **1106**, 136 (2011).

[153] M. Unsal, “Theta dependence, sign problems and topological interference,” Phys. Rev. D **86**, 105012 (2012).

[154] A. V. Yung, “Instanton Vacuum in Supersymmetric QCD,” Nucl. Phys. B **297**, 47 (1988).

[155] V. A. Rubakov and O. Y. Shvedov, “Sphalerons and large order behavior of perturbation theory in lower dimension,” Nucl. Phys. B **434**, 245 (1995).

[156] P. Argyres and M. Ünsal, “A semiclassical realization of infrared renormalons,” Phys. Rev. Lett. **109**, 121601 (2012).

[157] P. C. Argyres and M. Ünsal, “The semi-classical expansion and resurgence in gauge theories: new perturbative, instanton, bion, and renormalon effects,” JHEP **1208**, 063 (2012).

[158] G. V. Dunne and M. Ünsal, “Resurgence and Trans-series in Quantum Field Theory: The CP(N-1) Model,” JHEP **1211**, 170 (2012).

[159] G. V. Dunne and M. Ünsal, “Continuity and Resurgence: towards a continuum definition of the CP(N-1) model,” Phys. Rev. D **87**, 025015 (2013).

[160] A. M. Din and W. J. Zakrzewski, “General Classical Solutions In The Cp**(n-1) Model,” Nucl. Phys. B **174**, 397 (1980).

[161] “Interpretation and Further Properties of General Classical CP**(n-1) Solutions,” Nucl. Phys. B **182**, 151 (1981).

[162] W. J. Zakrzewski, *Low Dimensional Sigma Models*, (Taylor and Francis, 1989).

[163] F. Bruckmann, “Instanton constituents in the O(3) model at finite temperature,” Phys. Rev. Lett. **100**, 051602 (2008).

[164] W. Brendel, F. Bruckmann, L. Janssen, A. Wipf and C. Wozar, “Instanton constituents and fermionic zero modes in twisted CP**n models,” Phys. Lett. B **676**, 116 (2009).

[165] M. Shifman and A. Yung, “Large-N Solution of the Heterotic N=(0,2) Two-Dimensional CP(N-1) Model,” Phys. Rev. D **77**, 125017 (2008), [Erratum-ibid. D **81**, 089906 (2010)].

[166] P. A. Bolokhov, M. Shifman and A. Yung, “BPS Spectrum of Supersymmetric CP(N-1) Theory with ZN Twisted Masses,” Phys. Rev. D **84**, 085004 (2011).

[167] E. B. Bogomolny, “Calculation Of Instanton - Anti-instanton Contributions In Quantum Mechanics,” Phys. Lett. **B91**, 431 (1980).

[168] J. Zinn-Justin, “Multi - Instanton Contributions In Quantum Mechanics,” Nucl. Phys. B **192**, 125 (1981).

[169] J. Zinn-Justin, *Quantum field theory and critical phenomena*, (Oxford, 2002).

[170] U. D. Jentschura and J. Zinn-Justin, "Instantons in quantum mechanics and resurgent expansions," Phys. Lett. B **596**, 138 (2004).

[171] I. I. Balitsky and A. V. Yung, "Instanton Molecular Vacuum In N=1 Supersymmetric Quantum Mechanics," Nucl. Phys. B **274**, 475 (1986).

[172] I. I. Balitsky and A. V. Yung, "Collective - Coordinate Method for Quasizero Modes," Phys. Lett. B **168**, 113 (1986).

[173] A. I. Vainshtein, V. I. Zakharov, V. A. Novikov and M. A. Shifman, "ABC's of Instantons," Sov. Phys. Usp. **25**, 195 (1982) [Usp. Fiz. Nauk **136**, 553 (1982)]; reprinted in *ITEP Lectures on Particle Physics and Field Theory*, M. A. Shifman (Ed.) (World Scientific, Singapore, 1999).

[174] T. Schäfer and E. V. Shuryak, "Instantons in QCD," Rev. Mod. Phys. **70**, 323 (1998).

[175] N. Dorey, T. J. Hollowood, V. V. Khoze and M. P. Mattis, "The Calculus of many instantons," Phys. Rept. **371**, 231 (2002).

[176] S. Vandoren and P. van Nieuwenhuizen, "Lectures on instantons," (2008).

[177] L. M. Sibner, R. J. Sibner, and K. Uhlenbeck, "Solutions to YangMills equations that are not self-dual," Proc. Natl. Acad. Sci. **86**, 8610 (1989).

[178] L. Sadun and J. Segert, "Nonselfdual Yang-Mills connections with quadrupole symmetry," Commun. Math. Phys. **145**, 363 (1992).

[179] L. Sadun and J. Segert, "Stationary Points of the Yang-Mills Action," Commun. Pure Appl. Math **45**, 461 (1992).

[180] J. Burzlaff, "Nonselfdual Solutions Of Su(3) Yang-mills Theory And A Two-dimensional Abelian Higgs Model," Phys. Rev. D **24**, 546 (1981).

[181] J. Schiff, "Hyperbolic vortices and some nonselfdual classical solutions of SU(3) gauge theory," Phys. Rev. D **44**, 528 (1991).

[182] I. Jack and H. Osborn, "Green's Functions For The Dirac Equation For General Classical Solutions Of The Cp**(n-1) Model," J. Phys. A **15**, 245 (1982).

[183] K. -M. Lee and P. Yi, "Monopoles and instantons on partially compactified D-branes," Phys. Rev. D **56**, 3711 (1997).

[184] T. C. Kraan and P. van Baal, "Periodic instantons with nontrivial holonomy," Nucl. Phys. B **533**, 627 (1998).

[185] T. C. Kraan and P. van Baal, "Monopole constituents inside SU(n) calorons," Phys. Lett. B **435**, 389 (1998).

[186] S. Bolognesi and W. Zakrzewski, "Clustering and decomposition for non-BPS solutions of the $\mathbb{CP}^{N-1}$ models." Phys. Rev. D **89**, 065013 (2014).

[187] R. Dabrowski and G. V. Dunne, "Fractionalized non-self-dual solutions in the $\mathbb{CP}^{N-1}$ model," Phys. Rev. D **88**, 025020 (2013).

[188] R. Dabrowski and G. V. Dunne, "Superadiabatic particle number in Schwinger and de Sitter particle production," Phys. Rev. D **90**, 025021 (2014).

[189] R. Dabrowski and G. V. Dunne, "Time dependence of adiabatic particle number," Phys. Rev. D **94**, 065005 (2016).

[190] N. B. Narozhnyi and A. I. Nikishov, "The Simplest processes in the pair creating electric field," Yad. Fiz. **11**, 1072 (1970), [Sov. J. Nucl. Phys. **11**, 596 (1970)].

[191] A. P. Prudnikov, Y. A. Brychow, and O. I. Marichev, *Integrals and Series* (Gordon and Breach, Amsterdam, 1990), Vol. 1.